UNIVERSITA' DEGLI STUDI DI PAVIA

Dipartimento di Medicina Molecolare

Imprinting Disease Modelling by iPSCs and CRISPR/Cas9

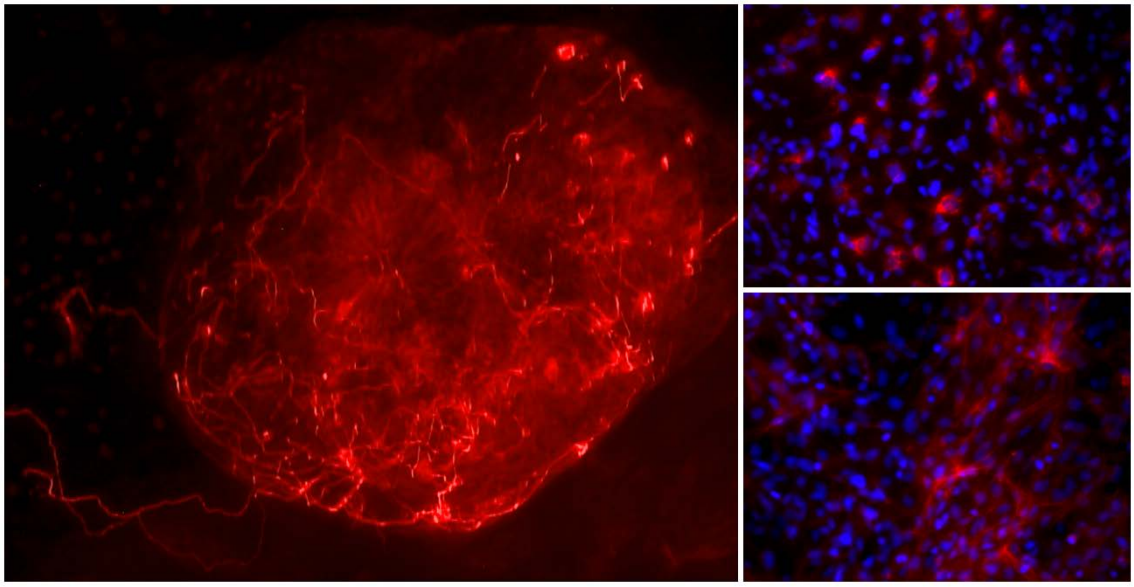

Cristina Barillà

Dottorato di Ricerca in
Genetica, Biologia Molecolare e Cellulare
XXX Ciclo – A.A. 2014-2017

UNIVERSITA' DEGLI STUDI DI PAVIA

Dipartimento di Medicina Molecolare

Imprinting Disease Modelling by iPSCs and CRISPR/Cas9

Cristina Barillà

Supervisor: Prof. Orsetta Zuffardi

Dottorato di Ricerca in
Genetica, Biologia Molecolare e Cellulare
XXX Ciclo – A.A. 2014-2017

Abstract

Chromosomal rearrangements occur in 1.8% of pregnancies (Forabosco A et al., 2009) and often lead to pregnancy interruption or early death of the newborn. The Kagami-Ogata syndrome is caused by rearrangements of a region on the maternal chromosome 14 that contains a cluster of genes regulated by imprinting mechanism. The Kagami-Ogata syndrome is often characterized by a severe phenotype that can, in some cases, cause the death of the patient in early ages. Even though the genes involved in the rearranged region are known, the molecular mechanisms related with the Kagami-Ogata syndrome have not been identified yet and the pathogenic role of these genes still needs to be investigated.

This study focuses on a family in which the Kagami-Ogata syndrome occurred in all the progeny with different degrees in the phenotype severity. We used sample from this family to generate iPSCs aiming to demonstrate an effect of this case's chromosomal rearrangement and, in particular, that the disease modelling using iPSCs is applicable for chr14 imprinting disorders. We also aimed to identify the gene(s) mainly responsible for the Kagami-Ogata syndrome's clinical features and to reveal the phenotype variability in comparison with patUPD14 mouse model prediction. In order to verify the role of *MEG3,* that has been predicted as the most important gene in Kagami-Ogata syndrome and patUPD14 pathogenesis, we modified our patient-derived iPS cell lines to rescue the expression of intact *MEG3*. Because some phenotypes can be correlated with malfunctioning of nervous system and because *MEG3*, one of the main genes investigated in this study, is mainly expressed in the brain, we further differentiated our patient-derived iPSCs into the neuronal lineage to study the transcriptional changing related with Kagami-Ogata syndrome.

Acknowledgements

I would like to thank my supervisor Dr. Orsetta Zuffardi for all opportunities that she gave me to work on this project and to learn more about genetics and molecular biology fields.

The second person who made this project possible is Dr. Dieter C. Gruenert. He accepted me as visitor researcher in his lab in UCSF, San Francisco (Ca, USA) and mentored and guided me to move this project forward.

In Dr. Gruenert lab I also had the mentorship from Dr. Shingo Suzuki and Dr. Roy G. Sargent who taught me many of molecular biology techniques and the strategy to carry out the basic biology research. Precious help came also from Mr. Keisuke Chosa.

As last, I would like to say thank you to the patients and their family who accepted to provide samples for this project wishing that our results will help to support other families.

Abbreviations

AFP: Alpha-Feto Protein
CGH-Array: Comparative Genomic Hybridization- Array
aSMA: alpha-Smooth Muscle Actin
BDNF: Brain-Derived Neurotrophic Factor
BPs: Breakpoints
bp or kb: basepare or kilobase
BSA: Bovine Serum Albumin
chr: chromosome
CMV: Cytomegalovirus
CRISPR/Cas9: Clustered Regularly Interspaced Short Palindromic Repeats/ CRISPR associated protein 9
DAPI: 4',6-diamidino-2-phenylindole
DNA: Desossiribonucleic Acid
DLK1: delta-like 1
DMEM: Dulbecco's Modified Eagle Medium
DMRs: Differentially Methylated Regions
EBNA: Epstein–Barr nuclear antigen
EBs: Embryoid Bodies
EGTA: Ethylene glycol-bis(2-aminoethylether)-*N,N,N′,N′*-tetraacetic acid
ES and hES: Embryonic Stem and human Embryonic Stem
FBS: Fetal Bovine Serum
Flt3L: fms-like tyrosine kinase 3 Ligand
bFGF: basic Fibroblast Growth Factor
GCV: Ganciclovir
GDNF: Glial cell-Derived Neurotrofic Factor
eGFP: enhanced Green Fluorescent Protein
gRNA: guide Rinbonucleic Acid
h-chr: human chromosome
HuMEC: human mammary epithelial cells
ICs: Imprinting Centers
IG-DMRS: Inter-genic Differentially Methylated Region
IL2: Interleukin 2
IL3: human interleukin 3
IL6: human interleukin 6
iPSC: induced Pluripotent Stem Cells

KO: Knock Out
KO-DMEM: Knock Out Dulbecco's Modified Eagle Medium
KSFM: Keratynocyte Serum Free Medium
KSR: Knock out serum replacement
LAM: Laminin
LCL: Lymphoblastoid cell line
lncRNA: long non-coding RNA
lincRNA: long intergenic non-coding RNA
matUPD: maternal Uniparental Disomy of chromosome 14
m-chr12: mouse chromosome 12
MEGs: Maternally Expressed Genes
MEF: Mouse Embryonic Fibroblasts
MEM: Minimum Essential Medium
miRNA: micro RNA
MLHC8e: modified LHC-8 medium with epinephrine
MLPA: Multiplex ligation-dependent probe amplification
MMC: Mytomicin C
MOI: Multiplicity of Infection
NEAA: Non Essential Amino-Acid
NHEJ: Non Homologous End Joining
NPCs: Neural Progenitors cells
Nt: nucleotide
patUPD: paternal Uniparental Disomy of chromosome 14
PB: Piggy Bac
PBase: Piggy Bac Transposase
PBMC: Peripheral Blood Mononuclear Cells
PBS or DPBS: Phosphate Buffer Saline without or with calcium and magnesium addiction
CAG: CMV early enhancer/chicken β actin/globin gene
PAM: Protospacer Adjacent Motif
PEGs: Paternally Expressed Genes
PET: Polyvinylpyrrolidone EGTA trypsin
PFA: paraformaldehyde
PHA: Phyto Emoagglutinin
PLO: Poly-Ornithyne
Puro: Puromycin
PWS: Prader-Willy syndrome
qPCR or PCR: quantitative Polymerase Chain Reaction

RNA: Ribonucleic Acid
Rocki: rho-kinase inhibitor
RPMI: Roswell Park Memorial Institute
RTl1: retrotransposone like-1
RTL1as: retrotransposone like-1 antisense
SCF: human stem cell factor
SFEMII: Serum-Free Expansion Medium II
SNORDs: small nucleolar RNA, C/D box
SSEA4: stage-specific embryonic antigen-4
T7E1: T7 endonuclease I
TALEN: Transcription activator-like effector nucleases
TUJ1: Neuron-specific class III beta-tubulin
TK: Thymidine Kinase
UPD: Uniparental Disomie of chromosome 14
WT: Wild Type
ZFN: Zinc Finger Nuclease

Contents

1. Introduction

An imprinting-related disease is defined as the genetic disorder characterized by phenotypes can be correlated with a parental origin of mutations. This disease is caused by aberrations on particular chromosomes that are characterized by mono-allelic expression of genes. These chromosomes contain a region called imprinting center (IC) which regulates the expression of downstream/upstream genes by DNA methylation. ICs are usually hyper-methylated on silent chromosome and hypo-methylated on expressed chromosome (Barlow DP and Bartolomei MS, 2014). The clearest example of imprinting diseases is uniparental disomy (UPD) characterized by the inheritance of two homologous chromosomes from only one parent. UPD itself is not necessarily to correlate with a pathologic condition, in fact its prevalence is approximately 1.65/10,000 and, in the most of cases, is not symptomatic. However, UPD shows a pathological condition when it causes a duplication of a recessive disease mutation or if it interests a chromosome carrying an IC, causing overexpression or no expression of imprinted genes. UPDs usually interest the entire chromosome but segmental UPDs are also known (Eggerman T. et al., 2015_A and B).

UPD14 is rare pathological condition that has been described for both paternal and maternal chromosome 14 and it has a frequency of <1/1,000,000 for both maternal and paternal UPD14 (Orphanet, http://www.orpha.net/consor/www/cgi-bin/?lng=IT). patUPD14 is caused by the inheritance of both chr14 from only the father and showed the bell-shaped thorax as the pathognomonic sign. Also, patUPD14 is usually associated with a severe phenotype which can be summarized with facial dysmorphisms, abdominal wall defects and polyhydramnios (Wang JC et al., 1991). In contrast, the matUPD14, caused by inheritance of the homologous 14s from only the mother, leads to a milder condition mainly characterized by growth failure (both pre- and post-natal) and early onset of puberty (Temple IK et al., 1991). The segmental UPD of chr14 is also known on both maternal and paternal UPD as UPD14-like. For example, matUPD14-like has been called Temple syndrome (#616222, OMIM, https://www.omim.org/) (Temple IK et al., 2007) and patUPD14-like is

known as Kagami-Ogata syndrome (#608149, OMIM) after its first report in 2008 (Kagami M et al., 2008).

Chromosomes 14 has two known ICs that are called IG-DMR (germ-line-derived inter-genic differentially methylated region) and MEG3-DMR (post-fertilization-derived DMR, mapped on the *MEG3* promoter region), located in 14q32.2. These two DMRs are hyper-methylated on the paternal chr14 and hypo-methylated on maternal ch14, regulating the *DLK1-MEG3* domain which contains two protein-coding genes (*DLK1* and *RTL1*) paternally expressed and several non-protein-coding genes (*MEG3, MEG8, RTL1as*, miRNAs and a cluster of SNORDs) maternally expressed (Wylie AA et al., 2000). These two DMRs are hierarchically functional: a methylation study on Kagami-Ogata syndrome patients showed that IG-DMR has the main regulatory role by affecting the methylation pattern of MEG3-DMR in the body, but not in the placenta. MEG3-DMR, when hypo-methylated, controls the expression of the surrounding PEGs and MEGs in both body and placenta. This report and others suggest that IG-DMR strongly affects on the expression of the genes in the *DLK1-MEG3* locus because MEG3-DMR is hypo-methylated, allowing the *MEG3* promoter to be functional when IG-DMR is hypo-methylated (normal status on maternal allele or epimutation on pathological paternal ch14), but MEG3-DMR is hyper-methylated when IG-DMR is hyper-methylated (normal status on paternal allele) or deleted (maternal deletion of IG-DMR) (Kagami M et al., 2010).

In this study, we focused on a family affected by Kagami-Ogata syndrome (Figure 1). Case 1 is the second child (the first child was a pre-term female, she died after a few hours of birth due to cerebral bleeding) of non-consanguineous parents. He was a pre-term male born at 33th week of gestation after rupture of the membranes and died at 6 months of age. At birth, he needed mechanical ventilation and in the following months he showed chronic breathing difficulties with severe feeding problems. Main phenotype in case 1 was characterised by severe developmental delay with severe hypotonia (difficulties in the head control at 5 months), hyposomia and hypotrophic muscle mass, bilateral inguinoscrotal hernia, and severe cervicothoracic scoliosis. He also showed mild dysmorphisms. Case 2 is the third child and sister of case 1, she was born at 34th week of gestation because of severe polyhydramnios and possible uterus rupture. At the birth,

she had no breathing activity requiring mechanical ventilation, but she recovered and started to be able to breath by herself. Case 2 showed feeding difficulties as well as case 1 with duodenal malrotation and mild dysmorphisms. Case 2 did not show other malformations. She showed a considerably milder phenotype when compared to case 1 and she could recover some of the clinical features even though developmental delay has been still observed. Both parents are apparently healthy without any known disease history in their family.

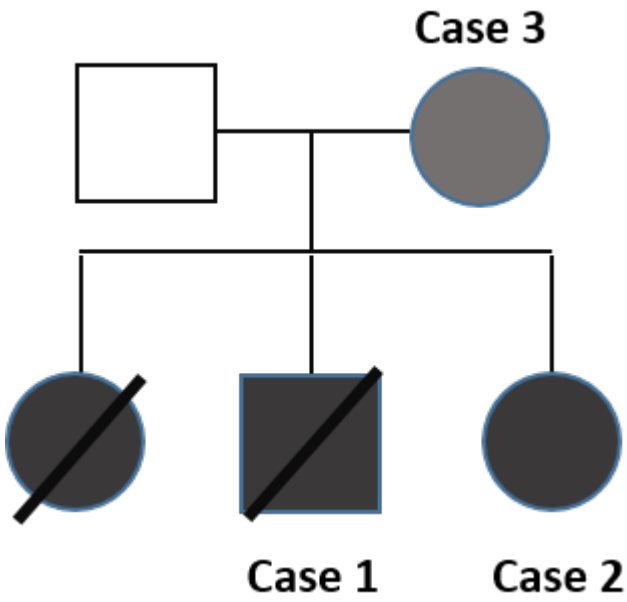

Figure 1. Pedigree of patients in this study. In dark grey, the affected children with 14q32.2 maternal deletion. In light grey, the apparently healthy mother (case 3) with 14q32.2 deletion of unknown origin.

2. State of the art

2.1 Mouse model of paternal UPD12

UPD has been investigated experimentally using animal models in order to trace the parental origin of chromosomes. UPD12 mouse is used as one of models for human UPD14 because mouse chr12 is the syntenic chromosome of human chr14. Studies on parthenogenetic, androgenetic and UPD12 embryos pointed out the possible presence of an imprinting region on chr12 in mouse. These studies, in fact, showed that two copies of paternal chr12 caused lethality at the embryonic stage with no fetus arriving at term, in contrast matUPD12 causes the lethality at the perinatal stage. Furthermore, patUPD12 shows placentomegaly, abnormal growth and development of skeletal muscles, bell-shaped thorax (the angulation of the ribs relative to the sternum is abnormally wide), lower ossification and abnormal abdominal distension. In contrast, matUPD12 shows the delay of placenta development, hyposomia, small skeleton and no delay in ossification (Georgiades P et al., 2000). The pathological phenotype in UPD12 mouse and its difference correlated with inheritance of the homologous chr12 could explain the presence of imprinted genes on chr12. In 2000, two genes have been proved to be imprinted on mouse chr12: *Dlk1* and *Gtl2*. In androgenetic and patUPD12 embryos, *Dlk1* expressed twice more when compared to normal mice and did not express in parthenogenic or matUDP12. *Gtl2* expression in these models was observed in opposite manner. The human homologues of *Dlk1* and *Gtl2* are localized on ch14q and this region in human also has been confirmed as imprinting regulated (Takada S et al., 2000; Miyoshi N et al., 2000). Following studies revealed that these two genes are not only imprinted genes on mouse chr12, but they are part of a cluster, around 1Mb, containing *Dio3* expressed paternally and long non-coding RNAs and C/D snoRNAs expressed maternally (Schmidt, J.V et al., 2000; Tsai CE et al., 2002; Yevtodiyenko A et al., 2002). Methylation studies showed that *Dlk1-Dio3* cluster is methylated on paternal chromosome and unmethylated on maternal chromosome in both mouse and human. In human, this methylation pattern in *DLK1-DIO3* cluster and in another imprinting domain, *IGF2/H19* domain, are unique because other imprinting regions are maternally methylated and paternally unmethylated. (Murphy SK et al., 2003). The identification of two DMRs in

the *DLk1-Dio3* domain allowed to confirm that the methylation status in these DMRs is the master regulator of surrounding genes through epigenetic switching: the deletion of maternal IG-DMR causes the paternalization of maternal m-chr12/h-chr14 with subsequent increment of *Dlk1*, *Rtl1* and *Dio3* expression and no Megs expression due to subsequent methylation at the promoter. On the other hands, when the paternal IG-DMR is deleted, no effect is observed on the methylation status of Megs' promoter and on these genes' expression pattern (Lin SP et al., 2003) (Fig.2). This hierarchical interaction of the two DMRs in mouse has been confirmed also in human (Kagami M et al., 2010). Interestingly, patUPD12 mouse model showed different imprinted genes' expression pattern in the placenta from that in embryos' body when maternal IG-DMR was deleted, even though higher expression level of *Dlk1*, *Rtl1* and *Dio3* were still detected compared with WT mice. More particularly, in ΔIG-DMR placenta, although Pegs' gene expression increment was observed, it was not as high as it observed from full paternalization of the maternal chromosome in embryos. Also, the expression of *Megs* is still detectable unlikely in embryos, suggesting that the maternal chromosome in the placenta is not completely silenced by the deletion of IG-DMR. Furthermore, while IG-DMR was methylated in both body and placenta, the DMR located on *Gtl2* promoter was differentially methylated only in the body, demonstrating that two DMRs in the *Dlk1-Gtl2* domain also are regulated in different way between embryos and placenta (Lin SP et al., 2007) (Figures 2 and 3).

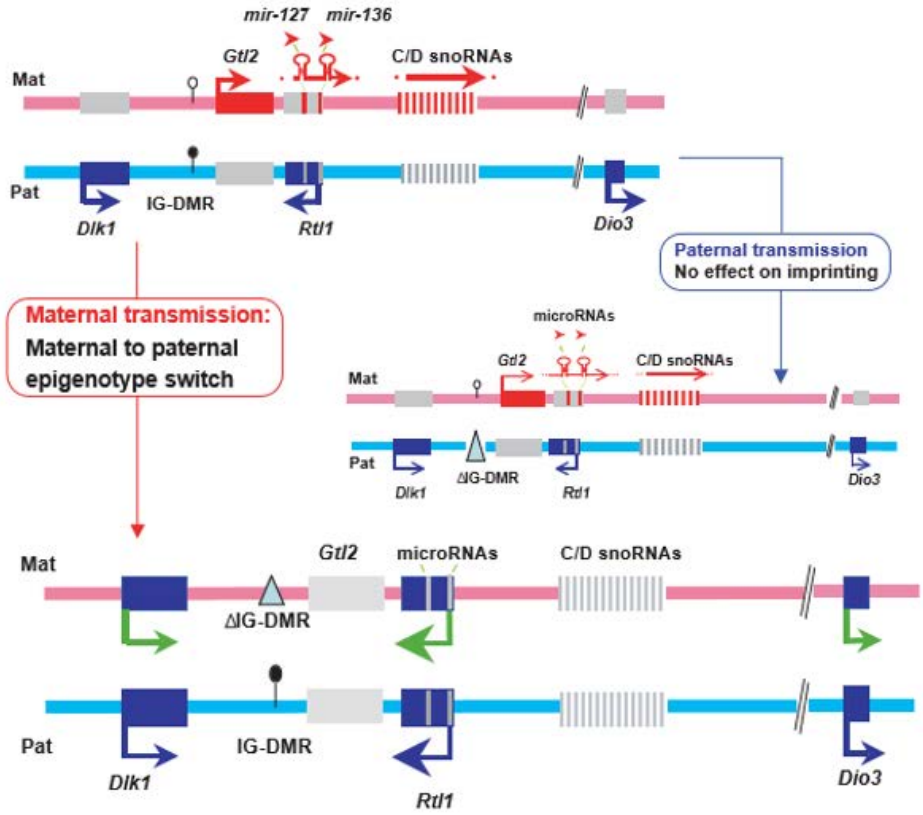

Figure 2. IG-DMR deletion in mouse chr12. The top shows the structure of mouse chr12 in normal expression conditions (in blue the paternally expressed genes, in red the maternally expressed genes). The authors created IG-DMR deleted mice and studied the methylation changes by tracing the parental origin of the deletion. From the panel we can see that only maternal inheritance of the IG-DMR deletion causes an epigenetic switch with consequent methylation of MEG3/Gtl2-DMR and silencing of Megs. In contrast the paternal deletion has no effect suggesting that the maternal IG-DMR controls the epigenetic status of the *DLK1-MEG3* domain by controlling the MEG3-Gtl2-DMR (Lin SP et al., 2003).

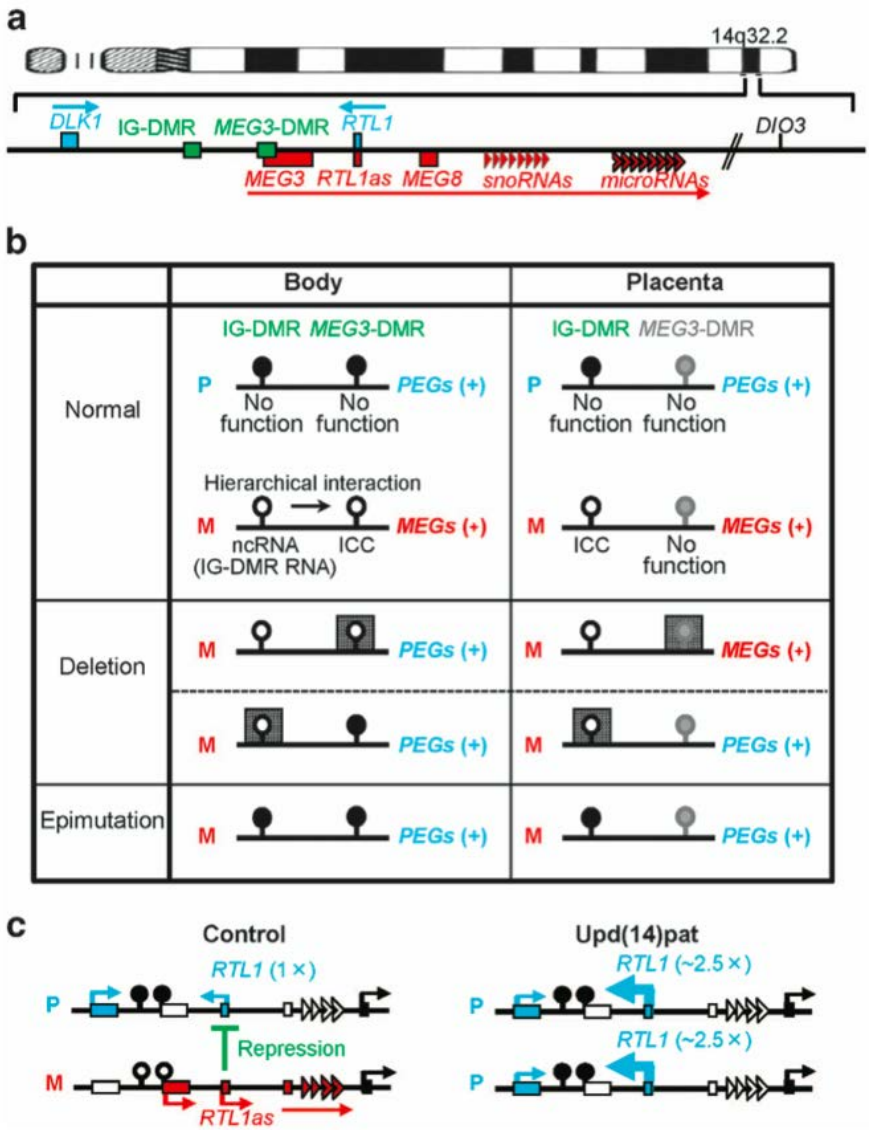

Figure 3. Methylation study on human samples from Kagami-Ogata syndrome patients. A) structure of human chr14. In blue the paternally expressed genes, in red the maternally expressed genes, in green the two DMRs. B) methylation analysis in embryos body and placenta in normal control, deleted patient and epimutated patient. C) gene expression analysis in placenta reveals that the activation of paternally expressed genes is not compatible with full paternalization of the deleted/mutated maternal chr14 in which it is expected to observe an increase of ≥4 times, as shown in the panel (Ogata T and Kagami M, 2016).

Methylation regulation has been investigated also from the point of histone modification level and the authors identified that there is no allele-specific alteration in mouse embryos at the IG-DMR. In contrast, Gtl2-DMR has been found hypo-acetylated at histones H3 and H4 on the transcriptionally silent paternal chromosome and hyper-acetylated on the transcriptionally active maternal chromosome, although the difference in histone methylation degree was not significant (Carr MS et al., 2007). Next, pathway models known to regulate histone modifications were applied to the study of *Dlk1-Gtl2* domain activation. However, none of known pathway showed any correlation. Recent studies in mouse ES cells and myoblasts revealed the existence of non-coding RNA derived from IG-DMR transcription, regulating histone modification and enhancing the expression of *Meg3/Gtl2* (Carr MS et al., 2007; McMurray EN and Schmidt JV, 2012; Kota SK et al., 2014; Hitachi K and Tsuchida K, 2017). No evidence has confirmed the IG-DMR non-coding RNA in human yet.

2.2 Paternally expressed genes in DLK1-MEG3 domain

The first imprinted gene in human *DLK1-MEG3* domain is *DLK1* (GRCh37/hg19 chr14:101,193,202-101,201,467_UCSC, https://genome.ucsc.edu/), a protein-coding gene that is expressed by the paternal chromosome 14. DLK1 (Delta Drosophila Homolog-Like 1) is a transmembrane protein expressed mainly at embryonic stage and its expression is suppressed in adult tissues except for preadipocytes, pancreatic β cells, thymocytes, B lymphocytes, cells in the adrenal gland and neuronal cells (Carlsson CD et al., 1997; Hansen LH et al., 1998; Kaneta M et al., 2000; Ohno N et al., 2001; Raghunandan R et al., 2008; Ferrón SR et al., 2011; Müller Det al., 2014; Rhee M et al., 2016). *Dlk1* KO-mice studies showed *Dlk1*'s important role in growth and development, perinatal survival, and adipose development. Phenotypes of KO-mice are overlapping that observed in patient with matUPD14, suggesting a possible causative role of *DLK1* gene in matUPD14 pathogenesis (Moon YS et al., 2002). Furthermore, a dose-dependent effect has been observed in overexpression models which causes organ abnormalities and post-natal lethality while the absence of expression can cause characteristic phenotypes such as poor growth in uterus and precocious puberty (da Rocha ST et al., 2009; Cleaton MA et al., 2016; Dauber A et al., 2017).

The 14q32 imprinted domain contains another paternally expressed protein-coding gene, *RTL1* (GRCh37/hg19 chr14:101,346,992-101,351,184_UCSC). RTL1 (retrotransposon-like 1) is a protein expressed during embryonic stage in both placenta and fetus with the essential role in the capillary stability, resulting in the regulation of the fetal-maternal interface during gas and nutrition exchange (Sekita Y et al., 2008). As mentioned above, *RTL1* is paternally expressed, however mouse model demonstrated that this gene is also maternally regulated because at the same genomic position of *RTL1* there is antisense sequence *RTL1as* which is coded on the opposite strand and expressed from the maternal chromosome. Mouse *Rtl1as* transcript is processed to originate a series of miRNAs which regulate the paternal *Rtl1* expression through RNA interference mechanism to decrease the RNA level of *Rtl1* (Seitz H et al., 2003; Davis E et al., 2005; Lin SP et al., 2007) (Figure 3). miRNA-127 derived from *RTL1as* seems to be more involved in this regulatory mechanism (Ito M et al., 2015). Both KO and overexpression mouse models have been created to study the role of *RTL1* and the effect of its alteration. Mice models showed that both absence and overexpression of *RTL1* are critical for fetal development and survival (Sekita Y et al., 2008).

The last protein-coding gene expressed by the paternal chromosome is *DIO3* (Deiodinase Iodothyronine type III). This gene is located at chr14:102,027,688-102,029,789 (GRCh37/hg19_UCSC) and it encodes a protein involved in the inactivation of thyroid hormones and essential for the correct thyroid function. Depletion of *DIO3* causes severe hypothyroidism (Huang SA et al., 2000; Hernandez A et al., 2006). Because thyroid malfunctioning is not observed in patients with segmental UPD14 involving the *DLK1-MEG3* domain, the association between *DIO3* and this domain is under debate yet. However, the differential methylation pattern between maternal and paternal chromosome 14 at the *DIO3* locus has been widely demonstrated, which has led some authors to hypothesize that a different imprinting center regulates *DIO3* expression and that differences in thyroid hormone at embryonic stage may have some role in the phenotype determination (Ogata T and Kagami M, 2016; Martinez ME et al., 2016).

2.3 Maternally expressed genes in DLK1-MEG3 domain

The other genes located in the 14q32 imprinted domain are all non-coding RNA and maternally expressed. *MEG3* (GRCh37/hg19 chr14:101,297,758-101,327,360_UCSC) is a long non-coding RNA expressed in many normal adult tissues with the role in cell proliferation and biological processes such as angiogenesis (Zhang X et al., 2010; Gordon FE et al., 2010; He C et el., 2017). To date, *MEG3* is the most studied gene in the *DLK1-MEG3* domain because it has been found that *MEG3* is sometime altered in tumors and, in some cases, it seems to have a critical role in influencing the prognosis of cancer, i.e. through regulation of tumor invasion. Furthermore, overexpression of this long non-coding RNA in cancer cell lines leads to an increase of apoptosis and differentiation capacity of the cells (Zhang X et al., 2010; Benetatos L et al., 2011; Wang P et al., 2012; Zhou Y et al., 2013; Qin R et al., 2013; Lu KH et al., 2013; Ying L et al., 2013; Sheng X et al., 2014; Tian ZZ et al., 2015; Luo G et al., 2015; Zhuang W et al., 2015; Peng W et al., 2015; Guo Q et al., 2016; Sun L et al., 2016; Zhang J et al., 2016; Huang ZL et al., 2017; Terashima M et al., 2017; Zhang CY et al., 2017). Inducible overexpression studies, in fact, showed that *MEG3* has a tumor suppressor activity through the activation of p53 (Zhou Y et al., 2007; Lu KH et al., 2013). This interaction has been confirmed also in *MEG3* epigenetic repression studies (Li J et al., 2016). The lack of *MEG3* expression has been also correlated with increase of angiogenetic genes and growth factor expression in mouse, suggesting a possible tumor suppressor activity by inhibiting the ability of the tissue to create new vessels (Gordon FE et al., 2010). Also, studies of cancer cells pointed out a series of other possible targets/correlated genes for *MEG3* activity, such as TGF-b pathway genes, PI3K, miRNAs, NOTCH1, PTBP1, genes involved in the epithelial-mesenchimal transition process, and etc (Mondal T et al., 2014; Guo O et al., 2016; Li Z et al., 2017; Terashima M et al., 2017; Zhang L et al., 2017; Gu L et al., 2017; Zhou X et al., 2017). In addition, a study was carried out to identify possible *MEG3* targets by RNA binding affinity and mass spectrometry and this study suggests that *MEG3* may be involved in the regulation of several biological processes by binding proteins involved in macromolecular complex assembly/organization, intracellular transport and so on (Liu S et al., 2015). Another study using human embryonic stem cells showed that the repression of *MEG3* causes morphological and growth changes in EBs and lower expression of neuronal

markers, such as PAX6, when compared to controls. Also, the expression of tested endoderm and mesoderm markers (SOX17 and HAND1, respectively) were increased. This suppression of neuronal lineage genes was observed also at the stem cell stage. These results suggest that *MEG3* may have a role in neuronal differentiation and maturation during cell fate determination (MO CF et al., 2015). Overall, *MEG3* has been considered as the most critical gene in the *DLK1-MEG3* domain in Kagami-Ogata syndrome.

MEG8 (GRCh37/hg19 chr14:101,361,107-101,373,305_UCSC) is a long non-coding RNA highly expressed in the adult mouse brain and skin, and at low level in heart. Mice studies suggested a possible important role in brain development during embryogenesis (Hagan JP et al., 2009; Gu T et al., 2012). Recently some papers published the existence of a new DMR inside of *MEG8* intron 2 whose methylation may be under the control of previously described MEG3-DMR. The role of MEG8-DMR has not been well characterized yet, but it has been found as hyper-methylated in Temple syndrome (matUPD14) and hypo-methylated in Kagami-Ogata syndrome, unlike previous prediction based on mouse model (Bens S et al., 2015; Beygo J et al., 2017).

SNORDs and miRNAs clusters are located inside of the *DLK1-MEG3* domain. The presence of small nucleolar RNA has been described also in the chromosome 15 imprinting domain which is associate with Prader-Willy/Angelman syndrome. In case of chromosome 15, the SNORDs cluster is paternally expressed. However, mouse SNORDs on chromosome 12 are maternally expressed, are located downstream of *MEG3* and also are brain specific (Cavaillé J et al., 2002; Benetatos L et al., 2013). miRNAs cluster contains 54 miRNAs, two of them are located in between *DLK1* and *MEG3*, but the most of them are located downstream of *MEG3* (Benetatos L et al., 2013).

2.4 Kagami-Ogata patients: genotype-phenotype correlation

Kagami M. et al., described first patients with segmental UPD14 in 2008. Since then, around 24 cases with epimutations affecting the DMRs or deletions on maternal ch14 have been reported (Kagami M et al., 2010; Irving MD et al., 2010; Kagami M et al., 2012; Classen C et al., 2013; Beygo J. et al., 2015; Kagami M et al., 2015; Corsello G et al., 2015; Rosenfeld JA et al., 2015; Ogata T. and Kagami M, 2016). The phenotype analysis from total of 53 reported cases with either total or segmental UPD14 (Table 1) showed that the main characteristic of these diseases is the bell-shaped thorax as well as mouse model during childhood and puberty. There are other characteristics can be observed in UPD14 patients, but they are not specific for the disease. Notably, the mortality is around 30% and in all reported cases it occurred before 4 years of age (Ogata T and Kagami M, 2016). The majority of reported cases has mutations or deletions spanning the DMRs, a few reports described patients with deletions inside of the imprinted domain not involving the DMRs (Rosenfeld JA et al., 2015; Corsello G et al., 2015). Also, at the best of our knowledge, reported Kagami-Ogata syndrome patients were studied the genotype-phenotype correlation only by comparing with mouse model and, however, no functional studies on these patients have been done. Taking these, the lack of expression of *MEG3* has been considered one of the possible responsible factors of the Kagami-Ogata syndrome, together with overexpression of *RTL1* (Kagami M et al., 2008). Despite the consideration about *MEG3*, there are clinical reports of patients carrying deletions at downstream of the MEG3-DMR and another carrying the deletion at downstream of *MEG3*, leading to the consideration that *MEG3* may not cause the UPD14 phenotype or at least it is not the major responsible (Rosenfeld JA et al., 2015). By performing molecular analysis in paraffin-embedded and fresh placenta samples from reported patients, the prediction of imprinted genes expression and methylation from mouse model was confirmed in favor of the hypothesis for the role of *RTL1* overexpression in Kagami-Ogata syndrome (KagamiM et al., 2008; Kagami M et al., 2012). Another example of imprinting diseases, Prader-Willy syndrome, caused by the loss of paternal expression of imprinted genes on chromosome 15, showed that point mutations in SNORD116 (small nucleolar RNA mapped inside of the Prader-Willy critical region) can cause the pathological phenotype observed in patients (Duker Al et al., 2010). These observations and discoveries have

brought in the field to consider that other genes or a combination of the genes in the *DLK1-MEG3* domain can be responsible for the Kagami-Ogata syndrome phenotype.

Table S1. Clinical features in patients with Kagami-Ogata syndrome											
	Upd(14)pat	Upd(14)pat	Epimutation	Deletion-1	Deletion-2	Deletion-3	Deletion-4	Deletion-5	Deletion-6	Deletion-7	Total
	Japanese	Non-Japanese	Japanese	Japanese	Japanese	Japanese	Japanese	Non-Japanese	Non-Japanese	Non-Japanese	
	(n=23)	(n=14)	(n=7)	(n=1)	(n=2)	(n=1)	(n=1)	(n=1)	(n=2)	(n=1)	(n=53)
Age at the last examination or death (year)	2.9 (0.0 ~ 15.0)	0.5 (0.5 ~ 9.0)	2.0 (0.0 ~ 5.5)	2,7	4.8 (0.7 ~ 8.9)	3,8	5,0	2,3	5.2 (4.8 ~ 5.5)	0	2.1 (0.0 ~ 15.0)
Sex (male:female)	9:14	5:9	4:3	0:1	1:1	0:1	0:1	1:0	1:1	0:1	21:32
Placentomegaly[a]	14/17	1/1	6/6	1/1	2/2	1/1	1/1	0/1	Unknown	0/1	26/31
Polyhydramnios	23/23	12/12	7/7	1/1	2/2	1/1	1/1	1/1	2/2	0/1	50/51
Prenatal growth failure[b]	0/23	1/8	0/7	0/1	0/2	0/1	0/1	0/1	0/2	0/1	1/47
Prenatal overgrowth[c]	13/23	0/8	5/7	1/1	2/2	1/1	0/1	0/1	0/2	0/1	22/47
Prenatal length (SDS)	+0.3 (–1.7~ +3.0)	Unknown	–0.6 (–0.9 ~ +1.4)	±0	Unknown	–0.1	+1.5	+1.4	–0.7 (0 ~ –1.4)	–1.1	±0 (–1.7 ~ +3.0)
Prenatal weight (SDS)	+2.2 (+0.1~ +8.8)	Unknown	+1.5 (+0.3 ~ +3.7)	+3.7	+2.6 (+2.4 ~ +2.8)	+2.5	+0.9	–1.6	0.0 (–1.6 ~ +1.5)	+1.5	+1.8 (–1.6 ~ +8.8)
Postnatal growth failure[d]	7/20	1/2	2/6	0/1	2/2	0/1	0/1	0/1	Unknown	Unknown	12/34
Postnatal overgrowth[e]	1/20	0/2	1/6	0/1	0/2	0/1	0/1	0/1	Unknown	Unknown	2/34
Postnatal length/height (SDS)	–1.6 (–8.7 ~ +1.1)	Unknown	–1.5 (–7.1 ~ +0.9)	–1.3	–2.7 (–3.3 ~ –2.2)	Unknown	–1.6	Unknown	Unknown	Unknown	–1.6 (–8.7 ~ +1.1)
Postnatal weight (SDS)	–1.0 (–6.0 ~ +2.4)	Unknown	–0.8 (–5.5 ~ +4.0)	±0	–1.7 (–2.2 ~ –1.3)	–1.3	–0.9	Unknown	Unknown	Unknown	–1.0 (–6.0 ~ +4.0)
Facial gestalt[f]	23/23	12/12	7/7	1/1	2/2	1/1	1/1	Unknown	2/2	1/1	50/50
Small bell-shaped thorax in infancy[g]	23/23	11/11	7/7	1/1	2/2	1/1	1/1	1/1	2/2	1/1	50/50
Coat-hanger appearance in infancy[h]	23/23	10/10	7/7	1/1	2/2	1/1	1/1	1/1	2/2	1/1	49/49
Omphalocele	7/23	1/11	2/7	1/1	0/2	0/1	0/1	Unknown	0/2	1/1	12/49
Diastasis recti	16/23	10/11	5/7	0/1	2/2	1/1	1/1	Unknown	2/2	0/1	37/49
Developmental delay	21/21	9/9	6/6	1/1	2/2	1/1	1/1	1/1	1/1	Unknown	43/43
Developmental/intellectual quotient	55 (29 ~ 70)	Unknown	52 (48 ~ 56)	Unknown	Unknown	Unknown	Unknown	Unknown	Unknown	Unknown	55 (29 ~ 70)
Feeding difficulties	20/21	8/8	7/7	1/1	2/2	1/1	1/1	1/1	1/2	Unknown	42/44
Hepatoblastoma	3/23	Unknown	0/7	0/1	0/2	0/1	0/1	Unknown	0/1	Unknown	3/36
Death	5/23	8/12	0/7	0/1	1/2	1/1	0/1	0/1	0/2	1/1	16/51
References	1–5	6–19	4,5,20	21	20	20	20	22	22	21,22	
			(plus 2 new cases)								

Table 1. Clinical study for genotype-phenotype correlation. The table shows the clinical feature of 53 patients with full or segmental patUPD14. From this analysis we can conclude that the main feature in patUPD14 is the presence of bell-shaped thorax that can be considered the patUPD14 pathognomonic sign (Ogata T and Kagami M, 2016).

2.5 LONG-NON-CODING RNAs

The development of high throughput analysis, such as whole genome sequencing and RNAseq, allowed better understanding for our genome structure. As hypothesized in the past, to date, we know that the majority of our genome is not translated, but still is transcribed. All un-translated RNA can be named "non-coding RNAs" and are usually distinguished based on RNA length in short- (<200nt) and long-non-coding RNAs (>200nt, lncRNA) (Kung JTY et al., 2013). lncRNAs are known to have an important role in gene regulation and in particular in epigenetic regulation, such as *H19* and *Xist* (Brannan CI et al. 1990; Brockdorff NA et al. 1992; Brown CJ et al. 1992). lncRNAs can be divided in different overlapping categories based on their origin: i.e. "lincRNAs" (long intergenic noncoding RNAs) are classified as lncRNAs encoded by region in between different genes. Usually lincRNAs are around 1kb in length and their structure is similar to an mRNA, in fact, they are usually polyadenylated, spliced and they can have different isoforms too (Guttman M et al. 2009; Cabili MN et al. 2011; Ulitsky I et al. 2011). This is the case of mentioned *Xist*, *H19,* but also others such as *HOTAIR* and *MALAT1* (Brannan CI et al. 1990; Brockdorff NA et al. 1992; Brown CJ et al. 1992; Rinn JL et al. 2007; Ji P et al. 2003). Another class of lncRNAs is encoded on the opposite strand of a known protein-coding gene and behave as antisense transcript (around 70% of sense transcripts have reported antisense counterparts) (Katayama S et al. 2005; He Y et al. 2008; Faghihi MA and Wahlestedt C 2009). The antisense coding region can be either overlapping the protein-coding gene or located in the regulatory regions at the 5' or 3' of the interested sense transcript (called sense-antisense or natural antisense transcripts, respectively). An example is the *Xist*/*Tsix* sense-antisense lncRNAs pairs that control X chromosome inactivation, but also protein-coding sense-antisense pairs such as *Kcnq1/Kcnq1ot1* and *Igf2r/Air* (Lee JT et al. 1999; Kanduri C et al. 2006; Lyle R et al. 2000). Also, some lncRNAs derive from transcription of pseudogenes regulating the gene expression through epigenetic or post-transcriptional regulation (Duret L et al. 2006; Elisaphenko EA et al. 2008). Furthermore, lncRNAs can be encoded inside of the introns of protein-coding genes or be encoded by enhancers, in both cases, poor details have been known (Guil S et al. 2012; Kim TK et al. 2010; Wang D et al. 2011).

MEG3 and *MEG8* are both lincRNAs and in particular *MEG3* shows polyadenylation signal and different isoforms (UCSC).

2.6 Induced Pluripotent Stem Cells

Induced pluripotent stem cell is a stem cell derived from primary cell cultures through epigenetic reprogramming and shows pluripotent character like embryonic stem (ES) cell. To date, it can be originated from different cell types such as fibroblasts or blood cells. Primary cells can be reprogrammed by the induction of specific expression pattern typic of ES cells. This induction can be obtained by exposing to the so-called Yamanaka factors, a combination of transcriptional factors that allow chromatin organization changes (Takahashi K and Yamanaka S 2006; Takahashi K et al., 2007). Since the discovery of the reprograming strategy, iPSCs have been generated from different samples and with different methods: stable DNA integration of the transcription factors using, i.e, Retrovirus transduction, integration-free reprogramming by using Sendai virus, virus-free techniques by using stable expression through bacterial-derived episomal vectors and so on (Shao L and Wu WS 2010).

The possibility to obtain pluripotent stem cells easily from primary cells brought researchers to apply this technologies in many fields, such as gene analysis, development and cells differentiation research, disease modelling and potential therapeutical strategy by using patient-specific iPSCs.

In particular by using patient-specific iPSC as human disease model, a lot of research and progresses have been done and made to elucidate the biology and the molecular mechanism underlaying diseases in order to develop better treatments (Unternaehrer JJ and Daley GQ 2011). The use of iPSC technology allows to have a stable and almost unlimited source of cells for functional experiments. iPSCs can be generated from a lot of different tissues, one of them is blood allowing less invasive withdraw even when the tissue of interest is a not accessible one. In fact, iPSCs can be differentiated in adult tissues through direct differentiation protocols, i.e. neurons or osteoblasts and so on (D'Aiuto L et al., 2014, Phillips MD et al., 2014). iPSCs technology became essential for modelling diseases that affect not proliferative or not easily accessible organs.

2.7 iPSCs application in chromosomal disorders

The iPSCs technology has been applied in a lot of different diseases including genetic disorders such as Cystic Fibrosis or Sickle-cells disease, but poor data are available regarding the usage of iPSCs for imprinting diseases (Ye L et al., 2009; Suzuki S et al., 2016). As mentioned above, the reprogramming step enables the chromatin to be accessible to active transcriptional factors during undifferentiated stages. Gene silencing and activation are necessary to determine the fate and the stage of a cell. In order to change a cell fate, we need to force changing gene expression pattern through the epigenetic modification. Therefore, one of concerns applying iPSC technology to imprinting diseases is the possible alteration at the imprinted status of the original cell type. In order to examine this possibility, the reprogramming of Prader-Willy patient's cells has been performed and it showed that the modelling of imprinting disease with the iPSC technology is possible as the DNA methylation pattern of the patient was maintained (Yang J et al., 2010). However, the question is still opened for specific domains, such as *DLK1-MEG3* locus, that are differently methylated between tissues.

Chromosomal aberrations are frequent and around 1 out of 500 newborn has trisomies, translocations, duplications or deletions with important impact on the patient life (Kim T et al., 2017). The necessity to find new treatments or have a better understanding of the mechanisms involved in chromosomal rearrangements' pathogenesis leads several trials of chromosome aberrations modelling using iPSCs technologies. As one of example, trisomy 21 related with Down syndrome was rescued in disease model iPSCs (Li LB et al., 2012). Recently also the modelling of ring chromosomes with iPSCs has been attempted to study the mechanisms of a cause forming the ring and to find possible therapies. Interestingly, the modelling was not succeeded because the selective pressure during the reprogramming caused the loss of the ring chromosome that was substituted by monosomy rescue (Bershteyn M et al., 2014). The described considerations and previous observations pointed out the unclear possibility to use iPSCs technology to model the Kagami-Ogata syndrome. Because, considering the importance of *DLK1-MEG3* domain during development, this domain may be necessary to determine the stem cell fate. In other words, the reprograming step could lead to switch the imprinting status to

compensate the lack of deleted genes expression, or fail.

2.8 Gene Editing

Our cells are evolutionary adapted to respond damages that can be occurred in our genomes. A lot of factors can induce a break in our DNA and physiologically our cells can activate several pathways in order to repair it. The main repair pathways involved in the double strand break are non-homologous end-joining (NHEJ) and the homologous recombination (HR). NHEJ is active during all phases of the cell cycle and it is usually considered as an error-prone repair. In fact, this pathway often leads to an introduction of insertion and/or deletion (indel) of genomic DNA (Lieber MR et al., 2003). Instead, HR is usually considered as an error-free repair and it is active during the S-phase of the cell cycle in which it uses a sequence (often the sister chromatid, Sonoda E et al., 1999) as the template to copy and repair the double strand break (Saleh-Gohari N and Helleday T 2004). In several decades, researchers have utilized this physiological DNA repair pathway to modify animal and human genomes in different ways, such as knock out and in, called "genome editing". In order to activate NHEJ or HR it is necessary to induce a double strand break in the host genome. This need brought the motivation to develop several molecular-cutting systems to target specific genes. The first protocol was utilizing zing-finger proteins to recognize the target DNA sequence and, in order to induce the cut, the peptides were bonded to FokI, a nuclease requires the formation of heterodimers resulting more specificity. The second system was called TALEN (Transcription Activator-Like Effector Nucleases), TALE protein is derived from the particular bacteria who uses it to help their infection in a plant by manuplating plant's transcriptions, since TALEs is constituted of a series of domain which can recognize specific DNA sequences and worked as transcriptional factors. As the same concept as Zinc Finger Nucleases, TALE is conjugated to FokI nuclease to obtain the sequence specific target. The improvement of this technique compared to ZFN was a lot more possibility to construct your own TALEN peptide by combining individual domains simply in a desired order to personalize it based on the target in individual scientist's hands (Gaj T et al., 2013). The other breakthrough in the gene editing technology was achieved by applying

an adaptive immune system in bacteria which uses an RNA-based recognition system to target exogenous genomes, such as virus genome, and digest it. This adaptive system is called CRISPR (Clustered Regularly Interspaced Short Palindromic Repeats)/Cas9 (CRISPR-associated nuclease) and because it is based on nucleotide-nucleotide recognition it is very easy to personalize and virtually target any region in the genomic DNA with the only restriction of the particular motif adjacent to targeting sequence (called Protospacer adjacent motif (PAM)), which is specific for each bacteria species (Garneau JE et al., 2012; Gaj T et al., 2013).

The combination of the so-called molecular scissors and the physiological repair pathway allows to modify the genome of interest relatively easily. For example, the only induction of the double strand cut can lead to the activation of the NHEJ pathway that induces mutations, and then have non-functional protein, or knock out an entire gene. On the other hands, the combination of the double strand break and an exogenous homologous (or high homology) sequence behaving as template (often called donor DNA or targeting DNA) activates the HR pathway inducing desired insertions/deletions or correction/induction of a specific point mutation (Gaj T et al., 2013).

3. Aims of the research

The Kagami-Ogata syndrome, as well as the patUPD14 syndrome, is one of rare genetic disorders that have not been well characterized yet. Mainly this disease's information derives from case reports with genotype-phenotype correlation analysis or from predictions relied on the mouse model. Furthermore, roles of genes present in the imprinted region have not been described or clear yet. *MEG3* is the most characterized gene for its function from several research groups and publications because of the role in carcinogenesis, although there is no report experimentally proofing the role in Kagami-Ogata syndrome.

This study focuses on the identification of molecular mechanisms involved in the pathogenesis of the Kagami-Ogata syndrome and specifically the contribution of the 14q32 imprinted genes. In order to achieve the final goal of the project, we focused on five aims:

1- obtain a sufficient number of patient-derived cells for the functional analysis. One of the challenges to reveal the molecular mechanism behind this disease is to obtain sufficient cell number to carry out the basic biology investigation. Because, in the most of cases, the primary cell culture from patient cannot be expanded more than several passages, resulting small sample sources. More importantly, in our case, it would be impossible to perform experiments requiring clonal isolation and expansion. Immortalization of patient cell is one of the options to overcome material source issue, however it has a limit to use as the application for the research, for example, because of karyotype instability. To avoid these problems and because we could not sample case 1 again, we reprogrammed primary skin fibroblasts and PBMCs to generate patient-derived iPS cells to have almost unlimited and stable source of sample for the study.

2- verify the suitability of iPSC technology for imprinting disease modelling on chromosome 14. iPSC generation requires whole genome reprogramming in order to change the accessibility of genes that are important during embryonic stage and silence genes related

with differentiation in a mature cell fate. It is essential then to confirm that the region of interest is not altered during reprograming which can cause chromatin structure changes.

3- verify the impact of the deletion on neuronal development and/or function by differentiating the patient-derived iPSCs into adult neurons. Some of the symptoms described in the Kagami-Ogata syndrome, such as autonomous feeding and breathing difficulties, may be explained by a neurological impairment. Because of this reason, we investigate the effect of deletion in neurons and eventual changes in gene expression.

4- demonstrate or disprove the hypothesized main role of *MEG3* in the determination of Kagami-Ogata syndrome phenotype by transcriptome analysis. *MEG3* has a role as tumor-suppressor and influences cell growth and differentiation and *RTL1* is crucial during embryogenesis. To date, these two genes in this imprinting region has been considered as responsible genes. In order to clarify the molecular mechanisms altered in Kagami-Ogata and patUPD14 patients, we decided to evaluate the role of *MEG3* individually as begin.

5- understand a reason of phenotype variability in patients show different phenotypes. As mentioned earlier in *Introduction*, we are able to study a family with two children affected by the Kagami-Ogata syndrome and apparent healthy mother. Interestingly, our three cases carry exactly the same deletion. While the different condition between the mother and affected children can be explained by a possible paternal origin of the chromosomal rearrangement, we cannot extend this hypothesis between the progeny. This family history let hypothesize that the deletion itself is not enough to explain the complexity of the symptoms.

This research provides more molecular information underlying in the Kagami-Ogata syndrome and patUDP14 to have a better understanding of the prognosis for the patient. Ultimately, the identification of the main causative gene of the Kagami-Ogata syndrome and patUPD14 could lead us to develop a novel therapeutic approach to improve the patient life quality

and lifespan. Furthermore, this research will be a proof of concept to apply *in-vitro* disease modeling to other imprinting diseases. The strategy described here can be applied to reveal molecular mechanism underlying other imprinting diseases and to find therapeutic approaches. To have a human model of diseases instead of animal model is very important, because we cannot exclude a variability in between species and the development of therapeutic strategy based on mouse predictions may have no or unexpected effects on the patients. The possibility to model virtually any disease with iPSCs technology is a valuable tool and it can be improved by combining other cutting-edges technologies such as gene editing and direct differentiation.

4. Materials and methods

4.1 Primary cell culture

Patient primary skin fibroblasts have been provided by Dr. Livia Garavelli (Reggio Emilia USL– IRCCS) and PBMCs have been provided by Dr. Antonio Percesepe (AOU-Parma) after the informed consent was signed by the patients' family. The fibroblasts have been cultured in 0.1% gelatin (Sigma Aldrich, Saint Louis, MO) coated flasks and fed every other day with MEF medium consisting of DMEM high glucose (Gibco, Grand Island, NY) supplemented with 15% FBS (Gibco), 1x Glutamax (Gibco), 1x NEAA (UCSF cell culture facility CCF, San Francisco, CA) and 1x penicillin/streptomycin (Gibco).

PBMC culture was optimized and compared between three different culture media: RPMI-1640 (UCSF cell culture facility CCF) supplemented with 1x Glutamax, 1x penicillin/streptomycin and 10% FBS, Yssel's medium (Gemini Bio products, Sacramento, CA), or StemSpan SFEMII supplemented with StemSpan CC100 containing cytokines, Flt3L, SCF, IL-3 and IL-6 (Stemcell Technologies, Vancouver, Canada). For both RPMI and Yssel's medium, 5 more additional conditions were tested: a supplement of 1) 2ng/ml IL2 (Gibco), or 2) 2μg/ml PHA-M (Sigma Aldrich), 3) co-culture with 10^5 MMC (Millipore, Billerica, MA)-treated LCL (ND00659, Coriell Biorepository, Camden, NJ) as feeder, and 4) the combination of co-culture with 10^5 MMC treated LCL and the supplement of 0.1μg/ml PHA or 5) the condition 4) with the supplement of 2ng/ml IL2. LCL were cultured in advanced RPMI (UCSF cell culture facility CCF) supplemented with 15% FBS, 2x Glutamax and 1x penicillin/streptomycin. Inactivation of LCL was optimized within different MMC concentrations, 8μg/ml, 20μg/ml, 50μg/ml an 100μg/ml. Briefly, $2.5x10^5$ cells were seeded in advanced RPMI, treated MMC for 1 hour and washed three times with DPBS (Gibco) before to seed back in culturing medium.

Buccal cells were cultured in MLHC8e (Gibco), HUMEC (Gibco) or KSFM (Gibco) directly on plastic plate or plates coated with following substitutes: Fibronectin/Collagen I (Corning, NY)/BSA (Sigma Aldrich), Laminin (Sigma Aldrich), Matrigel (Corning), 0.1% gelatin or on 3T3-J2

feeder layer (#EF3003 Kerafast, Boston, MA) with or without 10% FBS and 10μM ROCKi (Selleck Chem, Houston, TX). 3T3-J2 cells were cultured in DMEM supplemented with 10% bovine calf serum (VWR, Radnor, PA). Inactivation of 3T3-J2 cells was optimized using different MMC concentration at 1μg/ml, 2.5μg/ml, 5μg/ml, 10μg/ml and 15μg/ml with the incubation at 37°C for 1h.

CFBE41o- was cultured in MEM medium (UCSF cell culture facility CCF) supplemented with 10% FBS, 1x Glutamax, 1x penicillin/streptomycin on Fibronectin/Collagen I/BSA-coated flasks.

We obtained control PBMCs from Dr. Marcus O Muench (Blood Systems Research Institute at University of California, San Francisco UCSF).

Control iPSCs, fibroblasts and immortalized cell lines have been provided by the Dr. Gruenert laboratory at University of California, San Francisco UCSF.

4.2 Electroporation (Nucleofection)

Electroporation was carried out to deliver exogenous gene expression vector to immortalized cell, primary cell culture and iPSCs. The most of cell culture has been tested for its optimized transfection condition. Briefly, iPSCs are electroporated with P3 primary cell transfection reagent and program CA137 using 4D nucleofector X Unit (Lonza, Basel, Switzerland). CFBE41o- cells are electroporated using the 4D Nucleofector X Unit, with SF Cell line solution (Lonza) and Program DS120.

On the other hands, un-optimized primary cell culture, such as patient-derived fibroblasts, was tested in 8 different programs (CA137, CH138, DS150, EH100, EN150, EO144, FF113) with P3 primary cell transfection reagent on 4D nucleofector by transfecting pmaxGFP vector (Lonza) and observed the number of GFP positive cells (Figure 4). After the optimization process, the condition for the patient-derived fibroblasts was defined to use program CA137 or DS150 with P3 solution.

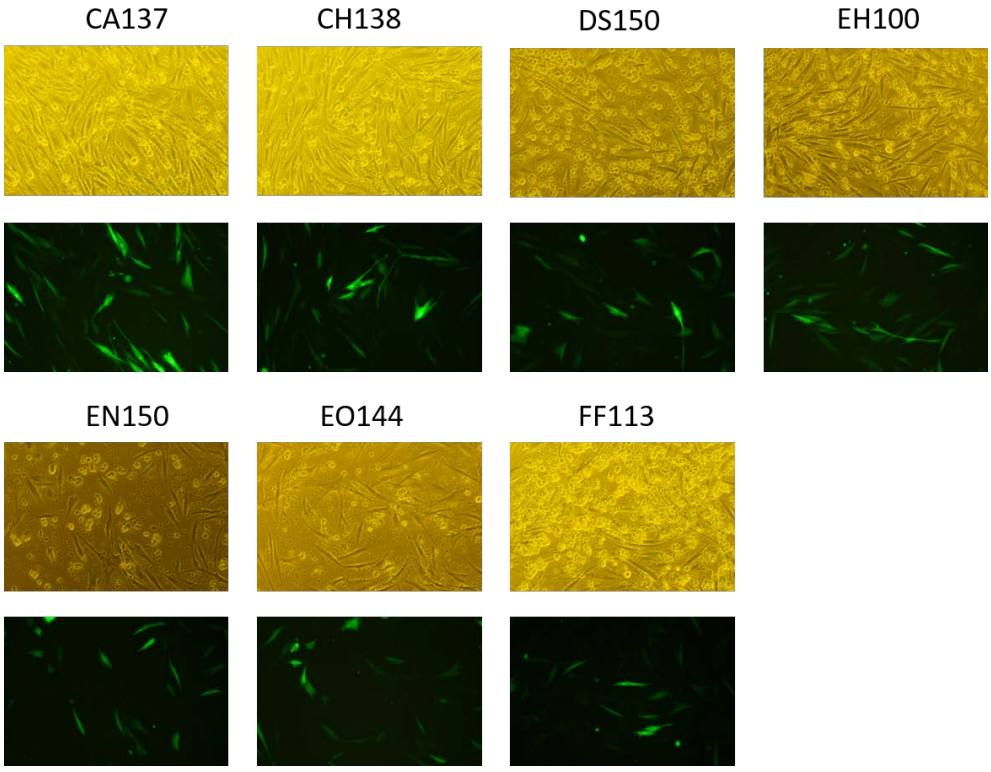

Figure 4. Optimization of electroporation condition for patient's fibroblasts. Microscopy analysis in bright field (top row) and in fluorescence field (bottom row). CA137 gave the best survival and transfection efficiency was slightly lower that DS150. These two conditions were chosen for further experiments.

4.3 iPSCs generation and culture

Fibroblasts are trypsinized with PET, a combination of polyvinylpyrrolidone, EGTA and trypsin (Sigma Aldrich), and resuspended into single cells to proceed following electroporation.

First iPSCs generation trial was conducted by the electroporation of episomal vectors carrying the Yamanaka factors: 1) pCXLE-EGFP+pCXWB-EBNA+pCXLE-hUL+pCXLE-hSK+pCXLE-hOCT3/4 (#27082, #37624, #27080, #27078, #27076 Addgene, Cambridge, MA), with program CA137 and DS150, and 2) pCXLE-hUL+pCXLE-hSK+pCXLE-hOCT3/4-shp53F (#27077 Addgene) with or without

pCXWB-EBNA using program CA137. Briefly, $2x10^6$ cells were electroporated as described above with condition 1) and 2) and then seeded on 0.1% gelatin-coated 60mm dish in MEF medium. The transfected cells were fed every other day for one week. On day 8 post-transfection, transfected cells were transferred on the inactivated MEF feeder layer and cultured in hES medium, consisting with KO-DMEM medium (UCSF CCF) supplemented with 20% KSR (USCF CCF), 1x glutamax, 1x NEAA, 55μM β-mercaptoethanol (Invitrogen, Carlsbad, Ca), 8ng/ml bFGF (MTI-Global Stem, Gaithersburg, MD), and by adding 10μM ROCKi in presence or absence of small molecules, 2μM SB431542 (Cayman, Ann Arbor, MI) and 0.5μM PD0325901 (Selleck chem). The culture was continuously fed with hES medium and kept up to day 30.

Sendai virus transduction technique was also utilized to reprogram fibroblasts. 10^5 cells were seeded in 1 well of 6well/plate one day before transduction (Figure 5). On the day of transduction (Day0), the fibroblasts have been challenged with Sendai virus (Cytotune-iPS reprogramming kit, Thermo Fisher, Waltham, MA), carrying the Yamanaka factors (hOCT3/4+SOX2+KLF4+MYC), at MOI of 5 or 10. Day1, the culture medium containing virus was refreshed with regular fibroblast culture medium and transduced fibroblasts were fed with it every other day. On day 7, transduced cells were transferred on inactivated MEF feeder layer and switched to hES medium with or without small molecules. Transduced cells were fed daily with hES medium from this time point.

Patient PBMCs were cultured in StemSpan SFEMII medium supplemented with StemSpan CC100 for four or eight days before reprogramming. 10^5 cells or $3x10^5$ cells from 4 days culture and $3x10^5$ cells from 8 days culture were seeded in 1 well of 12 well/plate and were challenged Sendai virus (KOS MOI=5, hc-Myc MOI=5, hKlf4 MOI=3, Cytotune-iPS 2.0 kit) with the centrifugation at 1000g for 30min by following the manufacture's protocol. On day3, cells were plated on inactivated MEF feeder layer and medium was switched to hES medium with or without small molecules (Figure 5). $2x10^5$ cells from case 3 culture were also transduced to test xeno-free condition: virus was removed on day 1 and then on day 3 we started the adaptation to ReproTeSR (Stemcell Technologies) on Matrigel-coated plates. ReproTeSR culture stopped at day 20.

When iPSC-like colonies appeared, cells were gradually adapted to mTeSR1 (Stemcell Technologies) and individual clones were manually picked (Figure 5), seeded on Matrigel-coated plates and expanded in mTeSR1. iPSCs were subcultured with ReLeSR (Stemcell Technologies) or StemPro Accutase (Gibco) in presence of 10μM ROCKi.

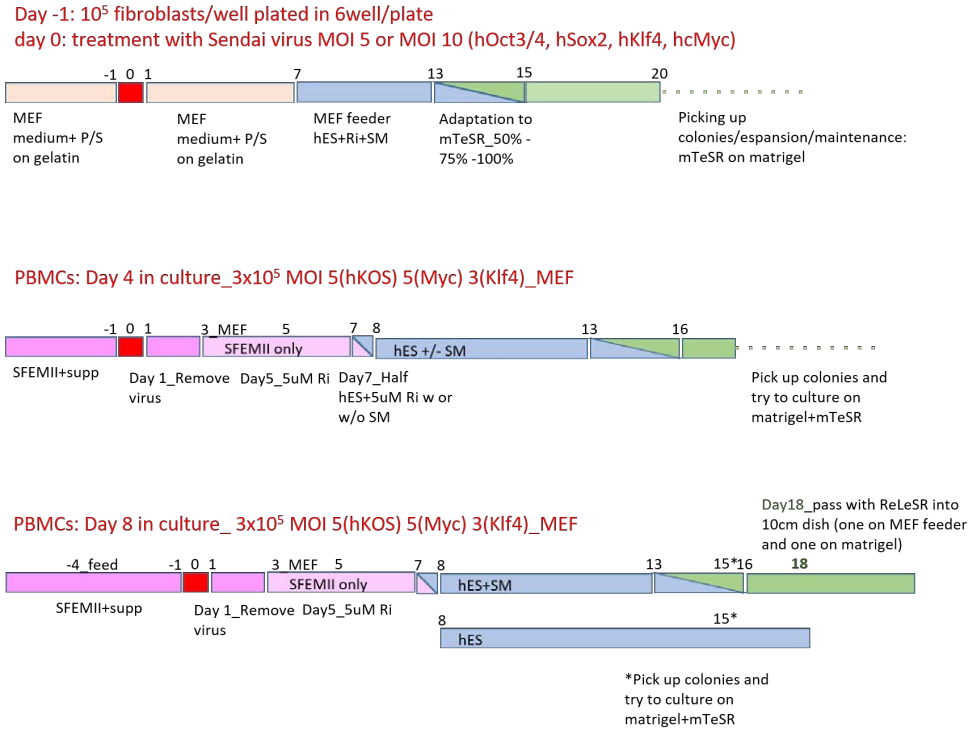

Figure 5. Reprogramming protocols from fibroblasts and PBMCs. The panel shows the timeline used for iPSCs generation from patients' sample. When iPSC-like colonies appeared the culture was gradually adapted to the iPSCs maintenance medium (mTeSR1). After colonies looked mature, individual colonies were manually picked and transferred to feeder-free culture (on Matrigel coated plates).

EBs were generated by harvesting the iPSCs colonies with ReLeSR by maintaining clumps and seeding them in Low Attachment plates (Corning). EBs were formed and cultured in suspension for one week in mTeSR1 supplemented with ROCKi. On day 7, EBs were transferred to 0.1% gelatin-coated 48well/plates and cultured with MEF medium to

establish an attached culture and to induce random differentiation into lineages derived from three germ layers.

4.4 Immunofluorescence Microscopy

iPSCs and EBs were washed with PBS twice and fixed with 4% PFA for 30minutes at room temperature with gentle agitation. Fixed cells were washed with cold PBS twice and permeabilized with 0.25% or 0.1% triton-x (Sigma Aldrich) for 10min at room temperature with gentle agitation. Permeabilized cells were washed three time with PBS and treated blocking solution containing 0.01% tween (Sigma Aldrich) in DPBS and supplemented with 5% goat serum (Sigma Aldrich) and 1% BSA (Sigma Aldrich) for 45min at room temperature with agitation. Then cells were incubated with primary antibodies (Table 2) in antibody solution (1% BSA in DPBST) at 4°C overnight. The following day, the primary antibody was removed by three times PBS wash and the secondary antibody (Table 2) was treated for 1h at room temperature. Cells were also stained by only secondary antibody to test non-specific binding of secondary antibody and as background. After incubation with secondary antibodies, cells were washed three times with PBS and then counterstained and mounted with DAPI Fluoromount-G (Southern Biotech, Birmingham, AL).

Ebs markers	
TUJ1 (TUBB3)	BioLegend (San Diego, CA)
SMA	Thermo scientific
AFP	Sigma Aldrich
ES markers	
Nanog	BD Biosciences (San Jose, CA)
Tra-I-60	Millipore (Burlington, MA)
Tra-I-81	Millipore
SSEA4	Abcam
Secondary Antibodies	
Goat anti-mouse IgG	Invitrogen
Goat anti-mouse IgM	Invitrogen

Table 2. Antibodies list.

4.5 Karyotype

iPSCs were treated with 0.1μg/ml Colcemid (Invitrogen) for 90min. After the treatment, medium was collected. Attached cells were washed with PBS and trypsinized with StemPro Accutase. All cells were collected, combined with the collected medium and centrifuged at 200g for 5min. The pellet was resuspended gently in hypotonic solution: 54mM KCl (Sigma), 20mM HEPES (Sigma) ph7.4 and incubated for 30min at 37°C. After the incubation, the cell suspension was gently inverted and added 1ml of fixative solution containing methanol (Sigma Aldrich) and acetic acid (Sigma Aldrich) in 3:1 ratio. Samples were immediately and gently inverted before centrifugation at 200g for 5min and then fixed thoroughly with fixative solution during gentle vortexing for 3 times. After overnight incubation at 4°C, cells were ready to be spread on glass slide for karyotype analysis. Chromosomes were stained using Quinacrine (Sigma Aldrich) for 30min incubation. Karyotype analysis was made through Genikon software (Nikon, Tokyo, Japan).

4.6 PCR and quantitative PCR

PCR technique was used for identifying patient breakpoints, genotyping of patient cells, sequence preparation and plasmid DNA construction. All primers were synthesized by Sigma Aldrich or Eurofins Genomics (Ebersberg, Germany). Primer pairs and PCR condition used in this study are listed in Table 3.

Quantitative PCR was performed to test gene expression level. Total RNA were collected and isolated with Direct-zol RNA miniprep with Trifast (Zymo Research, Irvine, CA) following the manufacturer protocol. cDNA was obtained using ProtoScript First Strand cDNA Synthesis kit (New England Biolabs) with the protocol specified by the manufacturer. All qPCRs were run on 7900 HT thermalcycler (Applied Biosystems) with power SYBR green PCR master mix (Life Technologies) at 95°C 10min, 95°C 15sec and 60°C 1min repeated 40 cycles. All primers are listed in Table 3. Results were analyzed with SDS2.4 software (Applied Biosystems). All data were analyzed using ΔΔCT method to show as relative data and normalized by housekeeping gene *GAPDH*.

Oligo name	seq	Oligo name	seq
BP14_MEG3_Rv	CCTTGTTTTGGAGCCAGGTA	TK FwII	CCCATGCACGTCTTTATCCT
BP14_MEG3_Fw	AACAAAAGACAGCCCCACAC	TK Rv	CCTCAGAAGCCATAGAGCCC
BP14_MEG8_Fw	CCTCCTTCCTTTGTCCCTTT	MEG3ex7-SNORD fw	TGTCTTAACAAAAACGCTGTTCTGAGGCGTTTGTG
BP14_MEG8_Rv	CATCCCCAGAAACTCACAACA	MEG3ex7-SNORD rv	ACGCCTCAGAACAGCGTTTTTGTTAAGACAGGAAACACATTTATTG
BP14 snord FW	GGTGGTTGGGTTAGGAGGAT	3'HA rv	ATTAATTAAGCGGCCGCCACTAATAACAACATTAAAGAGTCTGATTCAAAG
BP14 snord RV	ACAGAGCACGTGACCATGAA	T7E1_14q32 Fw	GAGAGTGGACCACGCAAGG
pCI-empty-T	AATTCGATGCCGGTACCAAAGTCTAGATAGCGC	T7E1_14q32 Rv	TTGGGCAGTGTTTCAATCAT
pCI-empty-B	GGCCGCGCTATCTAGACTTTGGTACCGGCATCG	P4 Rv	ACTGCCAAGTAGGAAAGTCCCATA
MEG3del-T	GACCCCAGCCCCTCTCCAGCTCGAAATC	CF2AP3 Fw	GCATTGTCTGAGTAGGTGTCATTC
MEG3del-B	GGCCGATTTCGAGCTGGAGAGGGGCTGGG	MEG3gDNA Rv	GATTCTGACACGGGCAAACAG
pCI-MEG3.2 T	AATTCAGCCCCTAGCGCAGACGGCGGAGAGCAGAGAGGGAG	5' MEG3_gDNA Fw2	GGTCAATCACCTACTCAACTAAGG
pCI-MEG3.2 B	CGCGCTCCCCTCTCTGCTCTCCGCCGTCTGCGCTAGGGGCTG	5'MEG3_insertion Fw1	CAGACCCGTGGGCTGGAC
BP14-gRNA1-T	CACCG CAGAACAGCCTTCTGCACAC	3'SNORD_gDNA Rv1	GAATAAAAATACACAACCCCCAAG
BP14-gRNA1-B	AAAC GTGTGCAGAAGGCTGTTCTGC	MEG3 ex2Fw	AAGGACCACCTCCTCTCCAT
BP14-gRNA2-T	CACCG GTGTGCAGAAGGCTGTTCTG	MEG3 ex3Rv	AGGAAACCGTGCTCCTAGTG
BP14-gRNA2-B	AAAC CAGAACAGCCTTCTGCACACC	MEG3 ex6Fw	GGAAGGGACCTCGAATGTG
BP14-gRNAn1-T	CACCGTTCTGCACACTGGTCCGTGT	MEG3 ex7Rv	CACTTCCCACATGCAGACAC
BP14-gRNAn1-B	AAACACACGGACCAGTGTGCAGAA C	MEG8ex2-F	TGTCGGAGGATCGTGTCAT
BP14-gRNAn2-T	CACCGCTGAGGCGTTTGTGAACCAA	MEG8ex3-R	AATCTTCTAGAGCCCCAGATCC
BP14-gRNAn2-B	AAACTTGGTTCACAAACGCCTCAGC	RTL1ex1 Fw	AACCAGACCGAGCACTCAAC
BP14-gRNAn3-T	CACCGAATTTCTCCCCCTGGGGATT	RTL1ex1 Rv	ACAGCGAGATGATGGACCTC
BP14-gRNAn3-B	AAACAATCCCCAGGGGGAGAAATTC	TUJ1-ex2F	GCAACTACGTGGGCGACT
BP14-gRNAn4-T	CACCGGTGTGCAGAAGGCTGTTCTG	TUJ1-ex3R	TCGAGGCACGTACTTGTGAG
BP14-gRNAn4-B	AAACCAGAACAGCCTTCTGCACACC	PAX6ex12-F	TCACCATGGCAAATAACCTG
5'HA fw	GCGAATTGGGGCGCGCCACAGAGAGAGGGCCCATTAGTTG	PAX6ex13-R	CAGCATGCAGGAGTATGAGG
Puro-14q32 fw	GGTGGTCTTTGGGGTTTAACCCTAGAAAGATAGTCTGCGT	MAP2ex3-F	CGAACTTTATATTTTACCACTTCCTTG
MEG3-Puro rv	TCTTTCTAGGGTTAAACCCCAAAGACCACCACTGAG	MAP2ex4-R	CCGTTCATCTGCCATTCTTC
NdeI rv	GGCGTACTTGGCATATGATACACTTGATGTACTGCCAAGTGG	p53-ex9 F	CCAGCCAAAGAAGAAACCAC
BbsI fw	TGGGAAGACAATAGCAGGCATGCTGGGGATGC	p53-ex11 R	CCCTTTTTGGACTTCAGGTG
Puro-MEG3ex7 fw	TCTTTCTAGGGTTAACTGACGAATGGAACATTTTGGATCAG	GAPDH F	ATGGAAATCCCATCACCATCTT
Puro-14q32 rv	TTAACCCTAGAAAGATAATCATATTGTGACGTACG	GAPDH R	CGCCCCACTTGATTTTGG
Puro Fw	GCTTGTCAATGCGGTAAGTG		

combination	pcr protocol	size	taq
BP14_MEG3 F-SNORD R	98°C 1min; 98°C 10sec, 62.5°C 10sec, 68°C 10sec, 30 cycles; 68°C 5min	731 bp	PrimerStar GXL (Clontech)
BP14_MEG3 F+R	98°C 1min; 98°C 10sec, 62.5°C 10sec, 68°C 10sec, 30 cycles; 68°C 5min	678 bp	PrimerStar GXL
BP14_MEG8 F+R	98°C 1min; 98°C 10sec, 60°C 10sec, 68°C 15sec, 35 cycles; 68°C 5min	340 bp	PrimerStar GXL
BP14_SNORD F+R	98°C 1min; 98°C 10sec, 62°C 10sec, 68°C 15sec, 30 cycles; 68°C 5min	897 bp	PrimerStar GXL
MEG3 ex2-3	95°C 10min, 95°C 15sec, 60°C 1min, 40 cycles	87 bp	Power Sybr green master mix (Thermo Fisher)
MEG3 ex6-7	95°C 10min, 95°C 15sec, 60°C 1min, 40 cycles	265 bp	Power Sybr green master mix
MEG8 qpcr	95°C 10min, 95°C 15sec, 60°C 1min, 40 cycles	104 bp	Power Sybr green master mix
RTL1 qpcr	95°C 10min, 95°C 15sec, 60°C 1min, 40 cycles	60 bp	Power Sybr green master mix
TUJ qpcr	95°C 10min, 95°C 15sec, 60°C 1min, 40 cycles	86 bp	Power Sybr green master mix
PAX6 qpcr	95°C 10min, 95°C 15sec, 60°C 1min, 40 cycles	52 bp	Power Sybr green master mix
MAP2 qpcr	95°C 10min, 95°C 15sec, 60°C 1min, 40 cycles	75 bp	Power Sybr green master mix
TP53	95°C 10min, 95°C 15sec, 60°C 1min, 40 cycles	173 bp	Power Sybr green master mix
GAPDH qpcr	95°C 10min, 95°C 15sec, 60°C 1min, 40 cycles	57 bp	Power Sybr green master mix
MEG3 insertion Fw+SNORDgDNA Rv	94°C 30sec; 94°C 15sec, 62°C 15sec, 68°C 7min, 35cycles	1,5 kb	Platinum DNA Polymerase (Thermo Fisher)
5' MEG3gDNA Fw+ P4	98°C 10sec; 98°C 10sec, 62.1°C 10sec, 68°C 8min, 35 cucles; 68°C 5min	7,2 kb	PrimerStar GXL
CF2AP3 Fw+ MEG3gDNA rv	95°C 1min; 95° 15sec, 62° 15sec, 72°C 30sec, 35 cycles; 72°C 2min	400 bp	MyTaq (Bioline, London, UK)
T7E1_14q32 Fw+ MEG3gDNA RV	98°C 10sec; 98°C 10sec, 62.1°C 10sec, 68°C 8min, 35 cucles; 68°C 5min	5,8 kb	PrimerStar GXL
T7E1_14q32 Fw+ Rv	95°C 1min; 95°C 15sec, 63°C 10sec,72°C 10sec, 35 cycles	647 bp	MyTaq
puro	95°C 4min; 95°C 30sec, 58.2°C, 72°C 45sec, 35 cycles; 72°C 5min	600 bp	DreamTaq DNA Polymerase (Thermo Fisher)
tk	95°C 4min; 95°C 30sec, 58.2°C, 72°C 45sec, 35 cycles; 72°C 5min	400 bp	DreamTaq DNA Polymerase
MEG3intron-BP14SNORD	94°C 30sec; 94°C 15sec, 60°C 15sec, 68°C 7min, 35 cycles	7,1 kb	MyTaq
RTL1 ex1.6 F+ ex1 R	98°C 10sec, 60°C 15sec, 68°C 60sec, 35 cycles	4,3 kb	PrimerStar GXL
5'HA Fw+MEG3 puroRv	98°C 10se, 62°C 15sec, 68°C 7min, 30 cycles	6,6 kb	PrimerStar GXL
Puro_MEG3ex7 Fw+MEG3_SNORD Rv	98°C 10se, 62°C 15sec, 68°C 7min, 30 cycles	6,2 kb	PrimerStar GXL
BbsI Fw+puro_14q32Rv	98°C 10se, 62°C 15sec, 68°C 1min, 30 cycles	361 bp	PrimerStar GXL
Puro14q32 Fw+NdeI Rv	98°C 10se, 62°C 15sec, 68°C 1min, 30 cycles	692 bp	PrimerStar GXL
MEG3_SNORD Fw+ 3'HA Rv	98°C 10se, 62°C 15sec, 68°C 1min, 30 cycles	1 kb	PrimerStar GXL

Table 3. Primers and protocols for qPCR and PCR.

4.7 Sequencing analysis

Sanger sequencing was performed by both Quintara Biosciences, USA and in house. PCR product containing the region of the interest was purified with QIAquick PCR purification kit following the manufacturer protocol and used for sequence analysis. In house, sequencing reaction was prepared using BigDye Terminator v1.1 (Invitrogen) by following the reaction cycle of 96°C 20sec, 50°C 5sec and 60°C 4min for 25 cycles as suggested by the manufacturer protocol, purified with DyeEZ 2.0 spin kit (Qiagen) and run on 310 Genetic Analyzer (Applied Biosystems).

4.8 Neuronal differentiation

iPSCs were harvested with StemPro Accutase and seeded at density of $2x10^5$ cells/cm^2 on Matrigel coated 6well/plates with Neuronal Induction Medium (Stemcell Technologies) supplemented with 10μM ROCKi during optimization, the cell density was decreased to $1.8x10^5$ cells/cm^2 for further experiments. Cells were subcultured with StemPro Accutase and maintained in STEMdiff Neural Induction Medium (Stemcell Technologies) at $1.5x10^5$ cells/cm^2 (decreased to 10^5 cells/cm^2) for 20 days (Figure 6). On day20, NPCs were harvested with StemPro Accutase and seeded on PLO (Sigma Aldrich) and Laminin coated plates at $4x10^4$ or $6x10^4$ cells/cm^2 (increased to $8x10^4$ cells/cm^2). Cells were then cultured in BrainPhys (Stemcell Technologies) supplemented with 1x NeuroCult SM1 Neuronal supplement (Stemcell Technologies), 1x N2 supplement-A (Stemcell Technologies), 20ng/ml BDNF (Sigma Aldrich), 20ng/ml GDNF (Sigma Aldrich), 1mM dibutyryl cAMP (Sigma Aldrich) and 200nM Ascorbic acid (Sigma Aldrich) or 1x NeuroCult SM1 Neuronal supplement alone (Figure 6).

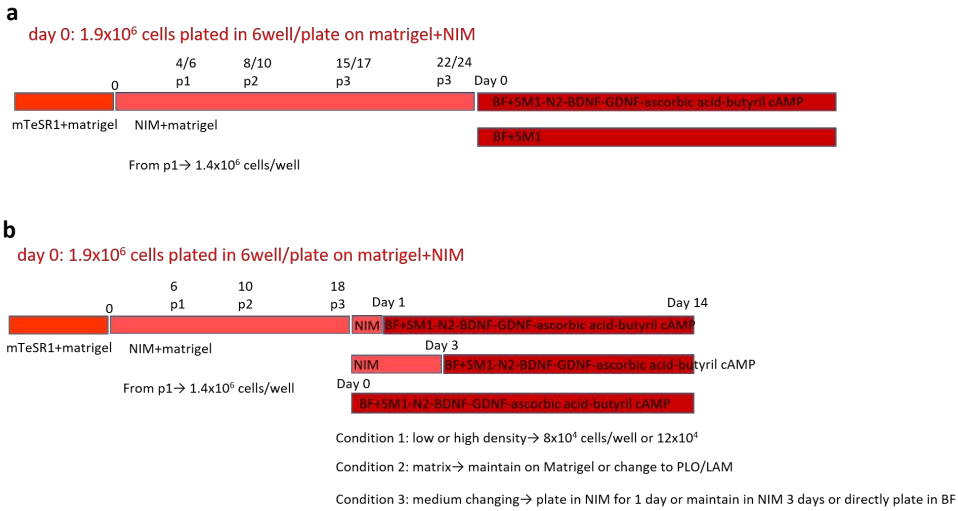

Figure 6. Neuronal differentiation protocols. a) First trial using the manufacturer protocol and optimizing the supplements suggested for the Brainphys medium. b) the optimization for plating and adaptation to Brainphys conditions. Two different cell densities (the density used in the first trial and 1.5 times more of original density) in two different coating conditions (Matrigel coated plate or the suggested coating combination PLO/LAM) and adapted to the brainphys in three different time points (seeding cells directly in Brainphys, plating in NIM and half medium changed to Brainphys on day1, and culturing in NIM for three days before switching).

4.9 Plasmid generation: MEG3 overexpression

All restriction enzymes used in this study are commercially available from New England Biolabs (Ipswich, MA). Oligos used in this section were synthesized by Sigma Aldrich (Table 3). Plasmid DNA constructs for *MEG3* expression were modified from pCI-MEG3 (#44727 Addgene, Figure 7), controls its expression under CMV promoter: 1) pCI-MEG3.2 represents the complete *MEG3* transcript from the latest assembly (NR_002766.2, GRCh38.p7). The regain lacked in the past assembly was completed by inserting synthesized oligonucleotides. Briefly, two single strand oligos (pCI-MEG3.2 T and pCI-MEG3.2 B, Table 3) were denatured at 95°C for 10min and slowly annealed and then annealed oligonucleotides were ligated in the EcoRI-BssHII site of pCI-MEG3. 2) pCI-MEG3.2-del mimics the deleted *MEG3* mutant found in our subject. Oligonucleotides

MEG3del T and B in Table 3 create the deleted *MEG3* fragment were prepared by annealing as described above and ligated inside of the KflI-NotI site of pCI-MEG3.2. 3) pCI-backbone is the empty plasmid vector to use as a mock control. Annealed oligonucleotides pCI-empty T and B in Table 3 were ligated in EcoRI-NotI site of pCI-MEG3 (Figure 7). *MEG3* expression vectors were also generated in pCAG backbone that controls gene expression under CAG promoter. pCAG plasmid vector expressing *MEG3* was generated from pCAG-GFP (#11150 Addgene) by substituting GFP with MEG3.2 from pCI-MEG3.2 at the EcoRI-NotI. pCAG-MEG3.2-del and pCAG-backbone were modified from pCAG-MEG3.2 and pCAG-GFP, respectively, as same strategy as above (Figure 7).

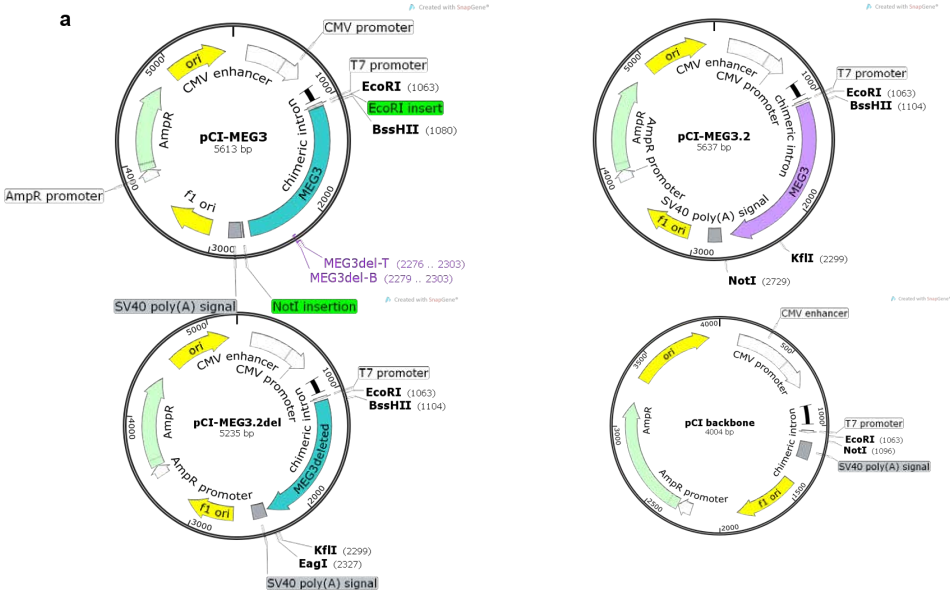

(Cont.)

(Cont.)

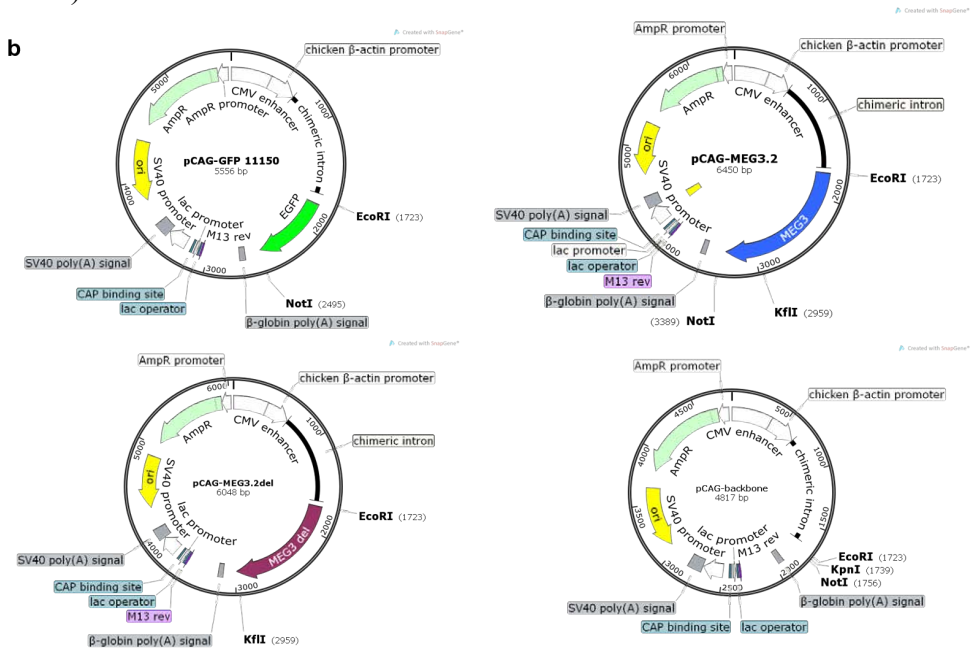

Figure 7. MEG3 plasmid DNA construction. A) The top panel shows the original pCI-MEG3 plasmid DNA (#44727 Addgene) and the derivative pCI-MEG3.2 expressing complete *MEG3* transcript from the latest assembly (NR_002766.2, GRCh38.p7). The bottom panel shows the deleted form of *MEG3* DNA and the mock vector. B) The panel shows the pCAG construction as organized with same expression in panel A.

4.10 MEG3 overexpression

$2x10^5$ cells of iPSC were transfected with serial amount of pCI-MEG3.2, pCI-MEG3.2del or GFP (0.4μg, 0.6μg, 1μg, 2μg, 4μg of plasmid DNA), RNA samples were collected after 48-72h post-transfection. $2x10^5$ CFBE41o- cells were nucleofected with 1.0 μg of pCI-MEG3.2 and total RNAs were harvested.

4.11 Plasmid generation: gene editing

CRISPR/Cas9 gRNAs were prepared by golden gate reaction, ligating annealed oligonucleotide (BP14-gRNAs T and B, Table 3) in pX330 with wt Cas9 or in pX462 with nickase activity (#42230 and #62987 Addgene). The insertion and anneal steps were performed by optimizing the protocol from Ran FA et al., 2013 (Figure 8).

Donor DNA was constructed to insert last intron and exon deleted in our subject with PCR cloning and Gibson assembly technique. Briefly, the *MEG3* allele starting from the patient breakpoint position to the poly-A signal of the longest reported transcript was cloned from a WT cell line using primer pairs 1) 5'HA Fw and MEG3 puro Rv, 2) Puro_MEG3ex7 Fw and MEG3_SNORD Rv, 3) MEG3_SNORD Fw and 3'HA Rv to recover MEG3 expression (Figure 9b). 1) 5'HA Fw and MEG3 puro Rv primers pair amplifies a part of the last intron of *MEG3* including 1kb homologous sequence with the upstream region of the patient's BPs junction. 2) Puro_MEG3ex7 Fw and 3'HA Rv primers pair amplifies 1kb homologous sequence with the downstream region of the patient's BPs junction. The PCRs products have been connected each other using recombinant PCR technique. In order to provide drug resistance to iPS cells for modified clones screening, the PiggyBac cassette containing Puromycin resistance gene as positive selection and thymidine kinase gene as negative selection, obtained from pCAGpuroTK plasmid DNA modified from pCAGpuroTK.neo (Ye L et al., 2014), kindly gifted by Dr. Yuet W Kan (Uiversity of California, San Francisco, USA), was combined with the modified *MEG3* genomic sequence prepared by recombinant PCR and inserted into the pUC19 backbone vector digested with BbSI and NdeI using Gibson assembly technique (In-Fusion HD cloning kit, Clontech, Mountain View, Ca) (Figure 9b).

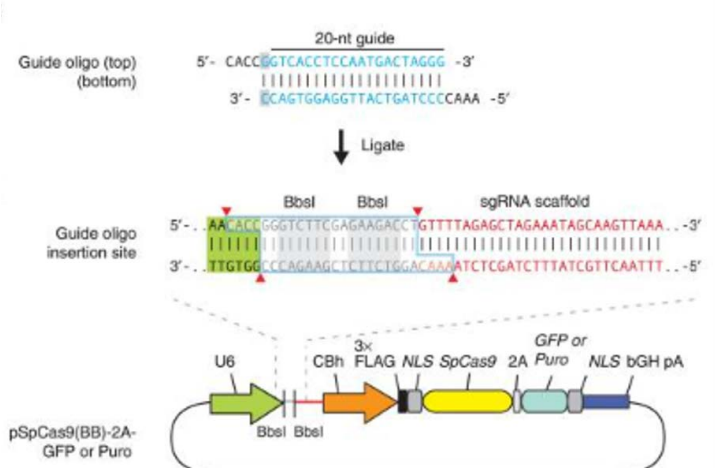

Figure 8. Target specific CRISPR/Cas9 construction. The panel shows the technique to construct CRISPR/Cas9 system targeting the gene of interest. The original plasmid DNA contains the cDNA encoding the Cas9 protein and the CRISPR RNA to build the cutting system. Furthermore, downstream of the U6 promoter two BbsI cutting sites are used to insert the target sequence with Golden Gate technique (Ran FA et al., 2013).

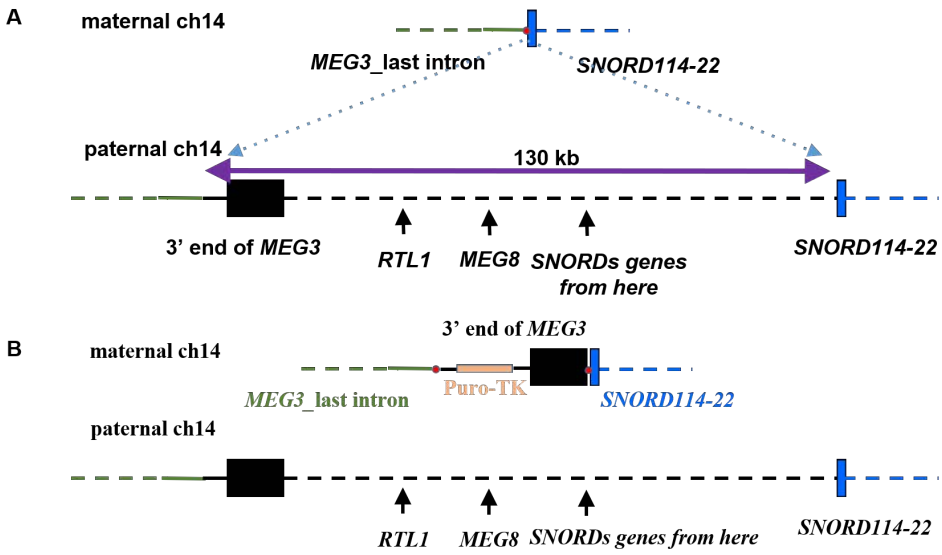

(Cont.)

(Cont.)

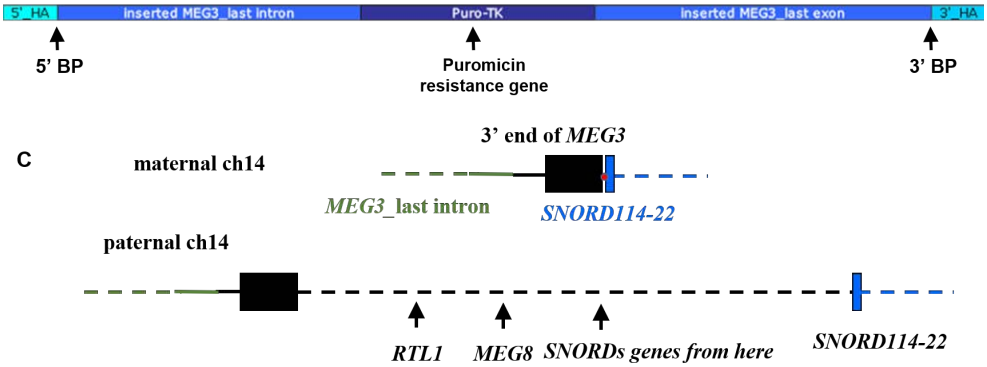

Figure 9. Gene editing experiment design. A) The scheme represents our patient genotype with the deletion on maternal chr14. Red dot represents the breakpoints junction. B) The scheme represents the maternal and paternal chr14 after the gene editing. Only maternal chr14 is modified by CRISPR/Cas9 and the donor DNA transfection. The donor DNA (showed below paternal chr14), in order to induce homologous recombination as mechanism of double strand repair, has 1kb homology arm at both 5' and 3' end of the construct. The puromycin resistance gene was inserted inside of *MEG3* last intron, upstream of its last exon. The *MEG3* cloned sequence starts from the identified 5' breakpoint and it ends at the poly-A signal of the longest transcript (UCSC). C) The scheme represents the maternal and paternal chr14 after excision of PB cassette though PB overexpression and GCV negative selection. Only the maternal chr14 is modified.

4.12 T7E1 assay

Individual CRISPR/Cas9 gRNAs were compared the efficiency of gene targeting by observing NHEJ induction through T7E1 assay. $4x10^5$ patient-derived iPSCs were transfected with 600ng of each gRNA and DNA was harvested after 3 days. Genomic DNA isolated with GeneJET genomic DNA purification kit (Thermo Fisher) was amplified through PCR (Table 3) and then the PCR product was purified with QIAquick PCR purification kit (Qiagen, Hilden, Germany). The purified PCR product was denatured at 95°C for 10min and reannealed by ramping temperature down from 95°C to 20°C with 0.1°C/sec in order to allow partially mismatched fragments to anneal. The annealed fragment was incubated with T7E1 endonuclease (New England Biolabs) that recognize and digest mismatches at 37°C for 1 hour. The final interpretation has been done on 2% agarose gel using the following formula:

$$\text{fcut} = \frac{\text{CleavageBand1} + \text{CleavageBand2}}{\text{CleavageBand1} + \text{CleavageBand2} + \text{UncleavedBand}}$$

$$\%\text{NHEJ}=100\text{x}(1\text{-}1\text{-}f_{cut})$$

4.13 MEG3 modification

1.5μg or 3μg of px330 CRISPR/Cas9 gRNA and 3μg donor DNA were transfected in $2\text{x}10^6$ cells using nucleofection technique with solution P3 and program CA137. On day2, puromycin (Sigma Aldrich) treatment was started at the concentration of 0.5μg/ml to select modified clones (Figure 9b). After approximately 10 days selection, individual clones were picked and expanded for further analysis. HDR inserted clones were identified by PCR using primer pairs 5'MEG3gDNAFw-P4 and MEG3intronFw-BP14SNORDRv (Table 3) and Sanger sequencing. PBase was overexpressed in modified clones to excise PB cassette. The modified PBase (R372A/K375A/D450N) (Li X et al., 2013) expression vector was kindly provided by Drs. YW Kan and Lin Ye in UCSF. Briefly, characterized modified clones were transfected with 2.25μg of PBase in $7.5\text{x}10^5$ cells using program B-016 and solution 1 (Lonza) on NucleofectorII (Lonza). 7 days after transfection, 2μM GCV (Cayman) was added in culture for 48 hours to perform negative selection. Individual clones were picked and expanded for the excision assessment. Excised clones were confirmed the insertion of deleted *MEG3* (Figure 9c) by PCR using primers pairs 1) T7E1_14q32 Fw and P4 Rv, 2) CF2AP3 Fw and BP14 SNORD Rv, 3) Puro Fw and P4 Rv, 4) TK Fw and Rv in Table 3. PCR products were tested by Sanger sequencing.

5. Kagami-Ogata syndrome model

5.1 Results

5.1.1 Patients' characterization

The patient who showed developmental delay, growth retardation and several dysmorphisms (case 1) was taken as the first subject and we sought out a genotype and phenotype correlation in this patient. First, we performed the CGH-Array to test and find any genetic rearrangement. We detected approximately 72kb duplication on chr2 (dup(2)(q14.3)_chr2:123,500,001-123,572,000, hg19) and 130kb deletion in 14q32 region (del(14)(q32.2q32.31)_chr14:101,320,247-101,450,247, hg19) (data not shown). Extending this analysis to the parents, we found the duplication on chr2 was inherited from the unaffected father, while the deletion on chr14 was inherited from the unaffected mother. The duplication from father on chr2 does not involve any reported genes (UCSC, https://genome.ucsc.edu), while the deletion from mother on chr14 involves several genes expressed based on the imprinting model (Figure 10). We were not able to extend the analysis to the grandparents so it was not possible for us to have the information whether the parents' rearrangements are *de novo* or inherited, and most importantly we were not able to determine which chromosome 14, maternal or paternal, is deleted in the mother (case 3). Based on the information we have from literatures, we hypothesize that the deletion in case 3 is on the paternal chromosomal because of the lack of clinical features. After the deletion in case 1 and case 3 was revealed, the prenatal diagnosis of case 2 was performed and we found out that she was carrying the same deletion on 14q32.2 although she showed a milder phenotype than case 1 did. In order to improve our knowledge about this particular deletion in this family, we performed MLPA analysis to check the methylation pattern and Sanger sequencing to identify the breakpoints (Figure 11). Since the deletion does not involve the DMRs, we expected that nothing affects on methylation pattern at the region of interest, in fact we did not observe any anomaly through MLPA analysis (data not shown), By performing the Sanger sequencing, we found that the proximal BP was located in chr14:101,315,665 and the distal BP was located in chr14:101,449,155 (UCSC, hg19). Interestingly the BPs

junction shows 3bp microhomology, suggesting that this deletion might occur through one of DNA repair mechanism; microhomology mediated end-joining (Figure 11). Same BPs were confirmed in case 2 and 3.

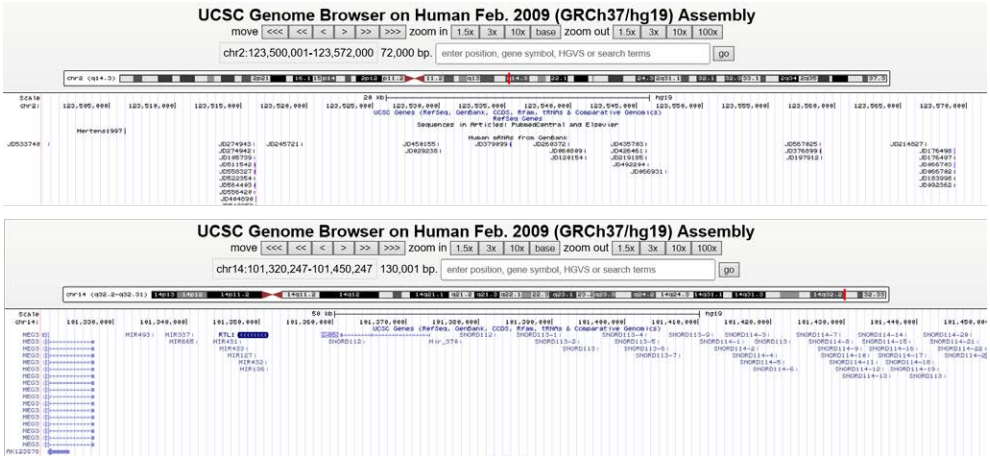

Figure 10. Patients' chromosomal aberrations. The top panel shows the region duplicated on chr2: there is no reported genes in this area in UCSC. The bottom panel shows the deletion on ch14: the deletion spans from the last intron of the imprinted gene *MEG3* to the cluster of SNORDs.

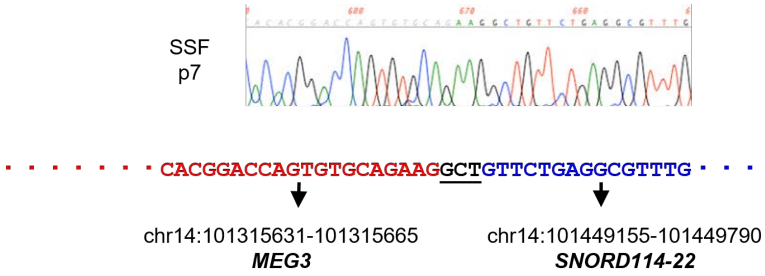

Figure 11. Breakpoints cloned in case 1 fibroblasts. By the optimized long PCR and Sanger sequencing we identified the exact location of the breakpoints of the deletion on chr14. The BPs junction is a three-base homology region between *MEG3* and SNORDs cluster suggesting a possible mechanism for the double strand break repair: microhomology end joining.

In order to confirm the expression pattern of deleted genes, we also performed qPCR analysis on patient fibroblasts with two different primary cell cultures as control (FHTF, fetal human trachea fibroblasts, and HTF, adult human trachea fibroblasts) after genotype confirmation in the region of interest (Figure 26). qPCR data showed no or barely expression of *MEG8* and last exon of *MEG3* (Figure 12b-c), confirming the prediction based on previous report and mouse model studies (in *State of the art*, MO CF et al., 2015). We also observed expression of *MEG3* itself (Figure 12a), suggesting normal activity of the DMRs as predicted by MLPA analysis. Furthermore, qPCR data suggests that the paternal chromosome is not activated to compensate for the lack of *MEG3* and *MEG8* expression from the maternal one. Interestingly, we observed almost no expression of *RTL1* (Figure 12d) despite the fact that, as discussed above (in *State of the art*), the mouse model predicts no expression of *RTL1* antisense (encoded on the maternal chromosome) and consequent overexpression of *RTL1* (encoded on the paternal chromosome) (Seitz H et al., 2003; Davis E et al., 2005; Lin SP et al., 2007; Ito M et al., 2015). In order to exclude the presence of mutation or micro-deletion/duplication affecting *RTL1* transcript stability, we sequenced the entire coding sequence of *RTL1* from case 1 and no mutation was found (data not shown).

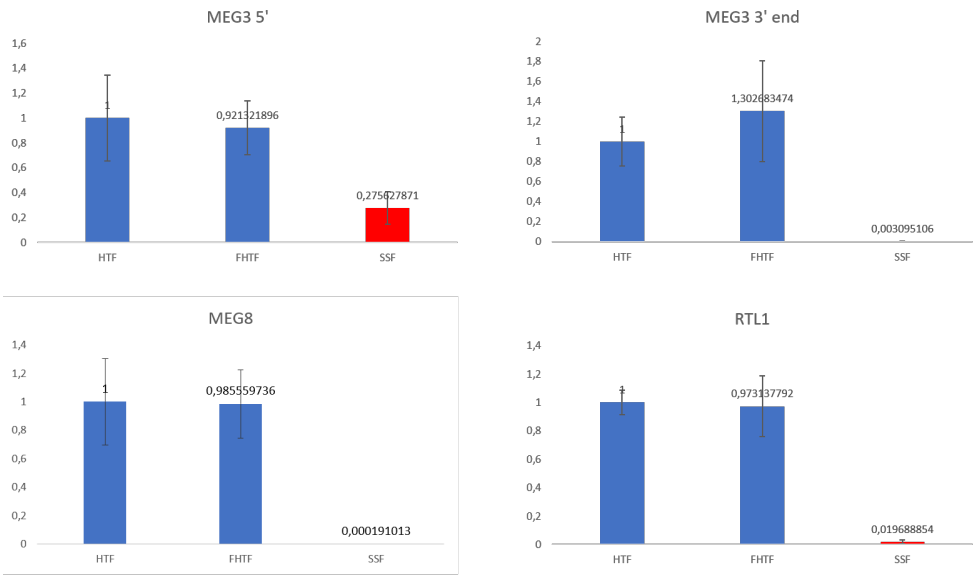

Figure 12. Expression analysis by quantitative PCR. The graphs show the relative

expression of *MEG3*, *MEG8* and *RTL1* in case 1 fibroblasts compared with two control fibroblasts. The relative value is calculated to HTF. *MEG3* was detected using two primers pairs: the top left graph shows the amplification using a primer pairs spanning exons 2 and 3. The top right graph shows the amplification of a primer pairs spanning exons 6 and 7 (exon 7 is deleted in the patient). From case 1 fibroblasts we expect no detection of *MEG8* and *MEG3* 3'. Bottom right graph shows that *RTL1* is barely expressed.

5.1.2 Buccal cells culture optimization

In order to study the effect of the deletion on patient's cells and to have enough cell sources to perform our experiments, we decided to prepare iPSCs from patient primary cells. First, we tried to use cells obtained with non-invasive techniques, such as buccal cells, to optimize its culture in our hands and to reprogram. Taking previous publications aimed to establish a buccal cells culture in order to perform molecular biology analysis (Michalczyk A et al., 2004), we harvested cells from mouthwash and seeded on matrix with keratinocyte culture condition. Because of variability in culture condition and efficiency due to the use of FBS in culture deriving from different providers, but also different lot numbers, we decided to use serum free-medium to optimize the protocol. Culture condition optimization (Figure 13) was performed on healthy donor buccal cells by testing combinations of different culture medium and extracellular matrixes (MLHC8e, HUMEC or KSFM; on plastic plate or Fibronectin/Collagen I/BSA-, Laminin-, Matrigel-, 0.1% gelatin-coated plates). The best condition seemed to be culturing with KSF medium on fibronectin coated plates (Figure 13). However, still the efficiency of live buccal cells' attachment (Figure 13) was very low and they could only survive for long term, but not proliferate. Another published technique to culture keratinocyte consists in co-culture with 3T3 cells as feeder cell layer (Sharma SM et al., 2012). 3T3 cells are derived from mouse embryonic fibroblasts and they are usually cultured in presence of calf serum. To use them as feeder cells, the inactivation through irradiation or MMC treatment need to be done so that they are not able to proliferate, but still maintain a culture condition favorable to keratinocyte culture. When we used MMC-inactivated 3T3-J2 cells as feeder layer (Figures 14 and 15), we observed that feeder was not capable to survive in serum-free condition, even with 10μM Rocki in the medium (Figure 15). No buccal cells growth in any

condition was observed for two months culture. Because we could not establish an efficient culture protocol for buccal cells in our hands, we did not test any of these conditions on patients' sample.

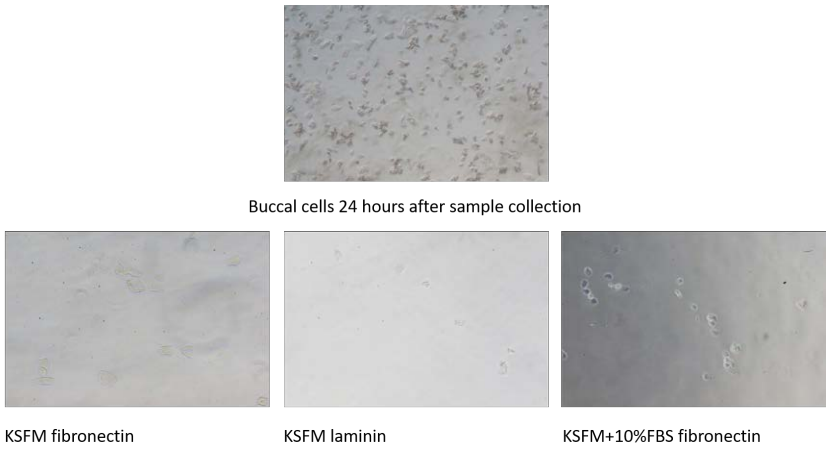

Figure 13. Buccal cells culture optimization. The top picture shows the representative field of cell culture harvested from healthy donor before refreshing the medium and removing unattached and survived cells. Pictures in the bottom panel show cell culture in different culture conditions (fibronectin or laminin coated plate in KSFM medium with or without 10% FBS supplement) after one month. Only on fibronectin and laminin we observed cell attachment and survival but no growth.

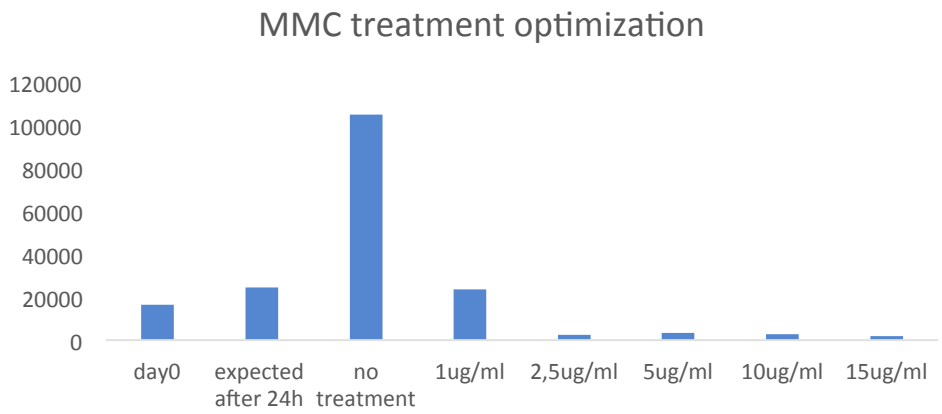

Figure 14. MMC treatment optimization for 3T3-J2. 3T3-J2 were treated with serial dilution of MMC (1, 2.5, 5, 10 and 15 μg/ml) and counted after one week. 1μg/ml of MMC allowed cells inactivate the proliferation and have them in stable conditions for one week.

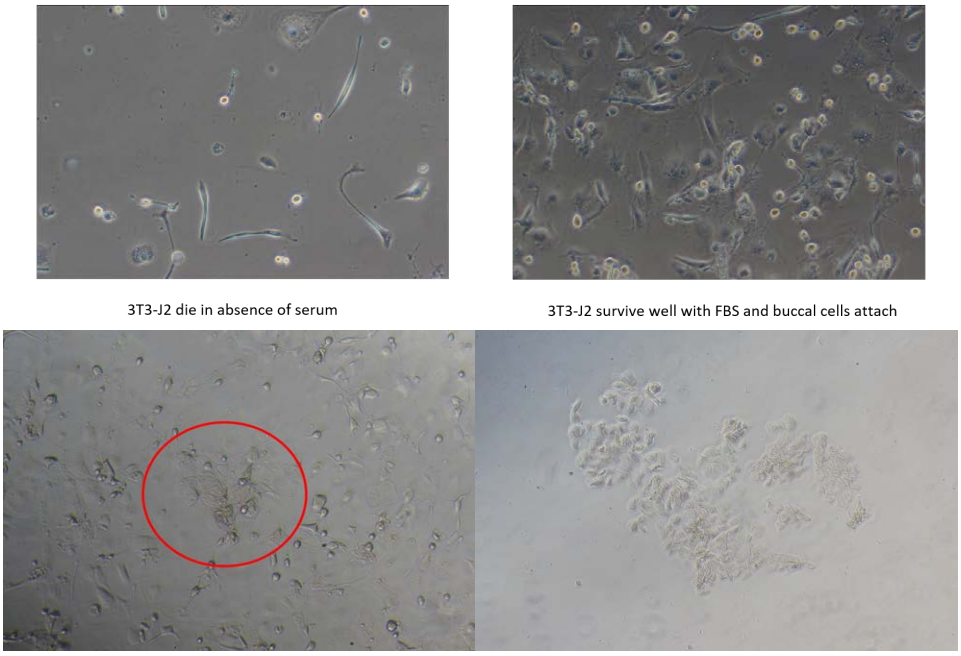

Figure 15. Buccal cells on 3T3-feeder layer. Buccal cells were cultured in four different conditions: 1) KSFM only, 2) KSFM supplemented with 10μM Rocki, 3) KSFM supplemented with 10% FBS, 4) KSFM supplemented with both 10μM Rocki and 10% FBS. Top two pictures show the condition of the feeder layer with or without serum supplement. Buccal cells were observed only in presence of healthy feeder cells (bottom left picture, the red circle shows the colony similar to that observed culturing on fibronectin-bottom right), no difference between with or without Rocki supplement, but no growth was observed.

5.1.3 PBMCs culture optimization

PBMC was another candidate cell type that we had the access to the patients and one of the most common cell types that we can easily obtain with less invasiveness. Before starting a culture and reprogramming, we also performed the culture optimization for PBMCs by taking healthy donor PBMCs (optimization was based on previous publication from Spits H and Yssel H 1996). First the inactivation protocol for LCL using MMC treatment was tested and we chose 8μg/ml as the concentration for the

feeder preparation (Figure 16). In RPMI-1640 with and without supplements, PBMC cultures did not show reasonable survival rate, around 80-90% of cells in culture died within four days (Figure 17). Between day 4 and day 6, the cell number kept decreasing in RPMI-1640 and in RPMI-1640 supplemented with IL2 or PHA. LCL+PHA with or without IL2 maintained survived cells better when compared to RPMI-1640 culture (Figure 17). Same conditions were tested in Yssel's medium but all cells died after 24 hours. When cultured in StemSpan SFEMII, cells still showed high mortality in first 4 days, but around 40% of them were still alive (Figure 18). At day 8 in StemSpan SFEMII, 60% of cells that were maintained in culture from day 4 were alive and subcultured. Overall, StemSpan SFEMII medium with StemSpan CC100 supplement was chosen for patient's cell culture followed by its reprogramming.

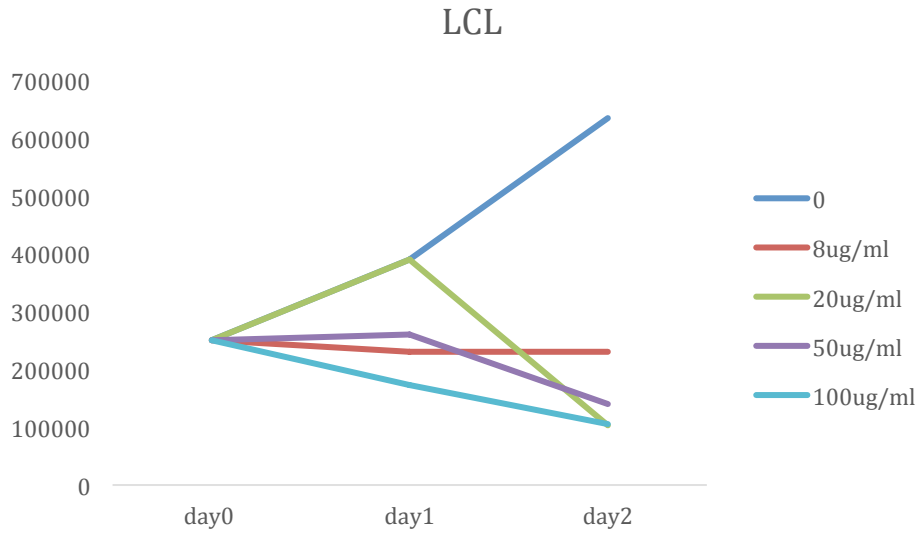

Figure 16. MMC treatment optimization for LCL. Cell number on day1 and day2 after MMC treatment. LCL were treated with serial dilution of MMC (0, 8, 20, 50 and 100μg/ml). 8μg/ml was used for further experiments.

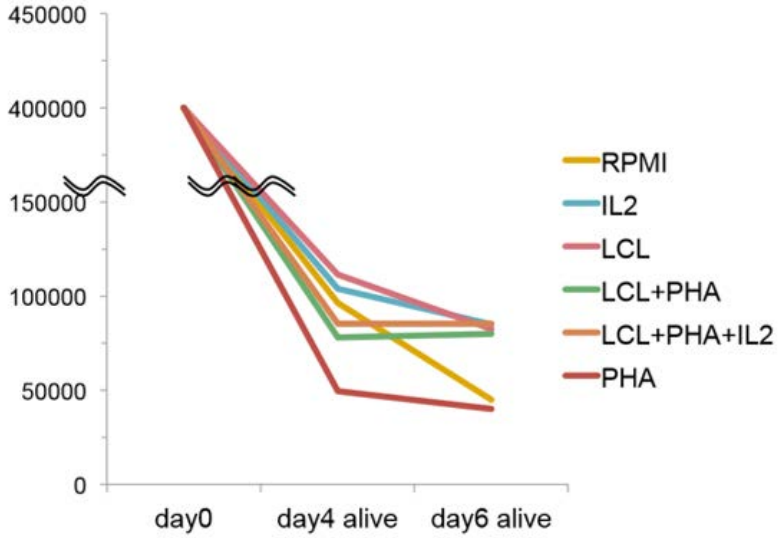

Figure 17. PBMC culture optimization in RPMI medium. Survived cell numbers on day4 and day6 in culture. IL2: RPMI-1640 supplemented with IL2, LCL: RPMI-1640 + inactivated LCL as feeder, LCL + PHA: LCL condition supplemented with PHA, LCL + PHA + IL2: LCL + PHA supplemented with IL2, PHA: RPMI-1640 supplemented with PHA.

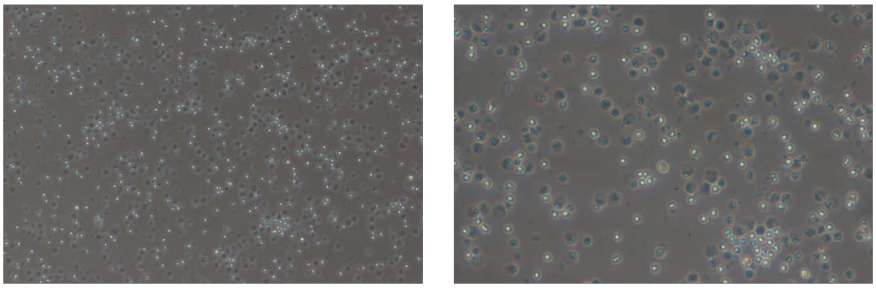

(Cont.)

(Cont.)

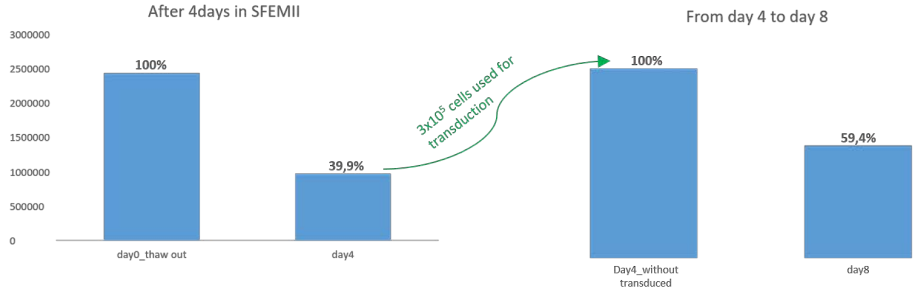

Figure 18. PBMCs culture optimization in SFEMII. The pictures at the top show patients PBMCs after 24 hours in SFEMII medium. Left graphs show the absolute live cell number after the first 4 days in culture. Relative % of survived cells to day0 is shown on the column. Right graphs show the survival rate between day4 and day8, calculated on the cells kept in culture from day4 after sampling cells for the reprograming protocol. Considering the total culture period, we calculated a survival rate of 23,7% after 8 days in SFEMII.

5.1.4 iPSCs generation

Fibroblast is the most common cell type for the reprogramming, although the sampling is more invasive. From case 1, since we were able to obtain fibroblasts, we reprogrammed patient's fibroblasts by testing two different methods: the electroporation of episomal plasmid DNAs expressing the Yamanaka factors and the transduction with Sendai Virus coding the same factors as described in *Material and Method*. First the method using episomal vectors was performed as described in *Material and Method*. We tried four different conditions/parameters for episomal vectors reprogramming, we first compared two different electroporation programs on 4D nucleofector and then we tried to substitute pCXLE-hOCT3/4 with pCXLE-hOCT3/4-shp53F comparing in between addiction or absence of pCXWB-EBNA. However, in all trials, almost no cells survived during the culturing on MEF feeder layer. Only one colony was observed when we used the combination of pCXLE-hUL+pCXLE-hSK+pCXLE-hOCT3/4-shp53F and medium was supplemented with small molecules, but it spontaneously differentiated and we stopped to culture (Figure 19).

Figure 19. Episomal vectors reprogramming. The picture shows the colony after one month on MEF feeder layer. Only one colony shown here was observed when pCXLE-hUL+pCXLE-hSK+pCXLE-hOCT3/4-shp53F were electroporated, but not other episomal vectors.

We next performed the Sendai Virus transduction method as described in *Material and Method* and it allowed us to observe colonies with iPSCs morphology, which were picked and expanded (Figures 20 and 21). The transduction of case 1 fibroblasts yielded 2 stable iPSC-like clones out of 27 colonies picked (Figure 21) when small molecules were added. Considering the mature iPSC colonies out of the total transduced cells, the reprogramming efficiency in case 1 was 0.001%.

Taking these information from trials of fibroblasts reprogramming, we only used the Sendai Virus transduction method for PBMCs samples from case 2 and 3. Although the manufacturer's protocol for PBMCs reprogramming suggests transducing the virus after only 4 days of culture, previous publications showed that a better yield in iPSCs generation could be obtained if cells are cultured longer in PBMCs expansion medium (Ye L et al., 2013). Therefore, we tested two different time points to transduce our cells 4 days and 8 days after culture in StemSpan SFEMII. For case 2 PBMCs, we observed 64 survived colonies and 446 colonies on MEF feeder layer with the transduction at day 4 and day 8, respectively. In both cases, the small molecules increased the survival rate and colony formation. The reprogramming efficiency for case 2 was similar to case 1 if cells where transduced on day4 but it increased up to 0,006% if transduced on day8. For case 3 PBMCs, we observed only 2 colonies and 33 colonies with the transduction at day 4 and day 8, respectively, confirming the better yield

from longer pre-culture in PBMC culture conditions (Figure 21). In spite of the appearance of colonies, we were not able to obtain any mature iPSC clone from case 3 (Figure 22). With case 3 transduced cells at day 8, we also tested feeder free reprogramming condition, culturing cells in Repro TeSR, but cells kept dying up to one week after transduction and only few differentiated cells survived till day 20 when protocol was terminated. Mature and stable iPSC-like clones (Figure 22) were examined characters of iPSCs by immuno-staining testing their stem cell features and pluripotency. All tested clones were positive for stem cell markers, NANOG, SSEA4, TRA-I-60 and TRA-I-81 (Figure 23). Pluripotency was tested by preparing EBs in suspension culture followed by adherent culture condition supplemented with FBS, results in a random differentiation in cells derived from three germ layers. All tested clones could generate EBs (Figure 24a) and were positive to the three germ layer markers AFP (Endoderm), αSMA (Mesoderm) and TUJ1 (Ectoderm) (Figure 24b-c). Chromosomal instability in iPSCs is occasionally observed due to the reprogramming step and/or long culture procedure. iPSC clones selected for further experiment were tested chromosomal abnormality through karyotyping. Of the two iPSC clones derived from case 1, both cell lines showed normal karyotype (Figure 25). In contrast, one of three tested iPSC clones from case 2 showed abnormal karyotype (data not shown). After all characterization, 2 clones from the reprograming of case 1 were chosen and designated as SSFiPS1 (Case 1 patient Fibroblast-derived iPSC clone 1) and SSFiPS7 (clone 7) and also 2 clones from case 2 were designated KHP2iPS8 (Case 2 patient PBMC-derived iPSC clone 8 from second transduction on day 8 of StemSpan SFEMII culture) and KHP2iPS11 (clone 11).

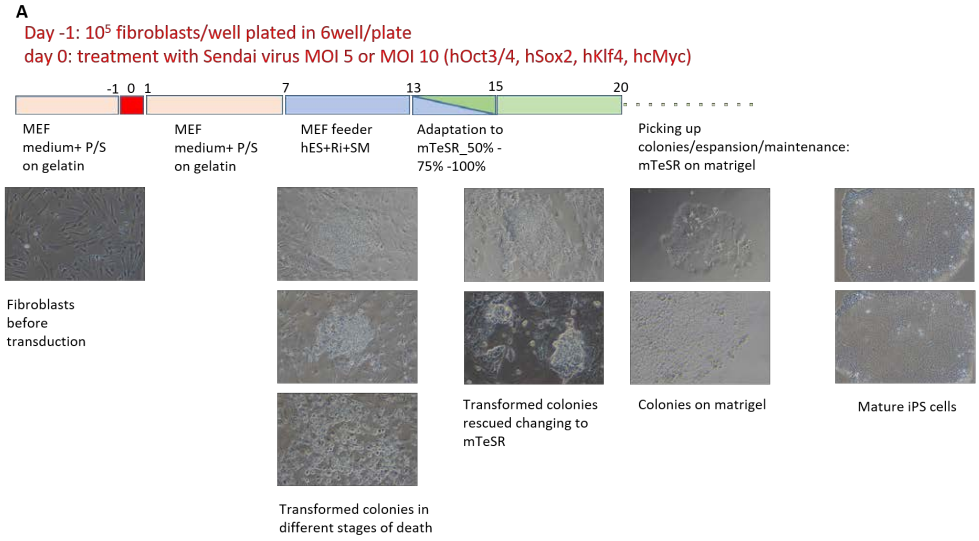
A
Day -1: 10^5 fibroblasts/well plated in 6well/plate
day 0: treatment with Sendai virus MOI 5 or MOI 10 (hOct3/4, hSox2, hKlf4, hcMyc)
-1 0 1
7
13
15
20
MEF medium+ P/S on gelatin
MEF medium+ P/S on gelatin
MEF feeder hES+Ri+SM
Adaptation to mTeSR_50% - 75% -100%
Picking up colonies/espansion/maintenance: mTeSR on matrigel
Fibroblasts before transduction
Transformed colonies in different stages of death
Transformed colonies rescued changing to mTeSR
Colonies on matrigel
Mature iPS cells

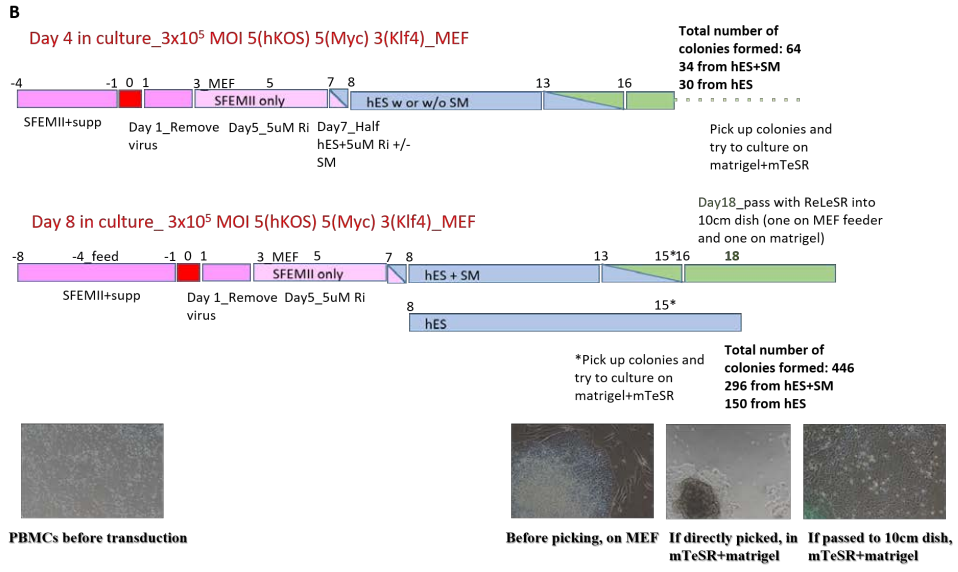
B
Day 4 in culture_3x10^5 MOI 5(hKOS) 5(Myc) 3(Klf4)_MEF
Total number of colonies formed: 64
34 from hES+SM
30 from hES
-4 -1 0 1 3_MEF 5 7 8 13 16
SFEMII only
hES w or w/o SM
SFEMII+supp
Day 1_Remove virus
Day5_5uM Ri
Day7_Half hES+5uM Ri +/- SM
Pick up colonies and try to culture on matrigel+mTeSR
Day 8 in culture_ 3x10^5 MOI 5(hKOS) 5(Myc) 3(Klf4)_MEF
Day18_pass with ReLeSR into 10cm dish (one on MEF feeder and one on matrigel)
-8 -4_feed -1 0 1 3_MEF 5 7 8 13 15*16 18
SFEMII only
hES + SM
SFEMII+supp
Day 1_Remove virus
Day5_5uM Ri
8 15*
hES
*Pick up colonies and try to culture on matrigel+mTeSR
Total number of colonies formed: 446
296 from hES+SM
150 from hES
PBMCs before transduction
Before picking, on MEF
If directly picked, in mTeSR+matrigel
If passed to 10cm dish, mTeSR+matrigel

(Cont.)

(Cont.)

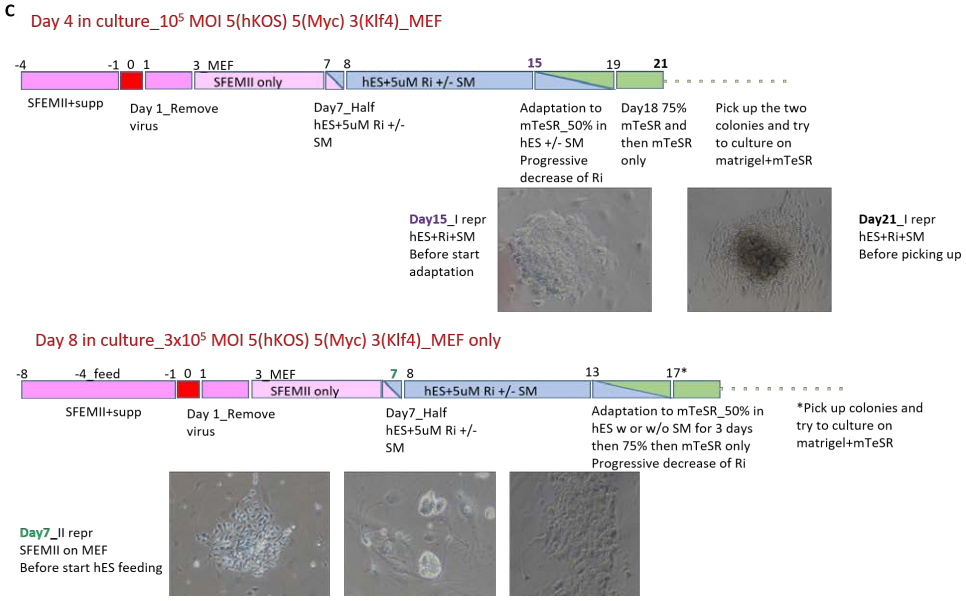

Figure 20. Morphology alteration in transduced patient's cell over reprogramming protocols. Pictures from transduced patients' cells a) Case 1 fibroblasts, b) Case 2 PBMCs, c) Case 3 PBMCs on days mentioned over reprograming protocol in time line.

A

SSF 10^5 cells/MOI	Number of colonies	Number of colonies
	MOI=5	MOI=10
Picked up	13	14
Differentiated	5 (38,5%)	5 (35,7%)
Cell death	7 (53,8%)	8 (57,1%)
keep growing	**1 (7,7%)**	**1 (7,1%)**

B

KHP $3x10^5$ cells/exp	Number of colonies	Number of colonies
	day4	day8
Picked up	21	34
Differentiated	13 (61,9%)	16 (47,1%)
Cell death	5 (23,8%)	1 (2,9%)
keep growing	**3 (14,28%)**	**17 (50%) + pool differentiated**

C

SKP 10^5 cells and $3x10^5$ cells	Number of colonies	Number of colonies
	day4	day8
Picked up	2	33
Differentiated	/	10 (30,3%)
Cell death	2 (100%)	23 (69,7%)
keep growing	**0**	**1 differentiated**

D

SSF: 0,001% in both MOI

SKP: 0% in both day4 and day6 experiments

KHP: 0,001% on day4 and 0,006% on day8

Figure 21. Summary of reprograming results. The tables show the number of picked colonies and the % of them becoming mature iPSC or differentiated or died from cases 1, 2 and 3 reprogramming. A) Case 1 fibroblasts (SSF), B) Case 2 PBMCs (KHP) and C) Case 3 PBMCs (SKP). D) The reprograming efficiency is shown and calculated as number of

mature colonies obtained out of the total cell number transduced. In KHP and SKP, the different efficiencies on day 4 and day 8 transduction are shown.

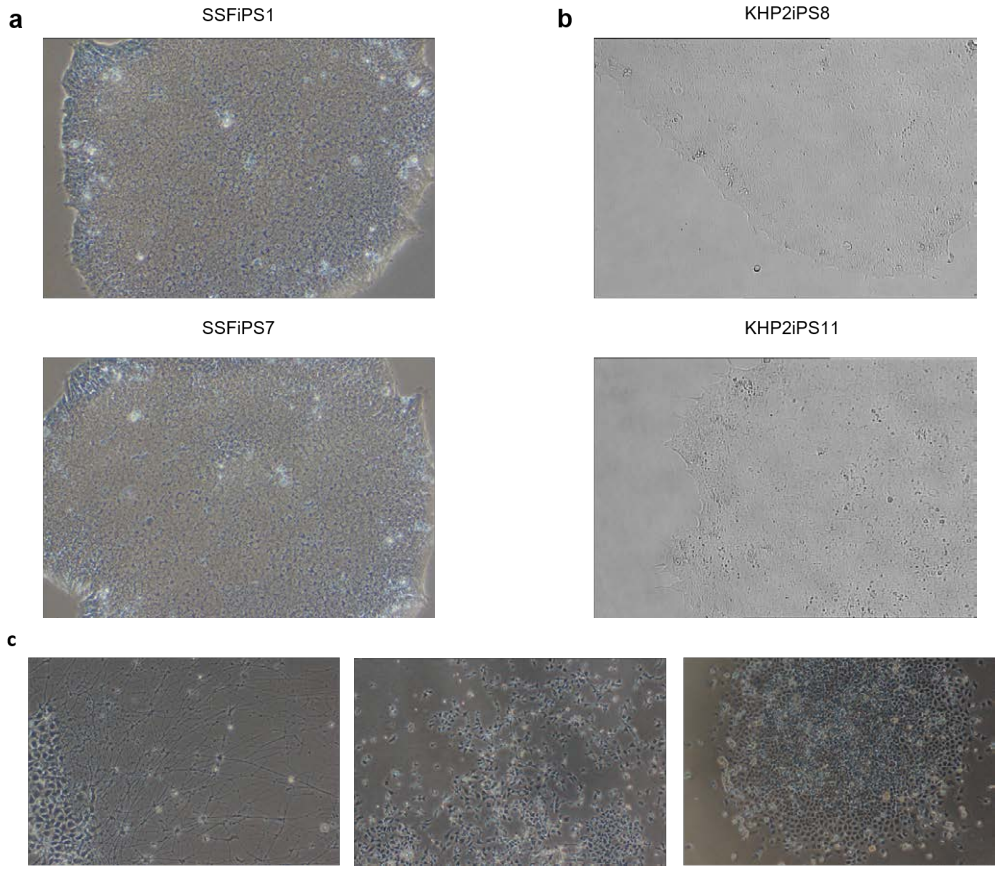

Figure 22. Mature iPSCs colonies. Representative culture of isolated clones from each patients' reprograming. a) Case 1-derived iPSCs clones. b) Case 2-derived iPSCs clones. In both cases iPSCs characteristics such as colony forming growth, well-defined edges of the colony, stem-like morphology in the nuclei/cytoplasm ratio can be confirmed. c) Case 3-derived clones. All of clones differentiated in different cell types or died during the reprogramming.

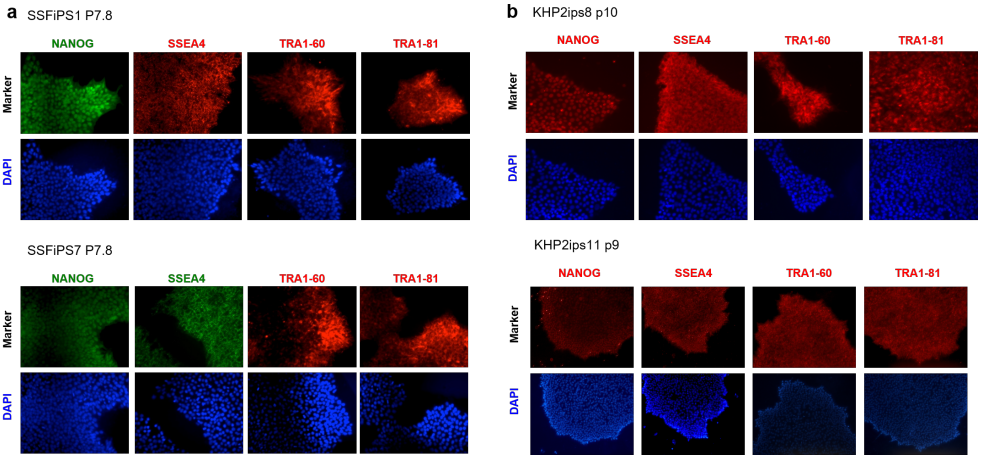

Figure 23. ES markers staining. Immunofluorescent microscopic analysis of iPS-like cells staining with NANOG, SSEA4, TRA1-60 and TRA1-81. DAPI was used as the counter staining. Representative staining is shown from a) clone1 and clone7 of case 1-derived iPSCs. (SSFiPS1 and SSFiPS7, respectively) and b) clone8 and clone11 of case 2-derived iPSCs (KHP2iPS8 and KHP2iPS11, respectively).

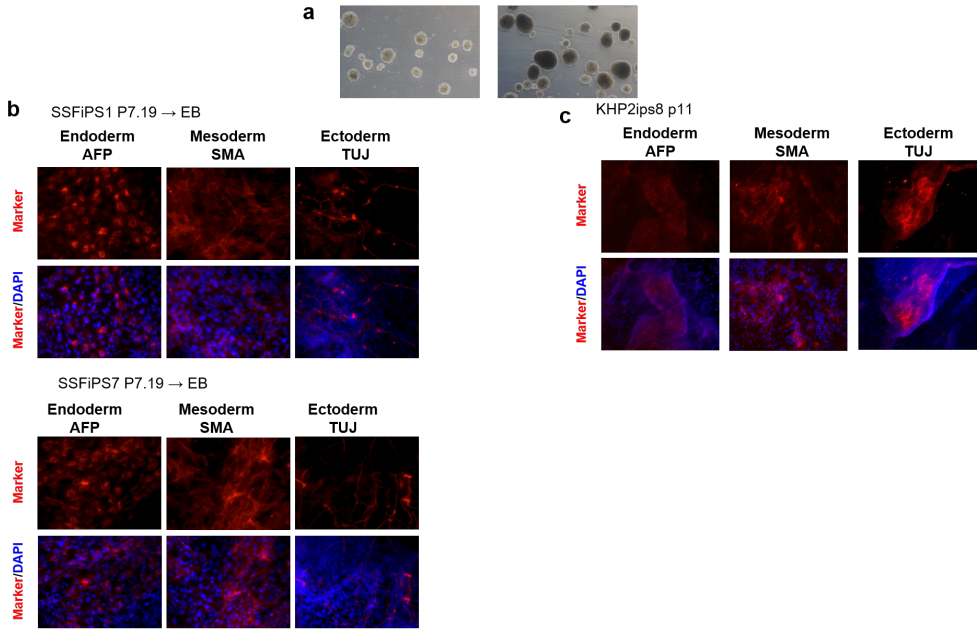

Figure 24. EBs markers staining. a) EBs in low attachment plates where iPSCs cannot grow as monolayer and create embryoid body-like clumps. Immuno-fluorescent microscopic analysis of EBs from b) SSFiPS1 and SSFiPS7 and c) KHP2iPS8 stained with

three germ layers markers, AFP (Endoderm), SMA (Mesoderm) and TUJ (Esoderm), after EBs are cultured in adherent condition.

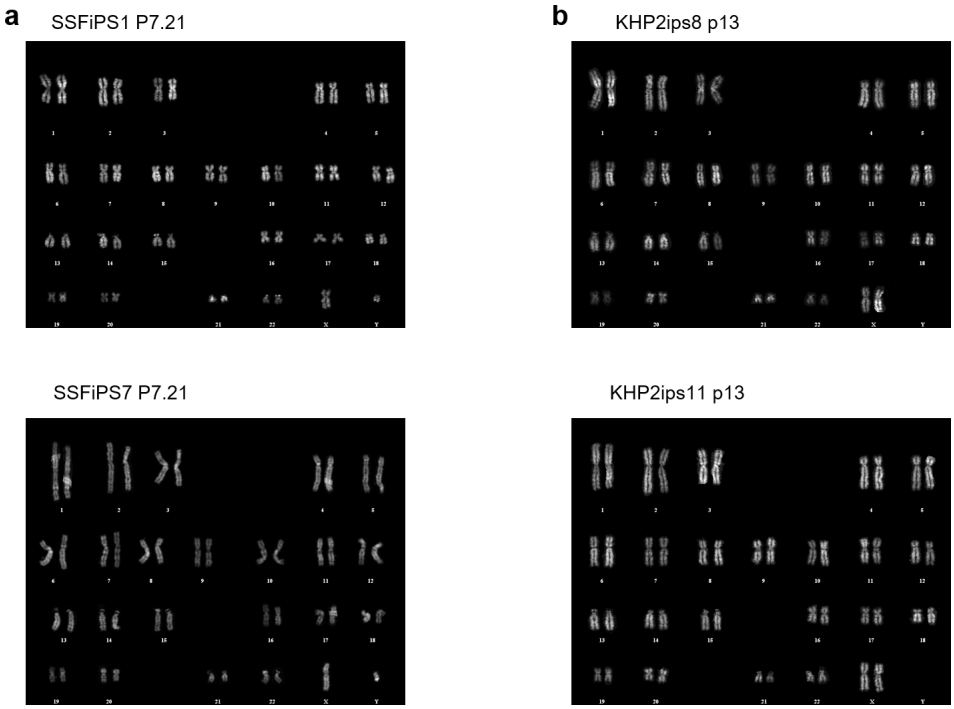

Figure 25. Karyotyping. a) SSFiPS1 and SSFiPS7 and b) KHP2iPS8 and KHP2iPS11 showed stable normal karyotype even after long culture condition**.**

5.1.5 Modeling suitability confirmation

In next, to verify the suitability of iPSC technology for imprinting disease modeling, genetic and epigenetic alterations of the interested region were examined. We performed genotype analysis through PCR and Sanger sequencing in our patient-derived iPSCs and controls on both WT and deleted allele. The diagnostic PCR was designed to selectively amplify only the deleted or the wt allele so that the heterozygote deletion can be detected in the patient and excluded in the controls. As expected, controls did not show amplification for the deletion diagnostic PCR (MEG3 Fw and SNORD Rv) and the patient showed amplifications for both deleted and wt allele (Figure 26). Sanger sequencing analysis confirmed the BPs junction

in the patients' reprogrammed cells (Figure 27). In order to verify if the reprogramming affected the expression pattern of our interested genes, we performed qPCR analysis on our patient-derived iPSCs and controls iPSCs provided from Dr. Gruenert group (CF2iPS3, CF3iPS2). We confirmed the absence or very low expression of patient deleted genes compared with controls (Figure 28). The reprogramming is a way to breakthrough epigenetic barrier determines cell fate and stage, however these results suggested no activation of the paternal allele in our patients-iPSCs as a compensation and no methylation change due to the reprogramming.

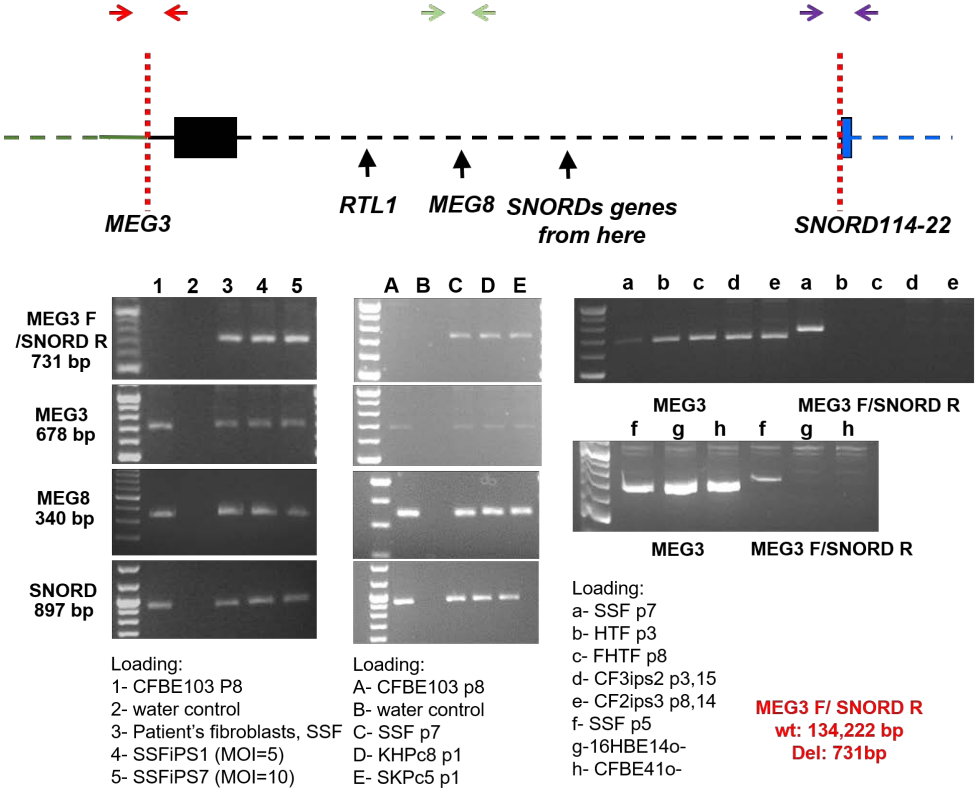

Figure 26. Genotyping by PCR. Patients' cells and control cell line (CFBE103, HTF, FHTF, 16HBE14o- and CFBE41o-) were tested to confirm the presence of the deleted allele by PCR. The top panel shows the scheme of diagnostic PCR: red arrows represent MEG3 Fw and Rv, green arrows represent MEG8 Fw and Rv, violet arrows represent BP14-SNORD Fw and Rv. Red vertical lines represent the position of patients' BPs. MEG3 Fw and SNORD Rv amplify 731bp with the BPs in the patient, while 134,222bp without the deletion. MEG3 Fw and Rv, MEG8 Fw and Rv, SNORD Fw and Rv amplify only the wt chr14 but not deleted allele.

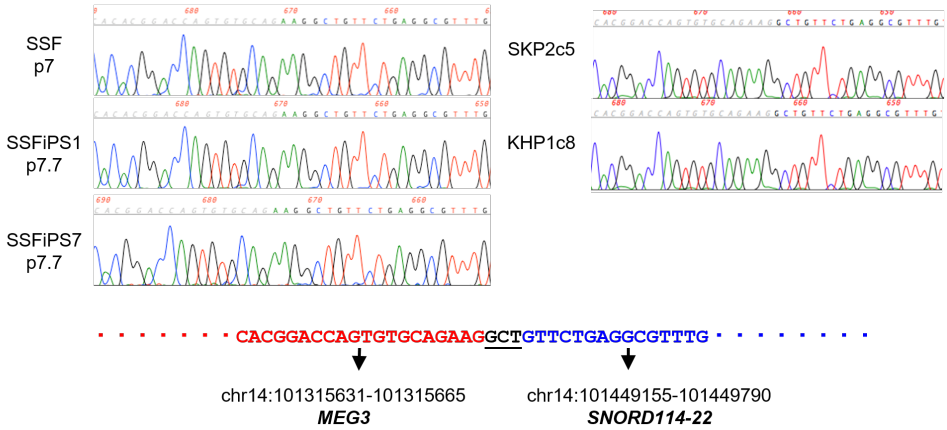

Figure 27. Breakpoints confirmation by Sanger sequencing in iPSCs. The chromatograms show the Sanger sequencing in case 1 fibroblasts (SSF p7), case 1-iPSCs (SSFiPS1 and SSFiPS7) and in case2 and case 3 clones (KHP1c8 and SKP2c5, respectively). The breakpoints junction is the same in between patients and it is maintained after the reprogramming. Positions are indicated based on UCSC, hg19.

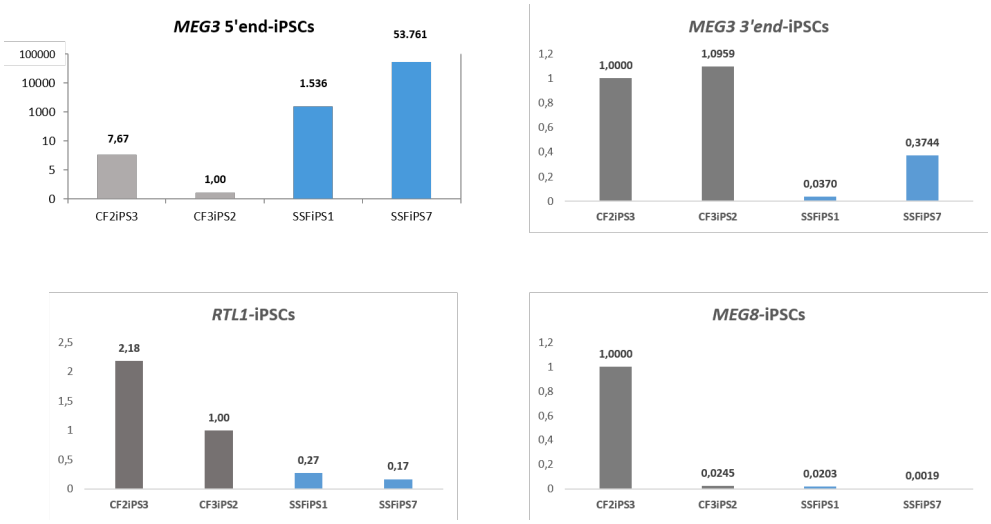

Figure 28. Quantitative PCR in patient-derived iPSCs. The graphs show the expression levels of *MEG3* (both 5' and deleted portion), *MEG8* and *RTL1* in patient-derived iPSCs relative to control iPSCs.

5.1.6 Neuronal differentiation

Some of the symptoms described in the Kagami-Ogata syndrome may be explained by a neurological impairment. Therefore, we tended to test the impact of the deletion on chr14 on neuronal development and/or function by directing the patient-derived iPSCs into adult neurons. A lot of protocols for the neuronal differentiation have been developed using specific supplements and growth factors to mimic the brain environment, such as BDNF, GDNF and so on. Differentiation from iPSCs into neurons was optimized on matrixes-coated plates but also on astrocytes feeder layer to provide the required factors (Liu H and Zhang SC, 2011; Kwon J et al., 2012; D'Aiuto L et al., 2014). The most common way to induce iPSCs differentiation into different cell types requires the formation of EBs in order to mimic the 3D environment and the physiological transition observed during embryogenesis. However, the step of EB formation is also a limit in the differentiation protocol due to the difficulties in standardize the culture conditions and reproduce a result (i.e. number of cells and size of EBs, which would effect on exposure of treatments). In this study, we chose to use one of established and standardized neuronal differentiation protocols, a commercially available system with the STEMdiff Neural Induction Medium (NIM) and BrainPhys Neuronal Medium, instead of establishing our own. Thus, we could normalize variabilities might come from in house protocol in order to assess true phenotype in our in vitro model for the Kagami-Ogata syndrome. STEMdiff Neural Induction medium is a complete medium that induces iPSCs differentiation into neural progenitors in feeder-free conditions and it is suitable for both EBs and monolayer protocols. BrainPhys is a maturation medium to induce the terminal differentiation of the progenitors. We chose BrainPhys Neuronal medium because it seems to induce a random differentiation into neurons: most of the available media allow the differentiation into specific neuronal subtypes but because we do not know which subset of neurons may eventually be affected by the Kagami-Ogata syndrome, we decided to use a medium that could better mimic the physiological cell diversity.

We used CF2iPS3 and CF3iPS2, provided by the Dr. Gruenert group to optimize the culture conditions. First, we followed the protocol suggested by the manufacturer to use the Neuronal Induction Medium and we observed higher growth rate than the one expected from the manufacturer protocol, even after plating the minimum cell density suggested. For further

experiments, we then decreased the cell density down to the half of the original density suggested. On day 20 in this culture medium, we switched to the neuronal maturation medium Brainphys (supplemented with SM1 alone or other growth factors as mentioned in *Material and Method*) and plated cells at the lowest suggested cell density on PLO/Laminin-coated plates. During switching culture condition, although we noticed a high cell death after 24 hours on PLO/Laminin, survived cells were kept in Brainphys culture up to 23 days. In order to check the features of survived cells, we examined the expression level of the neuronal differentiation markers such as TUJ1, PAX6 and MAP2 (Figure 31a), and observed an increase of these markers corresponding the culture in NIM. However, the expression level of TUJ1, PAX6 and MAP2 dropped down after switching to Brainphys with both SM1 alone and completed supplements, compatible with appearance of fibroblasts-like cells in culture (Figures 29 and 31a). We then tried to optimize the plating conditions to reduce cell death over switching culture conditions using CF2iPS3 only and we compared two different cell densities, two different coating protocols (Matrigel or PLO/Laminin) and three adaptation protocols to the Brainphys (Brainphys culture on day 0, 1 and 3 from the time point to switch the culture condition) (Figure 30). The gene expression level of neuronal markers was also tested after 14 days from the plating and observed that the condition seeded at higher density on PLO/Laminin and adapted to Brainphys after three days on PLO/Laminin induced higher expression level of all three neuronal markers (Figure 31b), even though the exposure to Brainphys was shorter than other conditions. We can reasonably decide that the longer transition from NIM to BrainPhys should be used for further experiments.

We applied the optimized conditions to two control iPSCs (CF2iPS3 and CF2iPS3 Ic8e11), two patients-derived iPSCs (SSFiPS7 and KHP2iPS8) and we traced the cell density and morphology changes during the differentiation steps (Figure 32). Because the density seemed to be a critical factor for success in neuronal survival and differentiation, we used again half of the plating density in NIM suggested by the provider and we increased the plating density on PLO/Laminin up to two times more than the original cell density used during the first optimization step. We used the same parameters for all cell lines. We observed a high variability in response to the protocol in term of cell survival and morphology changing, not only in between patients-derived iPSCs and controls but also in between the two controls (Figure 32). In other words, we could not reproduce the

differentiation on CF2iPS3. These data suggest that there may be a variability related with the deletion but, because of discrepancy in the control cell line, individual cell lines/clones may need different parameters to induce the differentiation. We did not test neuronal markers expression because of the uncompleted data set and because further optimization is required.

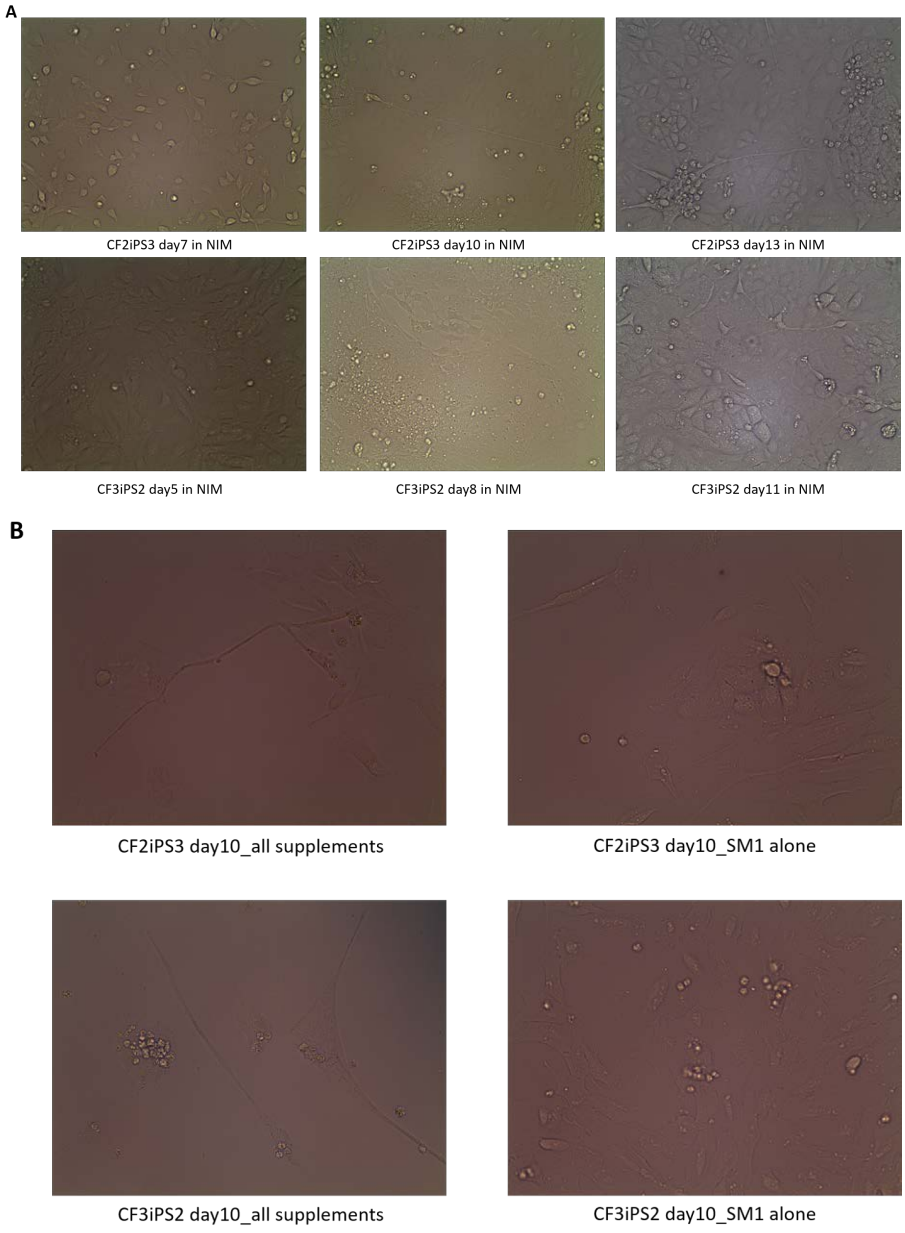

Figure 29. First optimization of neuronal differentiation. A) Three time points of the neuron induction in STEMdiff Induction Medium (NIM) for CF2iPS3 and CF3iPS2. B) Differentiated iPSC-derived neurons after 10 days in BrainPhys medium.

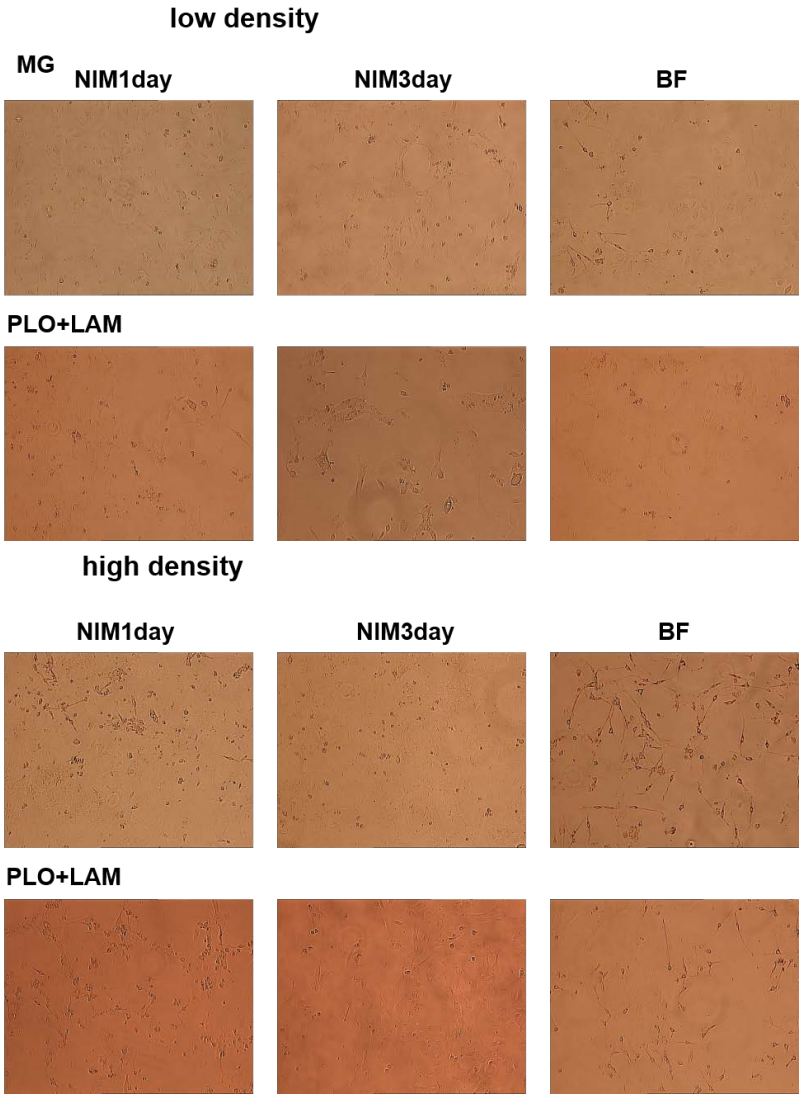

Figure 30. Plating optimization. The panel shows the summary of the conditions to optimize the switching to the BrainPhys: MG=Matrigel, PLO+LAM= PLO/Laminin, low density= $4x10^4$ cells/cm^2, high density= $6x10^4$ cells/cm^2, NIM 1 day= cells were seeded in NIM and adapted to BrainPhys after 24 hours, NIM 3 day= cells were seeded in NIM and adapted to BrainPhys on day 3, BF= cells were seeded in BrainPhys.

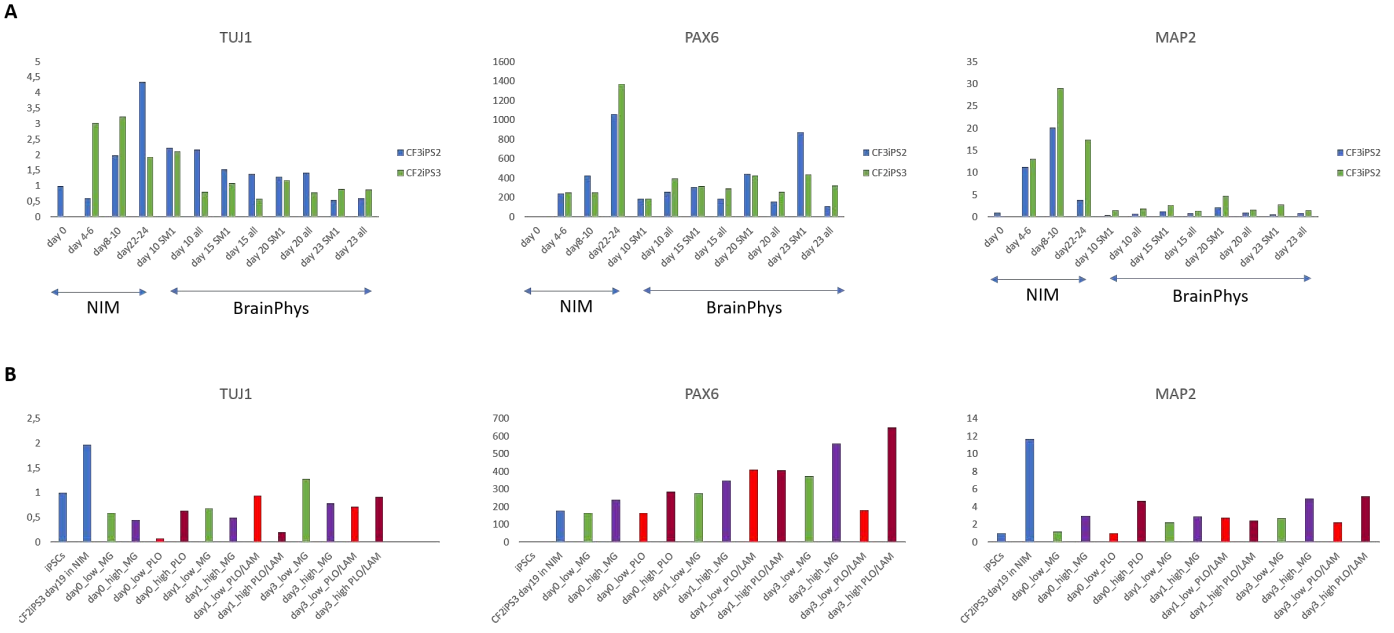

Figure 31. Neuronal markers. A) The graphs show the expression level of neuronal markers TUJ1, MAP2 and PAX6 during the differentiation protocol following the manufacturer suggestions. In blue CF3iPS2 used as comparison for the relative expression data, in green CF2iPS3. B) The graphs show the relative expression level of TUJ1, PAX6 and MAP2 in BrainPhys culture after 14 days. The coloring shows different densities and coating protocols during the switching to BrainPhys: in green low density on Matrigel-coated plates, in violet higher density on Matrigel-coated plates, in light red low density on PLO/LAM-coated plates, in dark red high density on PLO/LAM-coated plates.

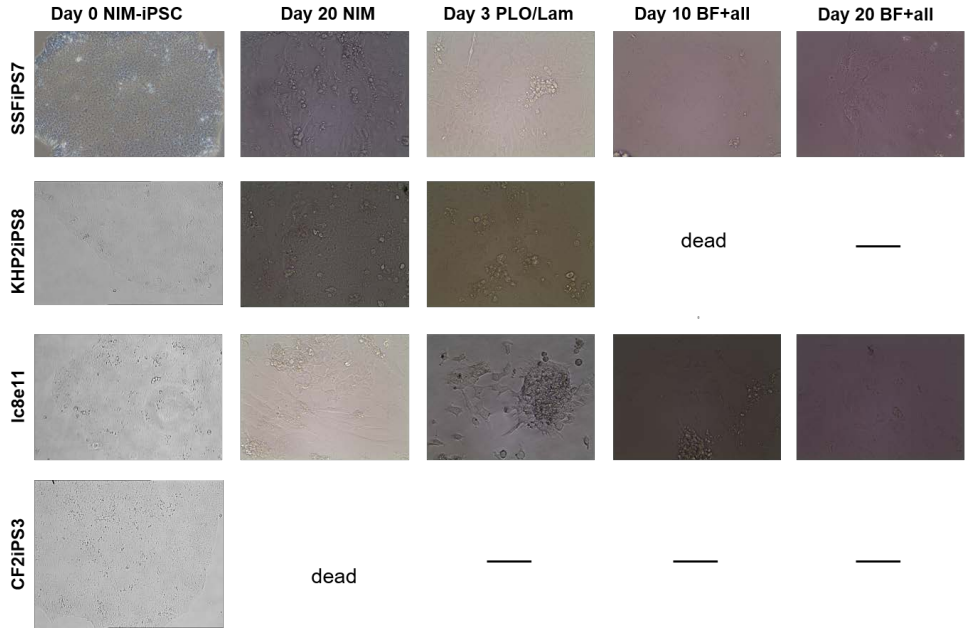

Figure 32. Neuronal differentiation in patients iPSCs and controls. The panel shows the morphological changes in 5 different time points during neuronal induction and maturation protocol: on day 20 we switched to PLO/Laminin-coated plates, after 3 days we adapted to Brainphys, after day 10 and 20 we recorded the morphological changes during BrainPhys culture. SSFiPS7 and Ic8e11 (the control cell line) survived until day 30 in Brainphys, even though the mortality was very high during the switching. CF2iPS3 had crisis during the culture in NIM and we could not use as comparison. The morphology and cell survival are highly variable in between different cell lines.

5.2 Discussion

We studied a family carrying a deletion in 14q32.2 imprinted region and showing high variability in phenotype severity degree. We first characterized the deletion in case 1 through CGH-Array and Sanger sequencing allowing us to perform pre-natal diagnosis on patient 2. Expression level analysis revealed low expression of maternally expressed genes and interestingly also low expression of *RTL1*. The analysis confirmed that breakpoints were stable during maternal meiosis and we excluded that the phenotype variability was correlated with variable positions of the BPs.

(AIM 1) Because a few molecular biology information in Kagami-Ogata syndrome have been known, we attempted to study the family more deeply and analyze the differences in between patients at molecular level. Because we could not obtain same cell type from the three patients, we have a limit on the amount of cell sources and we should minimize the invasiveness of the withdraw from the newborn case 2, we decided to use iPSC technique which allows to obtain a reasonable cell type with almost unlimited cell sources and study from different patients. Furthermore, iPSC technique allows us to study cell types that we do not have access in donor such as neurons.

In order to avoid invasive tests, we tried to reprogram different cell types, fibroblasts from the deceased case 1 and buccal cells or PBMCs from case 2 and 3. Although the buccal cells were one from the least invasive sampling, the culture of buccal cells failed so we focused on PBMCs which still allow a less invasive withdraw compared with skin biopsy. Also, the reprogramming through episomal vectors failed and we focused on transduction method. By comparing the results obtained in our cell culture, we observed a higher efficiency rate when PBMCs were transduced than when fibroblasts were. In fact, we observed 6 times higher reprogramming efficiency (0,006% in PBMCs vs 0,001% in fibroblasts). Furthermore, we observed increment of efficiency in PBMCs reprogramming when cells were kept in culture for 8 days instead of following manufacture-suggested duration, 4 days (0,006% after 8 days vs 0,001% after 4 days). This can be explained by the enrichment of myeloid lineage who highly proliferate in StemSpan SFEMII, because the higher reprogramming efficiency from actively dividing cells is well confirmed and described by many of

literatures. In fact, from day4 to day8 culture, we confirmed higher maintenance of cell number than that from day0 to day4 (Figure 18). We do not know why the reprogramming of case 3 PBMCs was unsuccessful, but we could confirm the improvement in cell survival following the transduction in between day 4 and day 8 in StemSpan SFEMII but none of the colony became mature iPSCs. We can only speculate that the deletion might affect the reprogramming step, but as mentioned we do not know the origin of the deletion in case 3 so we do not have data to correlate un-succeeded reprogramming with a deletion on paternal chr14.

(AIM 2) The characterization of patient-derived iPSCs showed that from both fibroblasts and PBMCs the reprogramming was complete and we obtained stable mature iPSCs. Our iPSCs show the morphology and the markers expression typic of stem cells and they demonstrated to be pluripotent. Karyotype analysis revealed that culture conditions allow to keep stable iPSCs and not selective pressure is induced. Furthermore, the RNA expression level of 14q32.2 imprinted genes was maintained as in primary cells suggesting that the reprogramming protocol does not affect the epigenetic regulation of the *DLK1-MEG3* domain and that iPSCs are a suitable tool for the modelling of the Kagami-Ogata syndrome. Our data suggest that we created a reliable human model of the syndrome mimicking our patients molecular features. Also, because we used Sendai virus reprogramming, we do not have virus integration in the genomic DNA that may alter further results.

(AIM 3) We generated iPSCs for studying the impact of the deletion in adult cells such as neurons. In order to do so, we optimized a neuronal differentiation protocol on control iPSCs. We observed that our iPSCs were growing faster in NIM than expected from the manufacturer protocol so we adjusted the cell density to our culture conditions. In Brainphys, cell survival and RNA expression showed that high cell density and also the three-day transition step in between plating on PLO/Laminin and adapting to the BrainPhys allow a better neuronal maturation during the switching. After validating the protocol and applying it to our patient-derived iPSCs, we noticed too many variabilities even if the culture conditions were the same for all cell lines (plating cell density, confluence, number of passages before switching, exposure to the medium). In order to proceed with analysis, we need to improve the differentiation protocol by confirming if the variability is clone-specific or if, in case of patients' iPSCs, the deletion has some effects.

6. MEG3 rescue through CRISPR/Cas9

6.1 Results

The genotype and phenotype correlation studies had suggested that the lack of expression of *MEG3* is one of the possible responsible of Kagami-Ogata syndrome despite there is no evidence that directly prove its role and shows a mechanism underlying on this disease. In this study, to reveal the role of *MEG3* in Kagami-Ogata syndrome, we carried out molecular biological experiments using the human model that we have established with iPSC technologies.

6.1.1 MEG3 overexpression

The most commonly, the effect of gene expression alteration is tested by transient induction of gene down regulation through RNA interference or gene overexpression through expression vector because of its convenience. To verify the change in gene expression caused by the lack of *MEG3* observed in our patients, we first tested an effect of *MEG3* overexpression transiently in patient-derived iPSCs. pCI background vectors, driving a gene expression with CMV promoter, were transfected in iPSCs and *MEG3* expression was tested by quantitative PCR. Lower dosage transfection 0.2 and 0.6 μg/2x10^5 cells did not show significant expression of *MEG3* (Figure 33). Higher dosage transfection 1.0, 2.0 and 4.0 μg/2x10^5 cells were also performed and we observed high mortality, especially 4μg plasmid DNA transfection caused many cell death. As observed high mortality, we observed strong alteration of house keeping gene *GAPDH* expression, which leads apparent increment of *MEG3* expression in transfection dosage dependent manner (5, 19 and 182 times more relative to non transfected cells after normalizing by *GAPDH*, respectively, and 3.9, 6.0 and 6.7 times more without normalizing by *GAPDH*, respectively, Figure 33). Due to the concern from the alteration of *GAPDH* expression, we took another control to confirm the *MEG3* overexpression. Since *MEG3* overexpression from pCI vector is known to induce p53 overexpression (Zhou Y et al., 2007), we analyzed p53 expression level as control for the transfection efficiency. However we did not observe a correlation between

the amount of pCI-MEG3.2 transfected and the expression level of p53. To reproduce Zhou et al.'s observation, we tested *MEG3* overexpression in one of immortalized cell CFBE41o- and observed 534 times more expression (without the alteration of *GAPDH* expression) likely in other cell lines, such as HCT116 and U2OS cell lines (Zhou Y et al., 2007). These data suggested CMV promoter was not suitable promoter to express exogenous gene in iPSCs. Thus we switched the backbone plasmid DNA from CMV to CAG promoter, well known as strong promoter and as being stable in ES and iPSCs, and observed even more critical cell mortality compared with CMV promoter (Figure 34). Overall, considering high cell death following the pCAG-MEG3.2 transfection and unsure *MEG3* induction from transient overexpression in iPSCs, we closed the experiment as unsuccessful and moved on the gene modification technique.

Figure 33. Overexpression experiments. Relative expression data to non-transfected cells. A) 0.2 and 0.6 µg of pCI-MEG3.2 (red) or pCI-MEG3.2-del (green). B) Second transfection experiment with high amount of plasmid DNA (1, 2 or 4µg) and confirmation of transfection efficiency by testing p53 expression. *MEG3* expression analysis is shown both after the normalization with *GAPDH* and without normalization. C) pCI-MEG3.2 (1µg) transfection in immortalized cell line CFBE41o- and p53 confirmation. The graphs show low induction of *MEG3* expression in iPSCs compared with immortalized cell line and no correlation between increase of *MEG3* detection and p53 expression.

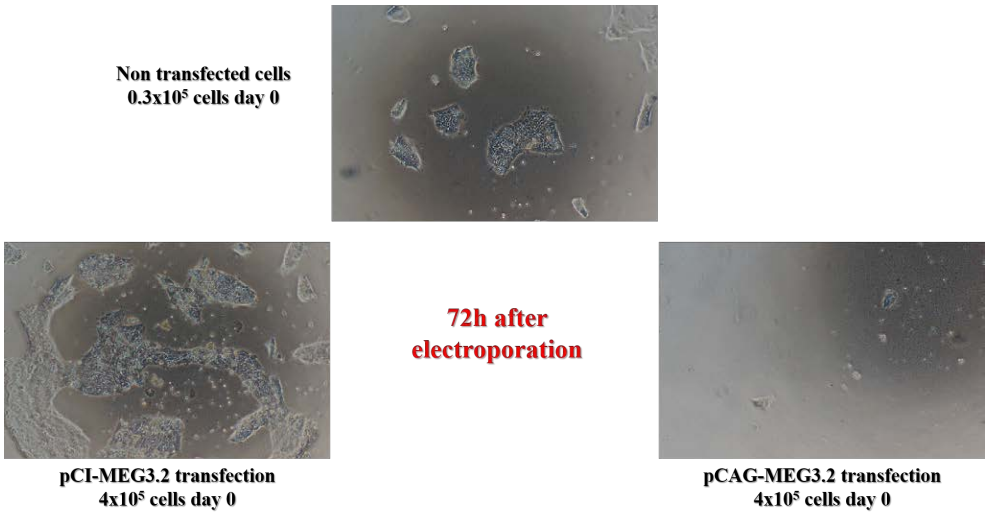

Figure 34. pCI versus pCAG transfection. The pictures show the cell survival 72 hours post-electroporation in control well, pCI-MEG3.2 and pCAG-MEG3.2 transfection (2μg).

6.1.2 MEG3 modification

Because of the technical difficulty to express *MEG3* in iPSCs through the transient transfection, we performed gene editing in our patient-derived iPSCs to correct the lacked region and to rescue *MEG3* expression controlled by the endogenous promoter. In this research, the gene editing strategy was designed to exchange the endogenous deleted allele to the exogenous targeting vector completes the lacked region through HDR enhanced by DSB introduction with CRISPR/Cas9 (Figure 38 bottom scheme). To do this, we developed the targeting vector contains the last intron and exon of *MEG3* and also CRISPR/Cas9 targeting allele specifically on the deleted maternal allele (Figure 35b), but not targeting vector, wt paternal allele and modified allele (expected modification on maternal ch14 in Figure 35a). Also, we utilized PiggyBac system in our targeting vector to select a modified iPSC via the drug selection and to remove that drug selection cassette (details on modification strategy in *Material and Method*).

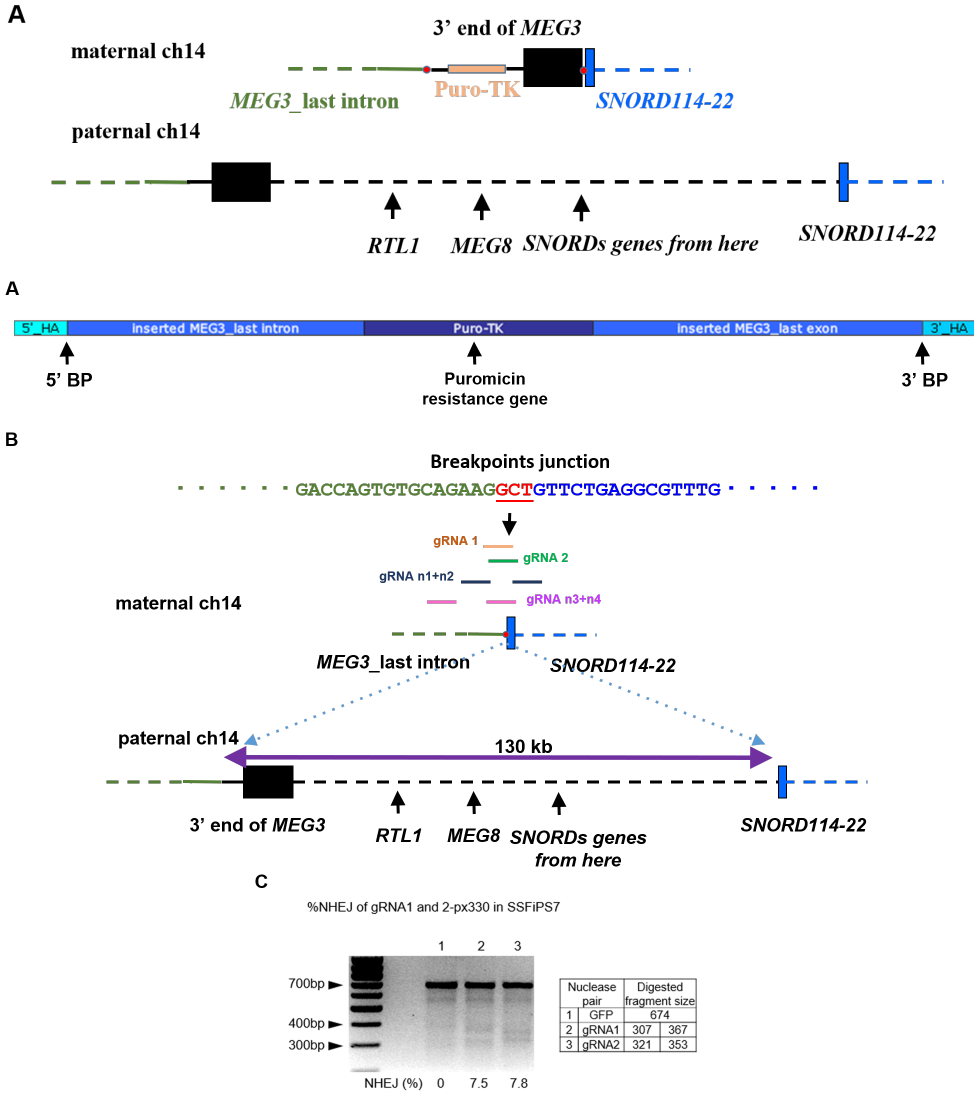

Figure 35. Breakpoints-targeting efficiency with allele-CRISPR/Cas9 system. A) Editing DNA design. The panel shows the scheme of paternal and maternal ch14 in patient's cells after *MEG3* insertion. Red dots on maternal chromosome represent the original BPs, B) Illustration shows several allele-specific guide RNAs designed in this study. gRNA1 and gRNA2 are inserted in the wt Cas9 vector. gRNAn1 and n2, and gRNA n3 and n4 are inserted in double nicking system, cause double strand break with two single strand cuts (Nick) through mutated Cas9s. C) T7E1 assay measuring the target efficiency. Only wt Cas9 induced a measurable cut in our patient-derived iPSCs. Thus, result from nicking pair is not shown.

From case 1 SSFiPS7 was chosen for the modification and transfected the donor DNA along with CRISPR/Cas9. Transfected iPSCs were selected for candidates of the modification by puromycin treatment. After around 10 days, 17 clones survived from the puromycin selection (Figure 36). Regarding case 2, we first modified KHP2iPS8 and obtained only 6 Puromycin resistant colonies. However, because of low survival after transfection and selection, we decided to perform the modification experiment on KHP2iPS11 as well, resulting 25 puromycin resistant colonies (Figure 36). We tested puromycin-selected clones by PCR and Sanger sequencing to confirm the MEG3 sequence insertion: 1) 5' inside-out PCR to target genomic DNA and plasmid derived DNA on 5' of *MEG3* sequence and 2) 3' inside-out PCR to target genomic DNA and plasmid derived DNA on 3' of *MEG3* sequence allowed to identify the modified clones vs un-modified clones, 3) 5' PB cassette junction and 4) 3' PB cassette junction allowed us to test the correct connection of the TTAA sequence, 5) *MEG3* and 6) SNORDs on the paternal chromosome to verify that no mutations were induced for unspecific Cas9 activity (Figures 36 and 37). Case 1 iPS7 had 76.47% of puromycin-selected clones that were positive for *MEG3* modification, from these c1, c4 and c7 (1.5μg gRNA) were sequenced and showed correct modification (Figure 37). Case 2 iPS8 had 100% of puromycin-selected clones that were positive for *MEG3* modification so, despite the low survival after selection, we decided to proceed with iPS8 for further experiments and c3 and c5 (3μg gRNA) were sequenced showing correct modification (Figure 37). Case 2 iPS11 had 84% puromycin-selected clones that were positive for inside-out PCR, but they were not deeply tested (Figure 36).

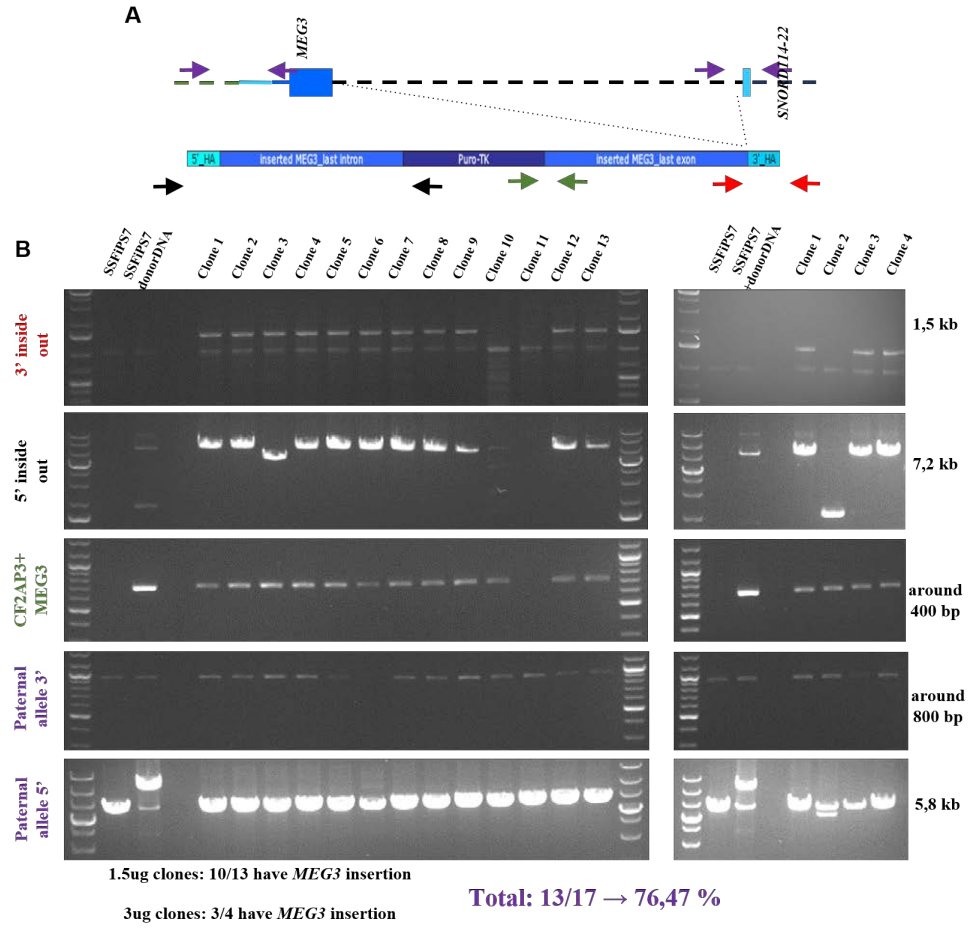
A
MEG3
SNORD114-22
5'_HA
inserted MEG3_last intron
Puro-TK
inserted MEG3_last exon
3'_HA
B
SSFiPS7
SSFiPS7 +donorDNA
Clone 1
Clone 2
Clone 3
Clone 4
Clone 5
Clone 6
Clone 7
Clone 8
Clone 9
Clone 10
Clone 11
Clone 12
Clone 13
3' inside out
5' inside out
CF2AP3+ MEG3
Paternal allele 3'
Paternal allele 5'
1,5 kb
7,2 kb
around 400 bp
around 800 bp
5,8 kb
1.5ug clones: 10/13 have MEG3 insertion
3ug clones: 3/4 have MEG3 insertion
Total: 13/17 → 76,47 %

(Cont.)

(Cont.)

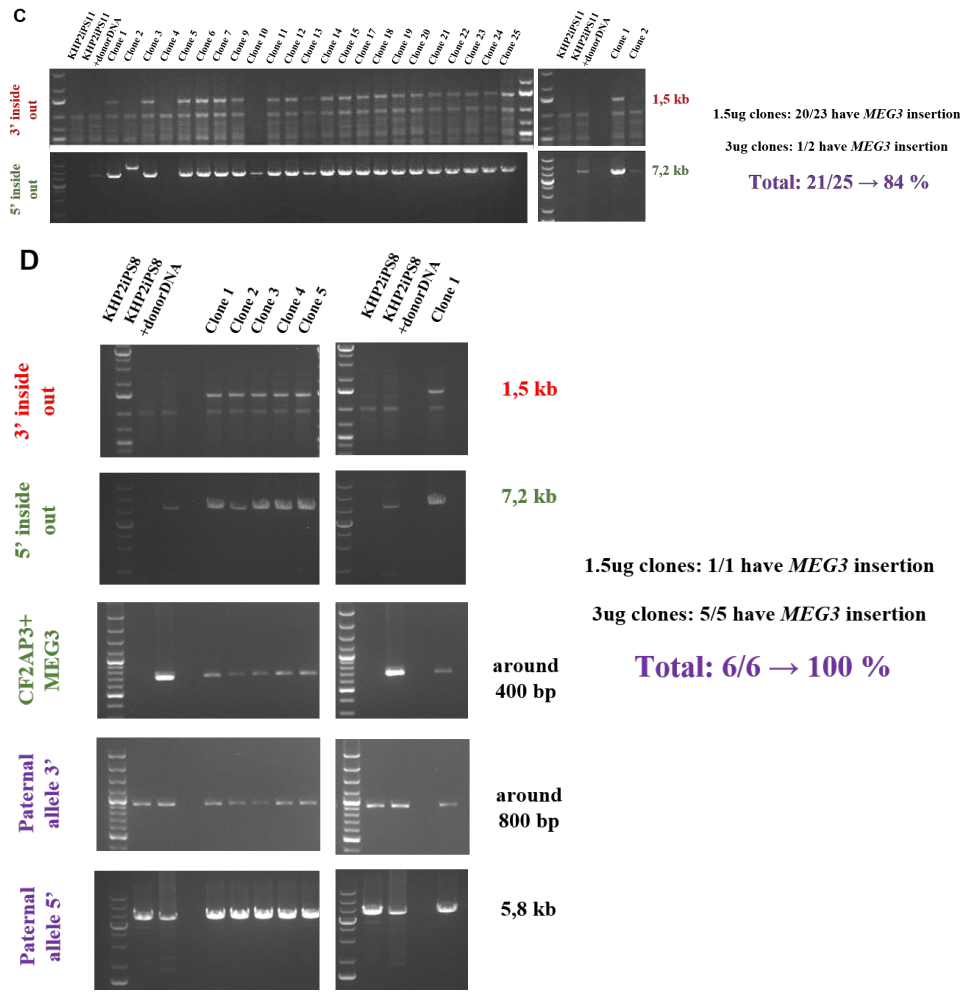

Figure 36. *MEG3* modification diagnostic PCRs. A) Scheme of the diagnostic PCRs: in black the 5' inside-out PCR spanning from the genomic DNA upstream of the homology arm to the puromycin resistance gene (5'MEG3gDNA Fw and P4 Rv, Table 3). In red the 3' inside-out PCR spanning from the inserted *MEG3* exon to downstream of the homology arm (MEG3 insertion Fw and SNORDgRNA Rv, Table 3). These PCRs allow to amplify specifically only the modified allele. The paternal chromosome in fact does not contain the puromycin resistance gene, while residual plasmid DNA does not contain the sequence upstream and downstream of the homology arm. At the same time the paternal allele, even though has the sequence recognized by the red primer pairs, cannot be amplified because the predicted PCR amplicon would be around 130kb. In black and in green the PCR designed to sequence the 5' and 3' junction of the PB cassette, respectively (5'MEG3gDNA Fw and P4 Rv, CF2AP3 Fw and MEG3gDNA Rv primers pairs, Table 3).

5'MEG3gDNA Fw and P4 Rv primers pair allows to amplify only modified allele because the human genome does not contain the puromycin resistance gene targeted by P4 Rv. In violet the primers pairs used to sequence the paternal chromosome 14 in order to confirm that no mutation occurred (BP14_MEG3 Fw and Rv, BP14_SNORD Fw and Rv, Table 3). B) 13 clones out 17 of SSFiPS7 showed expected size and expected pattern of amplification. C) 21 out of 25 KHP2iPS11 puromycin resistant clones were positive for the insertion but they were not deeply investigated because D) all the KHP2iPS8 resistant clones resulted to be inserted and we chose to use iPS8 for further experiments. Each color of primers pairs (arrows) in scheme A is corresponding of PCR condition shown at left of panels B, C and D.

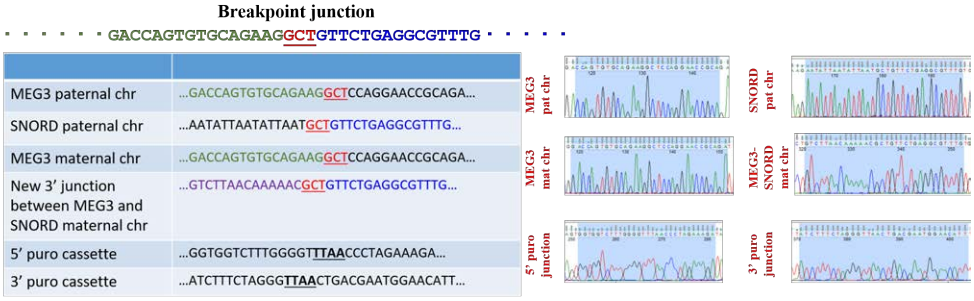

Figure 37. Confirmation of *MEG3* modification by Sanger sequencing. On the left it shows the sequence obtained after the *MEG3* insertion by Sanger sequencing of the PCR products from Figure 36. The green shows the *MEG3* sequence upstream of the breakpoint, blue for the SNORDs downstream. Coloring is maintained in the modified sequence as reference. On the right the chromatograms from Sanger sequencing are shown. From SSFiPS7 clones 1, 4 and 7 (1.5µg of gRNA) were sequenced. From KHP2iPS8 clones 3 and 5 (3µg of gRNA) were sequenced to confirm desired modification on maternal allele.

PB cassette contains exogenous promoter for the puromycin resistance gene and thymidine kinase gene expression so, in order to avoid potential interference with endogenous *MEG3* expression in our experiments, we excised PB cassette by transfecting and expressing the PB transposase in modified clones (Figure 38). Candidates of successful excision were negatively selected by GCV treatment. Case 1 iPS7c1 had 27 PB cassette negative clones (PB^-: Puromycin and TK sequence negative by PCR) out of 30 picked GCV selected clones. Clone 4 and 7 from Case 1 iPS7 also were taken to the excision process and c4 and c7 showed 16 out of 17 and 12 PB^- out of 12 GCV-selected and -picked clones, respectively (Figure 39a). Case 2 iPS8c3 and c5 are also chosen for the excision and had 12 out of 12 and 15 PB^- out of 15 GCV-selected and -picked clones,

respectively (Figure 39b). iPS7 c7 GCV selected clones were excluded from further experiment because PCR characterization showed that all of them were negative for excision confirmation PCR (Figure 39a) and positive for original deletion suggesting that c7 was originally mixed population between modified and unmodified (random donor DNA-integrated) cells.

Several PB negative clones from each modified clone were further characterized by Sanger sequencing to confirm the correct excision of the PB cassette (Figure 40). Although almost all clones tested showed correct excision, 2 sequenced clones from case 1 iPS7c1 interestingly showed 7bp deletion upstream of the TTAA sequence used to originally insert the PB cassette, suggesting un-expected recombination through PiggyBac transposition can happen (data not shown). iPSCs character (Figure 41) was also tested by ES markers and EBs markers staining. All tested clones showed positive staining for ES markers (Figure 42) and different degree in three germ layer differentiation potential (Figure 43). Karyotyping showed heterogeneity of chromosomal stability between tested excised clones. For example case 2 iPS8c3.6 had abnormal karyotype (data not shown) while other tested excised clones were normal 46,XY or 46,XX (Figure 44). These characteristic analyses showed almost all clones still have same or similar features to the original iPSCs, suggesting that the modification process itself did not affect on iPSCs features critically. However practically there are some possibilities to have an alteration due to long culture, modification process and so on as we observed. Thus, all characteristic tests on iPSC feature are essential periodically and in each modification steps.

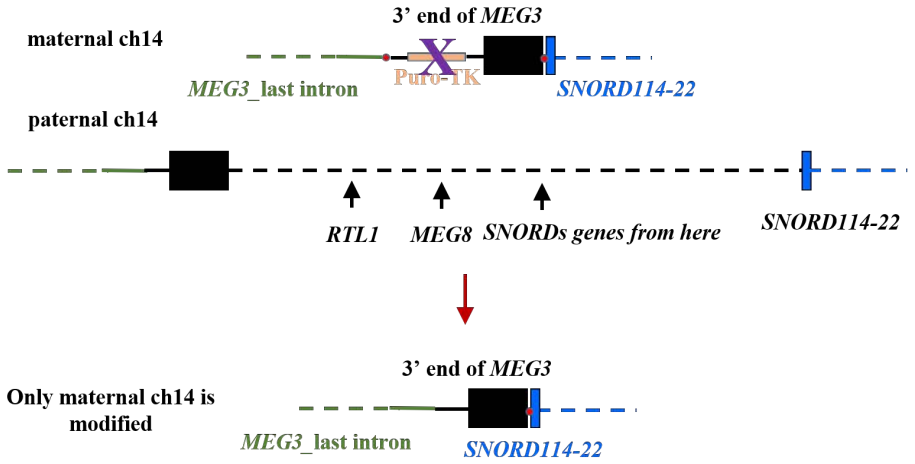

Figure 38. Excision experiment design. The panel shows the scheme of excision experiment to remove PB cassette (violet cross) and the expected result on the maternal chr14.

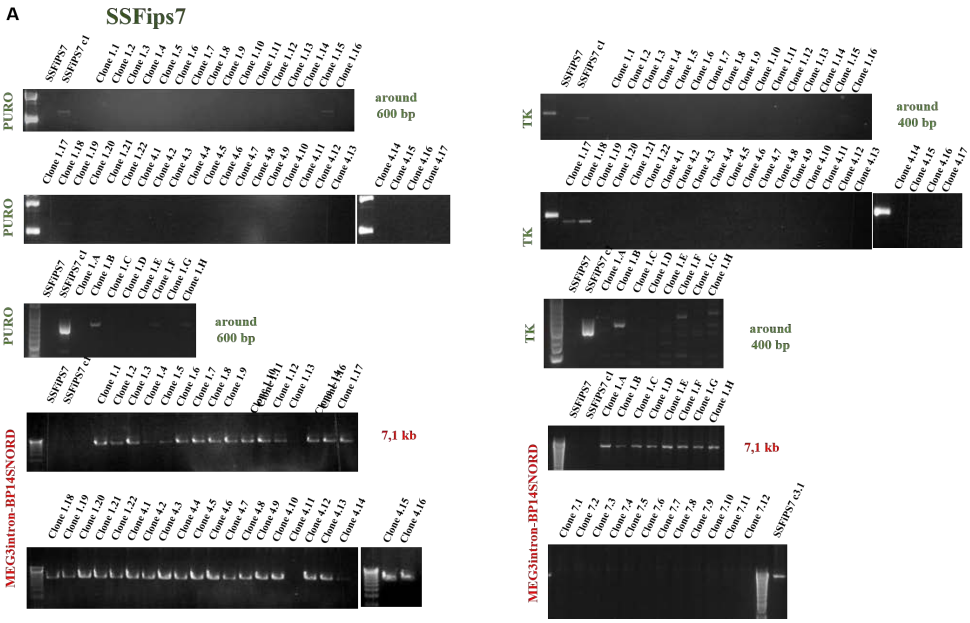

(Cont.)

(Cont.)

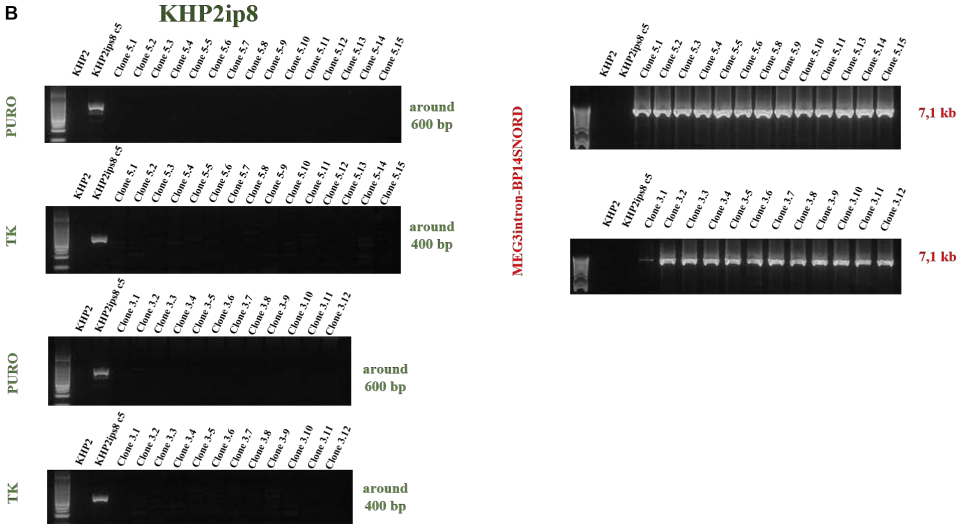

Figure 39. Excision confirmation. Diagnostic PCR for SSFiPS7 ganciclovir-selected clones (A) and KHP2iPS8 ganciclovir-selected clones (B). The PCRs tested amplify two primers pairs targeting the puromycin resistance gene (Puro Fw and P4 Rv, Table 3) and the mutated thymidine-kinase (TK FwII and TK Rv, Table 3), both expressed from the PB cassette. The third primers pair, MEG3intron Fw and BP14_SNORD Rv in Table 3, amplifies from the inserted intron of *MEG3* (in the original construct, it is located upstream of the PB cassette) and the SNORDs cluster (downstream of the PB cassette). Puro and TK are expected to be negative and we do not expect any amplification if the excision succeeded. In case of MEG3intron Fw and BP14SNORD Rv, the PCR product is expected 7.1kb in case of succeeded excision and around 11kb if PB cassette is still present. These results show that almost all clones from SSFiPS7 c1 and c4 and from KHP2iPS8 c3 and c5 were correctly excised. The quality of these data is confirmed by the negative results obtained in SSFiPS7 c7 excision in which no clone seems excised.

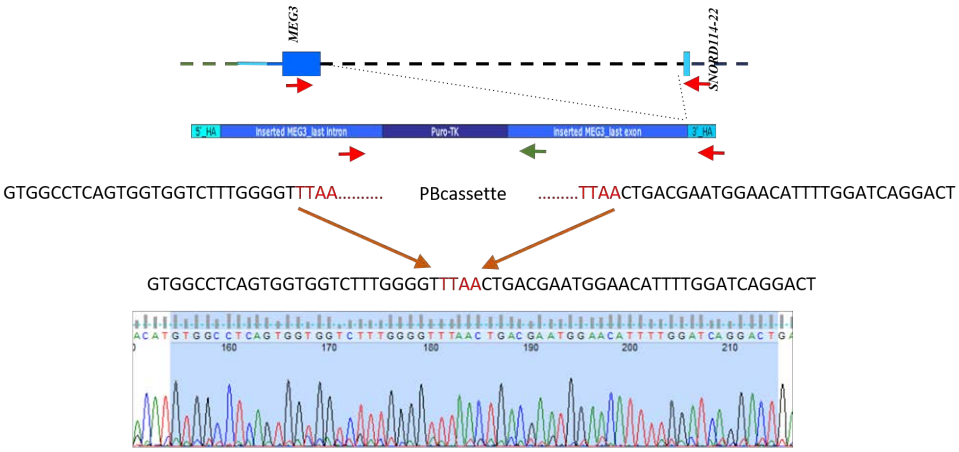

i.e. c5.3gcv
In red: PCR primers
In green: seq primer

Cell line	Puro	TK	MEG3intron-BP14SNORD
SSFips7 c1	3/22 + 0/8	3/22 + 0/8	22/22 + 8/8
SSFips7 c4	1/16	1/16	15/16
SSFips7 c7	0/12	0/12	0/12
KHP2ips8 c3	0/12	0/12	12/12
KHP2ips8 c5	0/15	0/15	13/13 tested

Figure 40. Sequence results for the PB cassette excision. The top of the figure shows the scheme of the PCR used for the excision confirmation and the sequencing results. Red arrows show the position of MEG3intron-BP14SNORD primers pair, green arrows show the primer used in Sanger sequencing. The table summarizes the number of clones that showed amplification for each primers pair. The results collected from SSFiPS7 c7 suggest that originally this clone probably was a mixed population of *MEG3* modified and un-modified cells.

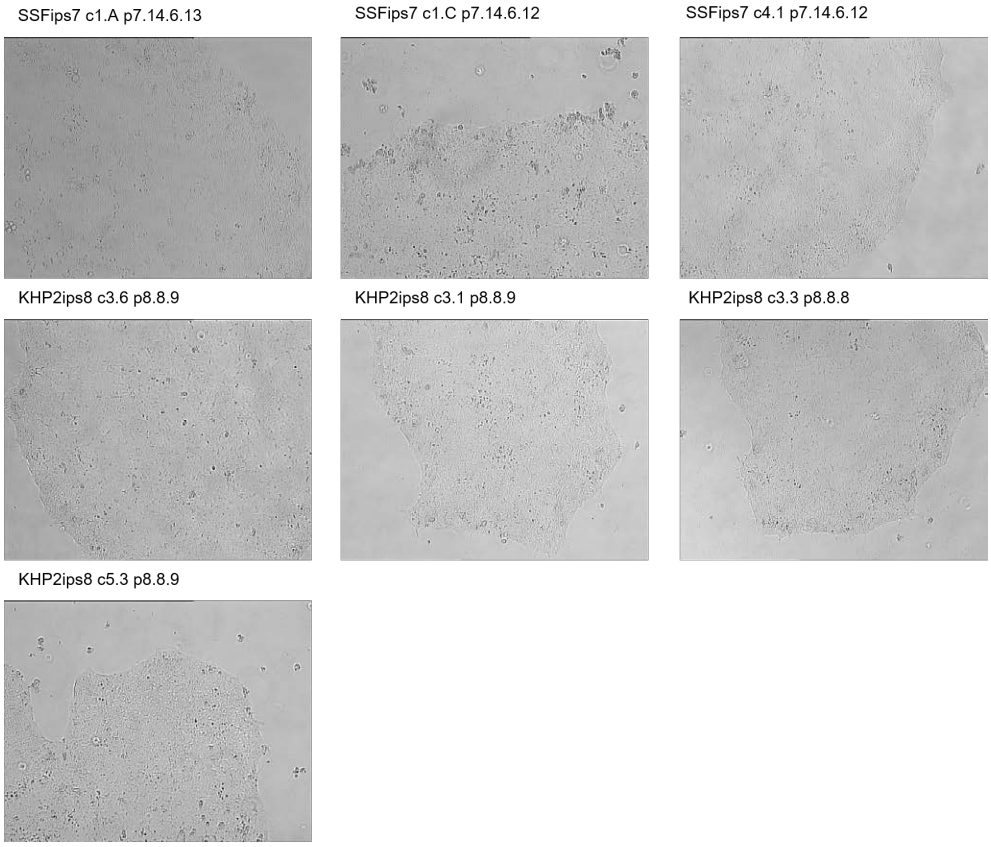

Figure 41. *MEG3* modified iPSCs morphology. The pictures show the iPSC colonies' morphology of some of the modified and correctly excised clones. They still maintain stem cell-like features, such as nuclei/cytoplasm ratio, distinguished border of colonies and so on.

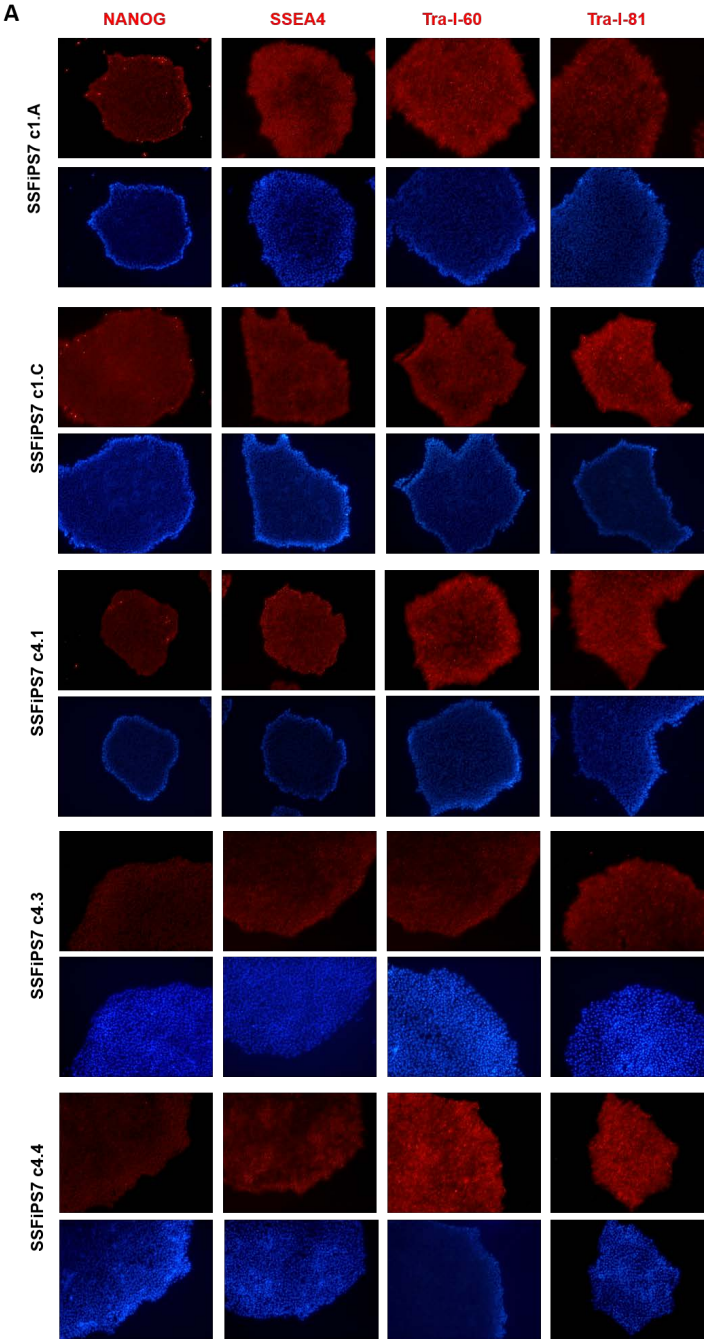
A
NANOG
SSEA4
Tra-I-60
Tra-I-81
SSFiPS7 c1.A
SSFiPS7 c1.C
SSFiPS7 c4.1
SSFiPS7 c4.3
SSFiPS7 c4.4

(Cont.)

(Cont.)

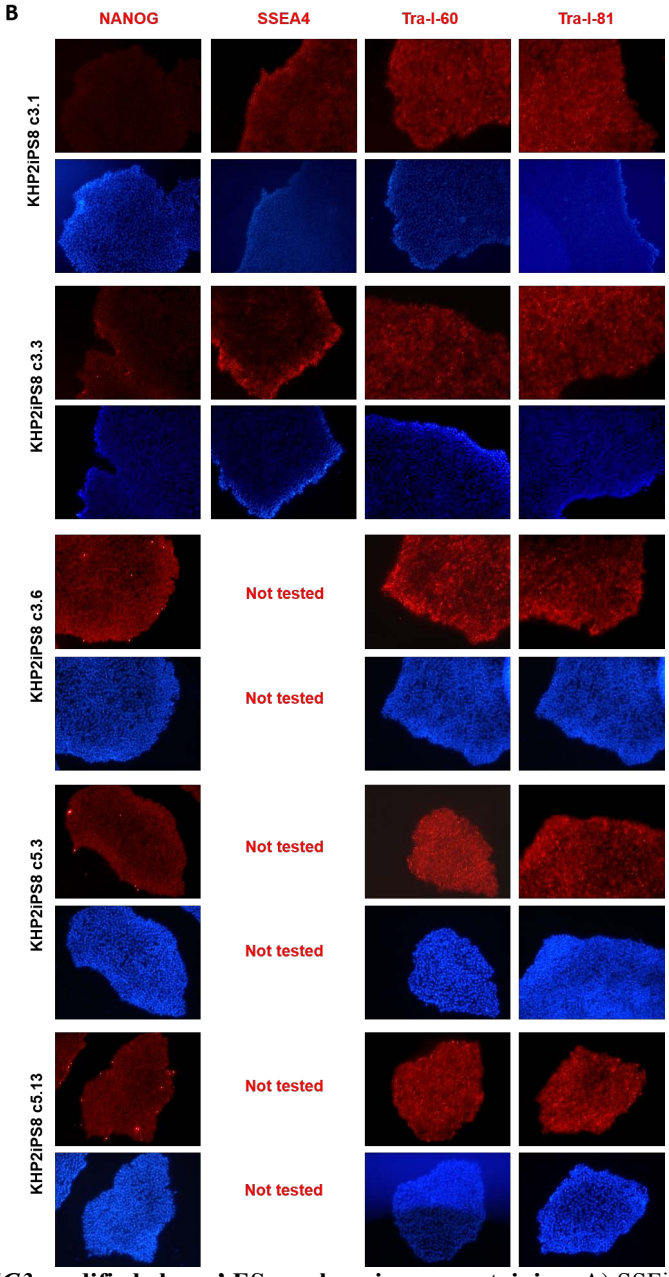

Figure 42. *MEG3* modified clones' ES markers immuno-staining. A) SSFiPS7 c1- and c4-derived clones, B) KHP2iPS8 c3- and c5-derived clones are tested for ES markers. All of modified and excised clones are positively stained.

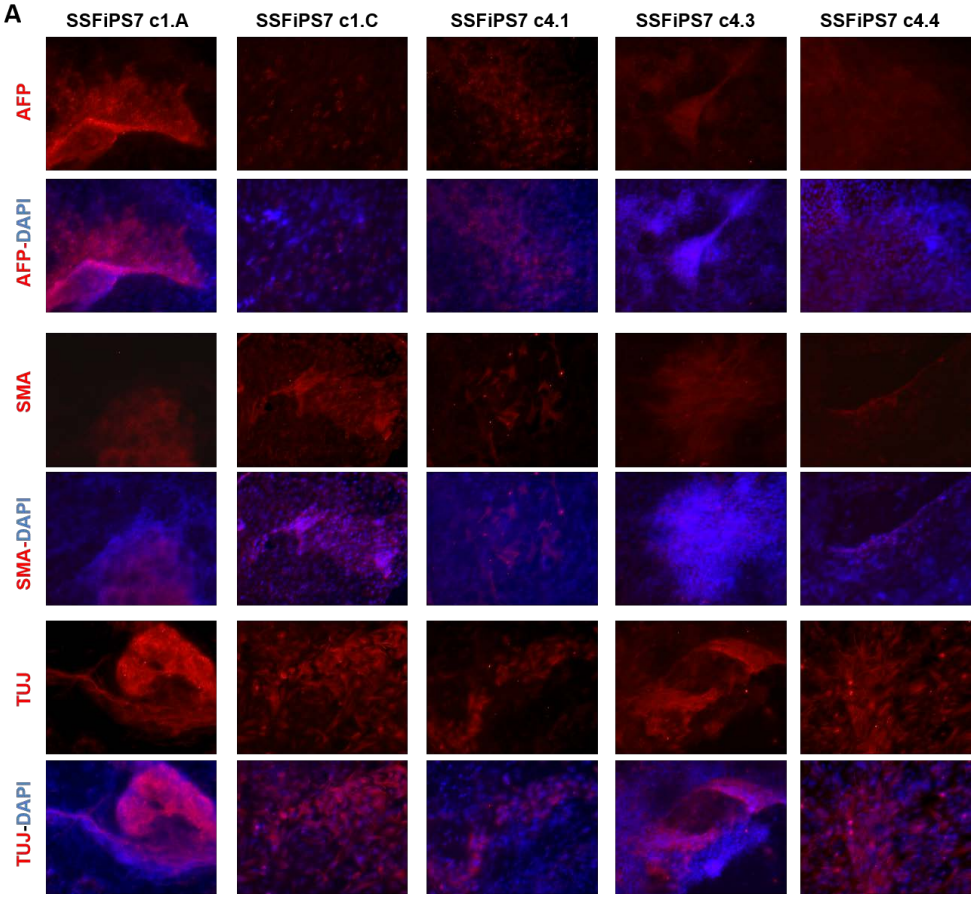
A
SSFiPS7 c1.A
SSFiPS7 c1.C
SSFiPS7 c4.1
SSFiPS7 c4.3
SSFiPS7 c4.4
AFP
AFP-DAPI
SMA
SMA-DAPI
TUJ
TUJ-DAPI

(Cont.)

(Cont.)

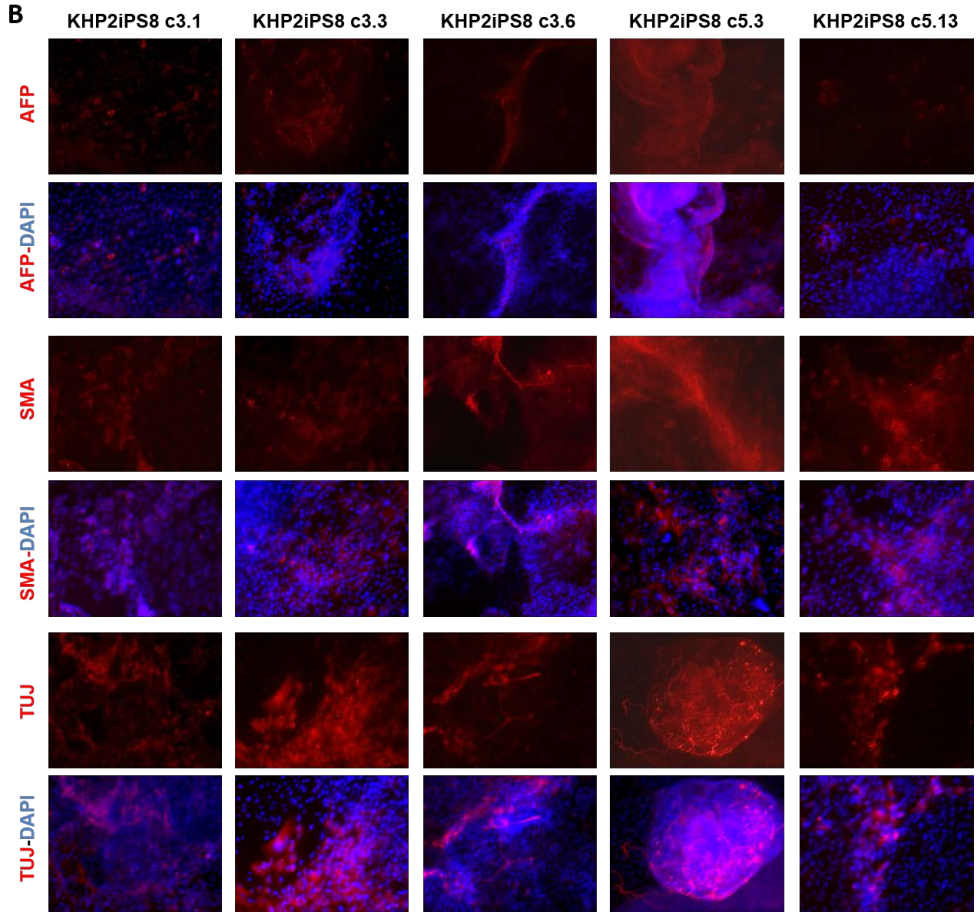

Figure 43. *MEG3* modified clones' EBs markers immuno-staining. A) SSFiPS7 c1- and c4-derived clones, B) KHP2iPS8 c3- and c5-derived clones are tested for three germ layer markers expression by immuno-staining. All tested clones are positively stained but the morphology and degree of markers staining is variable in between clones.

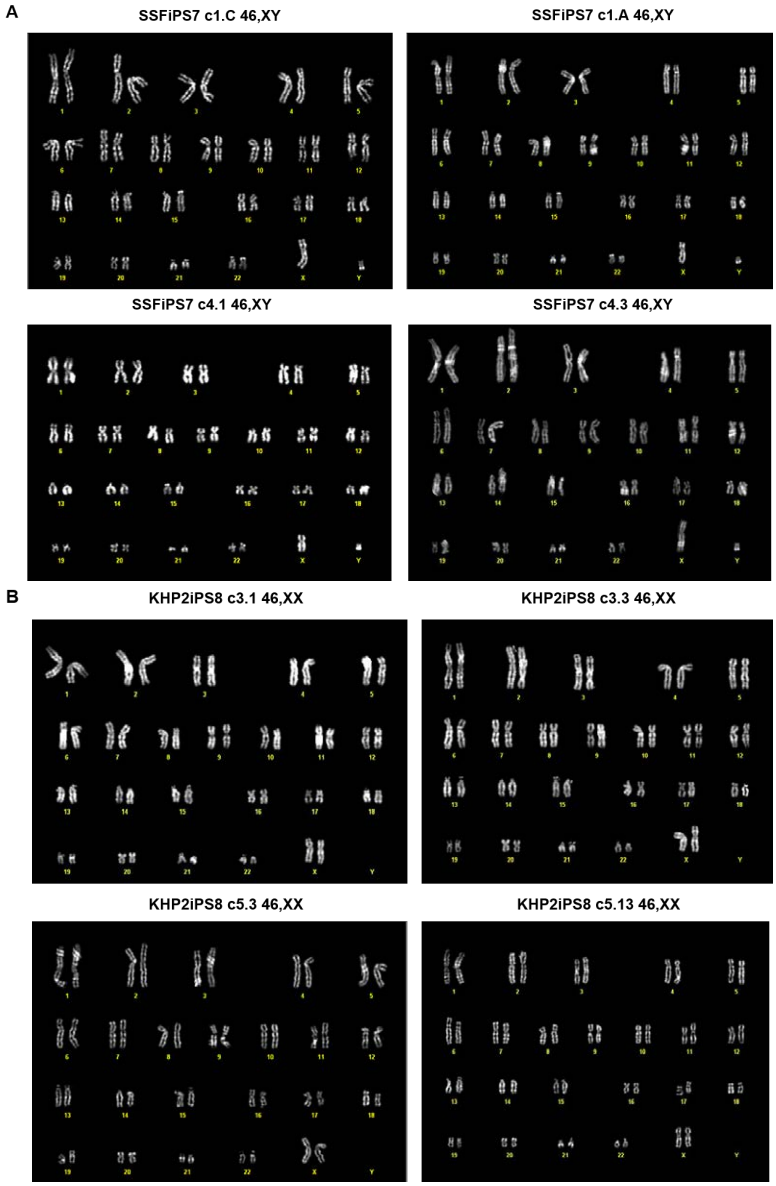

Figure 44. ***MEG3*** **modified clones' karyotype analysis.** Some of the modified and correctly excised clones from A) SSFiPS7 c1, c4 and B) KHP2ips8 c3, c5 were analyzed at karyotype level. All tested clones, but not KHP2iPS8 c3.6, showed a normal male (46,XY) or female (46,XX) karyotype.

6.1.3 Neuronal differentiation of modified clones

The generated *MEG3* modified clones were used to induce neuronal differentiation in parallel with original deleted iPSCs and controls. We used the conditions optimized on control iPSCs and already applied to the original patient-derived iPSCs. As well as SSFiPS7 and KHP2iPS8, we traced morphological changes of modified clones over neuronal differentiation experiment in the culture with NIM and BrainPhys (Figure 45). We observed again high variability in the response to the protocol between clones and some clones could not survive in even NIM until the switching time point. *MEG3* modified SSFiPS7 were more stable in culture and could be adapted to BrainPhys. However, KHP2iPS8 and its modified clones had lower tolerability to the culture condition and cell crisis was observed in all three cell lines at the first trial of differentiation. We did not test the expression of neuronal markers because of our observations in both original patients' iPSCs and *MEG3* modified clones. Overall further optimization is required to move forward testing a role of *MEG3* in Kagami-Ogata syndrome in adult neurons.

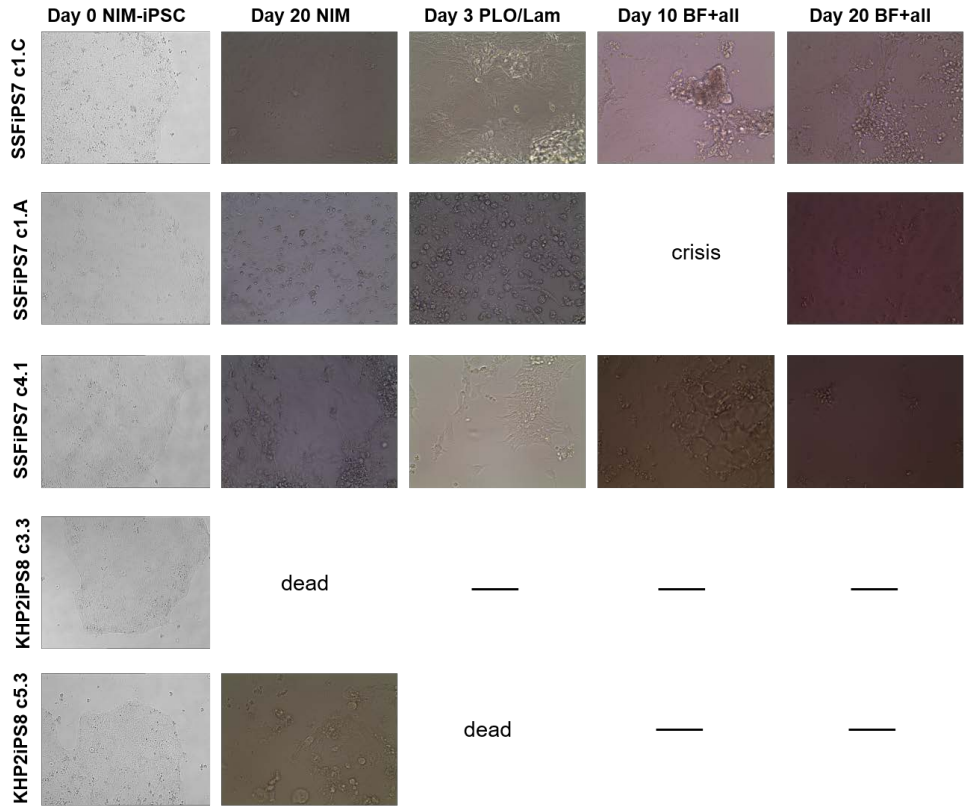

Figure 45. Neuronal differentiation in *MEG3* modified clones. The panel shows the morphological changes of tested clones in 5 different time points. We observed high variability in between the clones and low survival in KHP2iPS8-derived clones. SSFiPS7-derived clones survived better in NIM culture, but as well as original SSFiPS7 and KHP2iPS8, pictures show low survival at the BrainPhys adaptation time point (day 3 on PLO/Laminin).

6.2 Discussion

We studied a family carrying a deletion on the 14q32.2 imprinted region by iPSCs generation and CRISPR/Cas9 technique. In first session of this study, we characterized the expression level of the genes inside of the *DLK1-MEG3* domain in patient primary fibroblasts. As expected by the MPLA analysis, the deletion does not alter the DMRs activity and methylation leading to normal expression of *MEG3*. Despite many clinical reports have predicted *MEG3* is the most responsible gene in Kagami-Ogata syndrome, there is no direct evidence proved experimentally. In the case of our study, because the deletion is only on the last exon, but it is expressed, we may be able to answer the role of *MEG3* in this disorder by understanding if the transcribed deleted *MEG3* (delMEG3) is functional in our patient or not. Because of low expression level of delMEG3 in patients (Figure 12), we summarize at least the last exon of *MEG3* has an important role in its stability. This leads us two hypotheses in case that *MEG3* is responsible for this disease. 1) The deleted *MEG3* transcript is functional, but due to low expression from its instability, the patient is affected. 2) The deleted *MEG3* transcript is not functional and the patient is affected. In other words, a key regulatory/binding site is located on the last exon of *MEG3* that allows the lncRNA to be functional. In addition, 3) there is still a possibility that *MEG3* is not causative gene or not the main responsible gene in this disease. In order to evaluate these hypotheses, we used the patient-specific iPSCs we generated. First, overexpression of both wt and delMEG3 were attempted in patient-derived iPSCs. However, we were not able to obtain an assured increment of *MEG3* expression using the pCI vector. Especially, changes we observed were apparently from the alteration of *GAPDH* expression, which was highly possibly observed by higher mortality upon more plasmid DNA transfection. Because pCI vector drives gene expression by CMV promoter, it may not be strong induction enough in iPSCs as suggested by previous observation in ES cells (Norrman K et al., 2010). We then changed to a vector containing a stronger promoter sequence, the CAG promoter, so that we can reduce the amount of plasmid DNA transfected. However in this case the cell mortality was even higher after the electroporation and we were not able to analyze the results. Overall, due to high mortality, we concluded this overexpression system is not suitable for iPSCs. However, having the fact of cell death with reduced

amount of pCAG-MEG3.2, the *MEG3* overexpression might be succeeded from transient expression system even in iPSCs and it caused high mortality, which could be explained by the reported correlation between *MEG3* overexpression and p53 activation, a well-known tumor suppressor involved in apoptosis (Zhou Y et al., 2007).

Because of our difficulties in overexpression experiments, we decided to create a model of physiological *MEG3* expression by editing our patient-derived iPSCs especially because our patient still maintains intact promoter and most exons of *MEG3*. In this context, we considered three points to keep iPSC's accessibility to use in our study. 1) Modify only maternal allele, but not cause any unwanted mutation in paternal allele. This concern was solved by using allele-specific CRISPR/Cas9 guideRNA targets only the deleted maternal allele. 2) Rescue only *MEG3* in the patient-derived cell line so we can conclude *MEG3*'s role in this patient. This concern was solved by inserting only last intron and exon of *MEG3* deleted in the patient and making new breakpoints junction in the derivative cell line. 3) Remove exogenous region so only difference is the rescue of *MEG3* in patient cells. To isolate the modified clones, we utilized the drug selection marker incorporated with the *MEG3* modification. Due to exogenous promoter driving the drug gene expression, we may lose endogenous gene expression regulation surrounding it. This concern was approached by using PiggyBac system. Overall, we succeeded to model the system testing a gene involved with imprinting region and furthermore this will be used to reveal a role of imprinting genes in Kagami-Ogata syndrome.

We finally used modified clones for neuronal differentiation to test *MEG3*'s role in adult neurons, but some clones did not tolerate the protocol. Considering the KHP2iPS8 and its clones response to the differentiation protocol, we may hypothesize a specific response of this patient to the neuron induction due to the deletion, but we could not reproduce the differentiation in the control cell line too. Therefore, we cannot confirm our hypothesis. Furthermore, spontaneous differentiation during iPSCs culture (Figure 46) and during EBs formation showed a higher tendency of our patient-derived cells to differentiate into neurons-like cells, unlikely previous reports showing a decrease of neuronal markers' expression when *MEG3* was deleted (Mo CF et al., 2015) and unsuccess of our neuron induction method. Also, case 2 is the patient showing the milder phenotype

while the differentiation experiment would suggest a stronger impact from deletion on the neuronal tissues in this patient.

Taking together with the previous report regarding an impairment of neuronal differentiation in the lack of *MEG3* and our observations on iPSC culture spontaneous differentiation into neuronal lineage and EB formation experiment, it may suggest that the transcribed *MEG3* we detected is still functional in our patients and the pathological phenotype could derive from a different factor. To conclude, further optimization on the neuron induction protocol is essential to obtain stable neuronal differentiation.

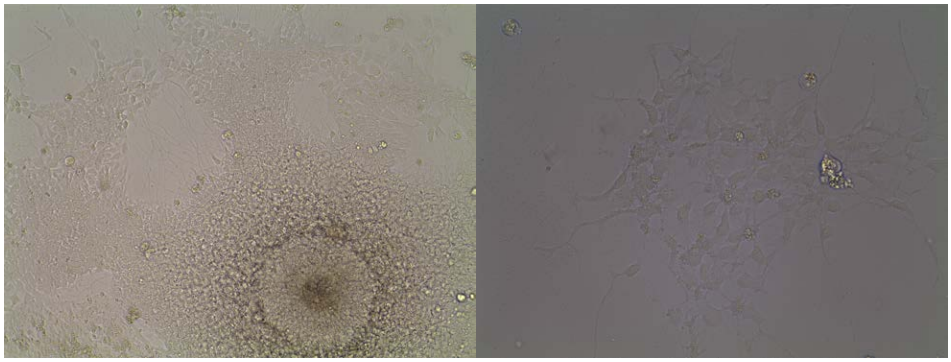

Figure 46. Spontaneous differentiation of iPSCs. Two examples of spontaneous neuron-like differentiation of iPSCs into neuron when cultured in mTeSR1. The left picture shows neuronal rosette (right bottom) and neuron-like cells extending axon (left top) in SSFiPS7 c1.A culture. The right picture shows neuron-like cells in KHP2iPS11 culture.

Considering another factor may be involved in this disease, we have interesting discovery from the expression study, related with *RTL1* expression. The mouse model and previous studies on patients' biopsies suggested an overexpression of *RTL1* due to absence of regulatory antisense expressed from the maternal allele, but as shown in the *Results*, we detected a lower expression of this gene compared with control cell lines (data confirmed in patient-derived iPSCs). This may be explained by species variability between mouse and human. Thus, we have run *in silico* analysis on miRBase (http://www.mirbase.org) which collects described miRNAs sequences and structures. From *RTL1* sequence, several miRNAs are predicted and reported. As mentioned in *State of the art*, *RTL1as* can be processed to generate some miRNAs and miRNA-127 is the most effective on *RTL1* regulation (Ito M et al., 2015). Running miRBase in human and

mouse *RTL1,* both generate miRNA-127. To confirm the target of it we then run prediction tools such as DIANA-TarBase v7.0 (http://www.diana.imis.athena-innovation.gr/DianaTools/index.php?r=tarbase/index). Interestingly, while the prediction website confirmed the targeting of *Rtl1* in mouse, it did not recognize human *RTL1* as potential target of hsa-miRNA-127. Overall, our approach making disease model from human subject could spotlight the molecular bases missing from past observations and this could enhance the importance of the human model in this disease to determine the role of both *MEG3* and *RTL1* in human. Finally, one of the most current case report showing the deletion on *RTL1* and its downstream, but not *MEG3* (Corsello G et al., 2015) and our observation on low expression level of *RTL1* let us hypothesize that *RTL1* can affect the phenotype variability in Kagami-Ogata syndrome.

7. Conclusions and perspectives

In our hands we could confirm that iPSC technology is a valuable tool to model the Kagami-Ogata syndrome and to study the molecular mechanism related with its pathogenesis. In contrast with previous reports we observed decreased level of *RTL1* and no obvious decrease of neuronal differentiation potential. Our results suggest that the modeling of Kagami-Ogata syndrome using human cells is necessary to completely understand the etiopathogenesis and the mechanism related with prognosis in Kagami-Ogata patients.

To date we obtained patient-derived iPSCs and modified patient-derived iPSCs expressing wild type *MEG3* and we are now validating the neuronal differentiation protocol to study the effect of *MEG3* in adult neurons. Our goal is to compare the gene expression of deleted patient-derived iPSCs with control iPSCs to study the effect of the deletion itself in our patients' cells. At the same time, we expect to compare original patient-derived iPSCs with the *MEG3*-rescued iPSCs in order to verify if the rescue of *MEG3* expression is enough to induce normal genes' expression when compared to healthy donor or not. With this experiment we expect to confirm or disprove the role of *MEG3* in the development of Kagami-Ogata syndrome and eventually find new targets of *MEG3* regulation.

In case of no effect from the rescuing experiment in disease's feature, we are planning to extend the investigation to *RTL1* and the other deleted genes. We still cannot exclude that a specific combination of the deleted genes, instead of a single gene, has a key role in the pathogenesis of the Kagami-Ogata syndrome. On the other hands, when *MEG3* is experimentally proved as the causative gene by this rescue experiment, we are planning to proceed with the confirmation of the gene expression data and also study more deeply about the molecular biology of *MEG3* (targets and stability) in order to find potential treatment targeting this lncRNA.

References

Barlow DP and Bartolomei MS. Genomic imprinting in mammals. Cold Spring Harb Perspect Biol 2014;6:a018382.

Benetatos L, Hatzimichael E, Londin E, Vartholomatos G, Loher P, Rigoutsos I, Briasoulis E. The microRNAs within the DLK1-DIO3 genomic region: involvement in disease pathogenesis. Cell. Mol. Life Sci. 2013;70:795-814.

Benetatos L, Vartholomatos G, Hatzimichael E. MEG3 imprinted gene contribution in tumorigenesis. Int J Cancer 2011;129:773-779.

Bens S, Kolarova J, Gillessen-Kaesbach G, Buiting K, Beygo J, Caliebe A, Ammerpohl O, Siebert R. The differentially methylated region of MEG8 is hypermethylated in patients with Temple syndrome. Epigenomics. 2015;7:1089-1097.

Bershteyn M, Hayashi Y, Desachy G, Hsiao EC, Sami S, Tsang KM, Weiss LA, Kriegstein AR, Yamanaka S, Wynshaw-Boris A. Cell-autonomous correction of ring chromosomes in human induced pluripotent stem cells. Nature. 2014;507:99-103.

Beygo J, Küchler A, Gillessen-Kaesbach G, Albrecht B, Eckle J, Eggermann T, Gellhaus A, Kanber D, Kordaß U, Lüdecke HJ, Purmann S, Rossier E, van de Nes J, van der Werf IM, Wenzel M, et al. New insights into the imprinted MEG8-DMR in 14q32 and clinical and molecular description of novel patients with Temple syndrome. European Journal of Human Genetics 2017;25:935-945.

Beygo, J., Elbracht, M., de Groot, K., Begemann, M., Kanber, D., Platzer, K. Gillessen-Kaesbach G, Vierzig A, Green A, Heller R, Buiting K, Eggermann T. Novel deletions affecting the MEG3-DMR provide further

evidence for a hierarchical regulation of imprinting in 14q32. Eur. J. Hum. 2015;23:180-188.

Brannan CI, Dees EC, Ingram RS, Tilghman SM. The product of the H19 gene may function as an RNA. Mol. Cell. Biol. 1990;20:28-36.

Brockdorff N, Ashworth A, Kay GF, McCabe VM, Norris DP, Cooper PJ, Swift S, Rastan S. The product of the mouse Xist gene is a 15 kb inactive X-specific transcript containing no conserved ORF and located in the nucleus. Cell 1992;71:515-526.

Brown CJ, Hendrich BD, Rupert JL, Lafrenière RG, Xing Y, Lawrence J, Willard HF. The human XIST gene: analysis of a 17 kb inactive X-specific RNA that contains conserved repeats and is highly localized within the nucleus. Cell 1992;71:527-542.

Cabili MN, Trapnell C, Goff L, Koziol M, Tazon-Vega B, Regev A, Rinn JL. Integrative annotation of human large intergenic noncoding RNAs reveals global properties and specific subclasses. Genes Dev. 2011;25:1915-1927.

Carlsson, C, Tornehave D, Lindberg KP, Galante N, Billestrup B, Michelsen L, Larsson I, Nielsen JH. Growth hormone and prolactin stimulate the expression of rat preadipocyte factor-1/delta-like protein in pancreatic islets: molecular cloning and expression pattern during development and growth of the endocrine pancreas. Endocrinology 1997;138**:**3940-3948.

Carr MS, Yevtodiyenko A, Schmidt CL, Schmidt JV. Allele-specific histone modifications regulate expression of the Dlk1-Gtl2 imprinted domain. Genomics 2007;89:280-290.

Cavaillé J, Seitz H, Paulsen M, Ferguson-Smith AC, Bachellerie JP. Identification of tandemly-repeated C/D snoRNA genes at the imprinted human 14q32 domain reminiscent of those at the Prader-Willi/Angelman syndrome region. Hum Mol Genet. 2002;11:1527-1538.

Classen CF, Riehmer V, Landwehr C, Kosfeld A, Heilmann S, Scholz C, Kabisch S, Engels H, Tierling S, Zivicnjak M, Schacherer

F, Haffner D, Weber RG. Dissecting the genotype in syndromic intellectual disability using whole exome sequencing in addition to genome-wide copy number analysis. Human Genetics 2013;132:825-841.

Cleaton MA, Dent CL, Howard M, Corish JA, Gutteridge I, Sovio U, Gaccioli F, Takahashi N, Bauer SR, Charnock-Jones DS, Powell TL, Smith GC, Ferguson-Smith AC, Charalambous M. Fetus-derived DLK1 is required for maternal metabolic adaptations to pregnancy and is associated with fetal growth restriction. Nat Genet. 2016;48:1473-1480.

Corsello G, Salzano E, Vecchio D, Antona V, Grasso M, Malacarne M, Carella M, Palumbo P, Piro E, Giuffrè M. Paternal uniparental disomy chromosome 14-like syndrome due a maternal de novo 160 kb deletion at the 14q32.2 region not encompassing the IG- and the MEG3-DMRs: Patient report and genotype–phenotype correlation. AJMG 2015;167:3130–3138.

da Rocha ST, Charalambous M, Lin SP, Gutteridge I, Ito Y, Gray D, Dean W, Ferguson-Smith AC. Gene dosage effects of the imprinted delta-like homologue 1 (dlk1/pref1) in development: implications for the evolution of imprinting. PLoS Genet. 2009;5:e1000392.

D'Aiuto L, Zhi Y, Kumar Das D, Wilcox MR, Johnson JW, McClain L, MacDonald ML, Di Maio R, Schurdak ME, Piazza P, Viggiano L, Sweet R, Kinchington PR, Bhattacharjee AG, Yolken R, et al. Large-scale generation of human iPSC-derived neural stem cells/early neural progenitor cells and their neuronal differentiation. Organogenesis. 2014;10:365-377.

Dauber A, Cunha-Silva M, Macedo DB, Brito VN, Abreu AP, Roberts SA, Montenegro LR, Andrew M, Kirby A, Weirauch MT, Labilloy G, Bessa DS, Carroll RS, Jacobs DC, Chappell PE, et al. Paternally inherited dlk1 deletion associated with familial central precocious puberty. J Clin Endocrinol Metab. 2017;102:1557-1567.

Davis E, Caiment F, Tordoir X, Cavaillé J, Ferguson-Smith A, Cockett N, Georges M, Charlier C. RNAi-mediated allelic trans-interaction at the imprinted Rtl1/Peg11 locus. Curr Biol. 2005;15:743-749.

Duker AL, Ballif BC, Bawle EV, Person RE, Mahadevan S, Alliman S, Thompson R, Traylor R, Bejjani BA, Shaffer LG, Rosenfeld JA, Lamb AN, Sahoo T. Paternally inherited microdeletion at 15q11.2 confirms a significant role for the SNORD116 C/D box snoRNA cluster in Prader–Willi syndrome. European Journal of Human Genetics 2010;18:1196-1201.

Duret L, Chureau C, Samain S, Weissenbach J, Avner P. The Xist RNA gene evolved in eutherians by pseudogenization of a protein-coding gene. Science 2006;312:1653-1655.

Eggermann T, Perez de Nanclares G, Maher ER, Temple IK, Tümer Z, Monk D, Mackay DJ, Grønskov K, Riccio A, Linglart A, Netchine I. Imprinting disorders: a group of congenital disorders with overlapping patterns of molecular changes affecting imprinted loci. Clin Epigenetics. 2015;7:123. (B)

Eggermann T, Soellner L, Buiting K, Kotzot D. Mosaicism and uniparental disomy in prenatal diagnosis. Trends Mol Med. 2015;21:77-87. (A)

Elisaphenko EA, Kolesnikov NN, Shevchenko AI, Rogozin IB, Nesterova TB, Brockdorff N, Zakian SM. A dual origin of the Xist gene from a protein-coding gene and a set of transposable elements. PLoS One. 2008;3:e2521.

Faghihi MA and Wahlestedt C. Regulatory roles of natural antisense transcripts. Nat. Rev. Mol. Cell Biol. 2009;10:637-643.

Ferrón SR, Charalambous M, Radford E, McEwen K, Wildner H, Hind E, Morante-Redolat JM, Laborda J, Guillemot F, Bauer SR, Fariñas I, Ferguson-Smith AC. Postnatal loss of Dlk1 imprinting in stem cells and niche-astrocytes regulates neurogenesis. Nature. 2011;475:381-385.

Forabosco A., Percesepe A., Santucci S. Incidence of non-age-dependent chromosomal abnormalities: a population-based study on 88965 amniocenteses**.** Eur J Hum Genet. 2009;17:897-903.

Gaj T, Gersbach CA, Barbas CF 3rd. ZFN, TALEN, and CRISPR/Cas-based methods for genome engineering. Trends Biotechnol 2013;31:397-405.

Garneau JE, Dupuis MÈ, Villion M, Romero DA, Barrangou R, Boyaval P, Fremaux C, Horvath P, Magadán AH, Moineau S. The CRISPR/Cas bacterial immune system cleaves bacteriophage and plasmid DNA. Nature 2010;468:67-71.

Georgiades P, Watkins M, Surani MA, Ferguson-Smith AC. Parental origin-specific developmental defects in mice with uniparental disomy for chromosome 12. Development 2000;127:4719-4728.

Gordon FE, Nutt CL, Cheunsuchon P, Nakayama Y, Provencher KA, Rice KA, Zhou Y, Zhang X, Klibanski A. Increased expression of angiogenic genes in the brains of mouse meg3-null embryos**.** Endocrinology. 2010;151:2443-2452.

Gu L, Zhang J, Shi M, Zhan Q, Shen B, Peng C. lncRNA MEG3 had anti-cancer effects to suppress pancreatic cancer activity. Biomed Pharmacother. 2017;89:1269-1276.

Gu T, He H, Han Z, Zeng T, Huang Z, Liu Q, Gu N, Chen Y, Sugimoto K, Jiang H, Wu Q. Expression of macro non-coding RNAs Meg8 and Irm in mouse embryonic development. Acta Histochem. 2012;114:392-399.

Guil S, Soler M, Portela A, Carrère J, Fonalleras E, Gómez A, Villanueva A, Esteller M. Intronic RNAs mediate EZH2 regulation of epigenetic targets. Nat. Struct. Mol. Biol. 2012;19:664–670.

Guo Q, Qian Z, Yan D, Li L, Huang L. LncRNA-MEG3 inhibits cell proliferation of endometrial carcinoma by repressing Notch signaling. Biomed Pharmacother. 2016;82:589-594.

Guttman M, Amit I, Garber M, French C, Lin MF, Feldser D, Huarte M, Zuk O, Carey BW, Cassady JP, Cabili MN, Jaenisch R, Mikkelsen TS, Jacks T, Hacohen N, et al. Chromatin signature reveals over a thousand highly conserved large non-coding RNAs in mammals. Nature 2009;458:223-227.

Hagan JP, O'Neill BL, Stewart CL, Kozlov SV, Croce CM. At least ten genes define the imprinted Dlk1-Dio3 cluster on mouse chromosome 12qF1. Plos one 2009;4:e4352.

Hansen LH, Madsen B, Teisner B, Nielsen JH, Billestrup N. Characterization of the inhibitory effect of growth hormone on primary preadipocyte differentiation. Mol Endocrinol. 1998;12:1140-9.

He C, Yang W, Yang J, Ding J, Li S, Wu H, Zhou F, Jiang Y, Teng L, Yang J. Long Noncoding RNA MEG3 Negatively Regulates Proliferation and Angiogenesis in Vascular Endothelial Cells. DNA Cell Biol. 2017;36:475-481.

He Y, Vogelstein B, Velculescu VE, Papadopoulos N, Kinzler KW. The antisense transcriptomes of human cells. Science 2008;322:1855-1857.

Hernandez A, Martinez ME, Fiering S, Galton VA, St. Germain D. Type 3 deiodinase is critical for the maturation and function of the thyroid axis. J Clin Invest. 2006;116:476-484.

Hitachi K and Tsuchida K. Myostatin-deficiency in mice increases global gene expression at the Dlk1-Dio3 locus in the skeletal muscle. Oncotarget. 2017;8:5943-5953.

Huang SA, Tu HM, Harney JW, Venihaki M, Butte AJ, Kozakewich HPW, Fishman SJ, Larsen PR. Severe hypothyroidism caused by type 3 iodothyronine deiodinase in infantile hemangiomas. New Eng. J. Med. 2000;343:185-189.

Huang ZL, Chen RP, Zhou XT, Zhan HL, Hu MM, Liu B, Wu GD, Wu LF. Long non-coding RNA MEG3 induces cell apoptosis in esophageal cancer through endoplasmic reticulum stress. Oncol Rep. 2017;37:3093-3099.

Irving MD, Buiting K, Kanber D, Donaghue C, Schulz R, Offiah A, Mohammed SN, Oakey RJ. Segmental Paternal Uniparental Disomy (patUPD) of 14q32 With Abnormal Methylation Elicits the Characteristic Features of Complete patUPD14. Am J Med Genet A. 2010;152A:1942-1950.

Ito M, Sferruzzi-Perri AN, Edwards CA, Adalsteinsson BT, Allen SE, Loo TH, Kitazawa M, Kaneko-Ishino T, Ishino F, Stewart CL, Ferguson-Smith AC. A trans-homologue interaction between reciprocally imprinted miR-127 and Rtl1 regulates placenta development. Development. 2015;142:2425-2430.

Ji P, Diederichs S, Wang W, Böing S, Metzger R, Schneider PM, Tidow N, Brandt B, Buerger H, Bulk E, Thomas M, Berdel WE, Serve H, Müller-Tidow C. MALAT-1, a novel noncoding RNA, and thymosin beta4 predict metastasisandsurvival inearly-stage non-smallcell lung cancer. Oncogene 2003;22:8031–8041.

Kagami M, Matsuoka K, Nagai T, Yamanaka M, Kurosawa K, Suzumori N, Sekita Y, Miyado M, Matsubara K, Fuke T, Kato F, Fukami M, Ogata T. Paternal uniparental disomy 14 and related disorders. Placental gene expression analyses and histological examinations. Epigenetics. 2012;7:1142-1150.

Kagami M, O'Sullivan MJ, Green AJ, Watabe Y, Arisaka O, Masawa N, Matsuoka K, Fukami M, Matsubara K, Kato F, Ferguson-Smith AC, Ogata T. The IG-DMR and the MEG3 -DMR at human chromosome 14q32.2: hierarchical interaction and distinct functional properties as imprinting control centers. plos genetics 2010;6:e1000992.

Kagami M, Sekita Y, Nishimura G, Irie M, Kato F, Okada M, Yamamori S, Kishimoto H, Nakayama M, Tanaka Y, Matsuoka K, Takahashi T, Noguchi M, Tanaka Y, Masumoto K, et al. Deletions and epimutations affecting the human 14q32.2 imprinted region in individuals with paternal and maternal upd(14)-like phenotypes**.** Nat Genet. 2008;40:237-242.

Kagami, M., Kato, F., Matsubara, K., Sato, T., Nishimura, G., Ogata, T. Relative frequency of underlying genetic causes for the development of UPD(14)pat-like phenotype. Eur. J. Hum. Genet. 2012;20:928-932.

Kagami, M., Kurosawa, K., Miyazaki, O., Ishino, F., Matsuoka, K., Ogata, T. Comprehensive clinical studies in 34 patients with molecularly defined UPD(14)pat and related conditions (Kagami-Ogata syndrome). Eur. J. Hum. Genet 2015;23:1488-1498.

Kanduri C, Thakur N, Pandey RR. The length of the transcript encoded from the Kcnq1ot1 antisense promoter determines the degree of silencing. EMBO J. 2006;25:2096-2106.

Kaneta, M., Osawa M, Sudo K, Nakauchi H, Farr AG, Takahama Y. A role for pref-1 and HES-1 in thymocyte development. J. Immunol. 2000;164**:**256-264.

Katayama S, Tomaru Y, Kasukawa T, Waki K, Nakanishi M, Nakamura M, Nishida H, Yap CC, Suzuki M, Kawai J, Suzuki H, Carninci P, Hayashizaki Y, Wells C, Frith M, et al., Antisense transcription in the mammalian transcriptome. Science 2005;309:1564–1566.

Kim T, Plona K, Wynshaw-Boris A. A novel system for correcting large-scale chromosomal aberrations: ring chromosome correction via reprogramming into induced pluripotent stem cell (iPSC). Chromosoma. 2017;126:457-463.

Kim TK, Hemberg M, Gray JM, Costa AM, Bear DM, Wu J, Harmin DA, Laptewicz M, Barbara-Haley K, Kuersten S, Markenscoff-Papadimitriou E, Kuhl D, Bito H, Worley PF, Kreiman G, Greenberg ME. Widespread transcription at neuronal activity-regulated enhancers. Nature 2010;465:182-187.

Kota SK, Llères D, Bouschet T, Hirasawa R, Marchand A, Begon-Pescia C, Sanli I, Arnaud P, Journot L, Girardot M, Feil R. ICR noncoding RNA expression controls imprinting and DNA replication at the Dlk1-Dio3 domain. Developmental Cell 2014;31:19-33.

Kung JT, Colognori D, Lee JT. Long Noncoding RNAs: Past, Present, and Future. Genetics. 2013;193:651-669.

Kwon J, Lee N, Jeon I, Lee HJ, Do JT, Lee DR, Oh SH, Shin DA, Kim A, Song J. Neuronal Differentiation of a Human Induced Pluripotent Stem Cell Line (FS-1) Derived from Newborn Foreskin Fibroblasts. Int J Stem Cells. 2012;5:140-145.

Lee JT, Davidow LS, Warshawsky D. Tsix, a gene antisense to Xist at the X-inactivation centre. Nat. Genet. 1999;21:400-404.

Li LB, Chang KH, Wang PR, Hirata RK, Papayannopoulou T, Russell DW. Trisomy correction in Down syndrome induced pluripotent stem cells. Cell Stem Cell. 2012;11:615-619.

Li X, Burnight ER, Cooney AL, Malani N, Brady T, Sander JD, Staber J, Wheelan SJ, Joung JK, McCray PB Jr, Bushman FD, Sinn PL, Craig NL. PiggyBac transposase tools for genome engineering. Proc Natl Acad Sci USA. 2013;110:E2279-E2287.

Li Z, Jin C, Chen S, Zheng Y, Huang Y, Jia L, Ge W, Zhou Y. Long non-coding RNA MEG3 inhibits adipogenesis and promotes osteogenesis of human adipose-derived mesenchymal stem cells via miR-140-5p. Mol Cell Biochem 2017;433:51.

Lieber MR, Ma Y, Pannicke U, Schwarz K. Mechanism and regulation of human non-homologous DNA end-joining. Nat Rev Mol Cell Biol 2003;4:712-720.

Lin SP, Coan P, Teixeira da Rocha S, Seitz H, Cavaille J, Teng PW, Takada S, Ferguson-Smith AC. Differential regulation of imprinting in the murine embryo and placenta by the Dlk1-Dio3 imprinting control region. Development 2007;134:417-426.

Lin SP, Youngson N, Takada S, Seitz H, Reik W, Paulsen M, Cavaille J, Ferguson-Smith AC. Asymmetric regulation of imprinting on the maternal and paternal chromosomes at the Dlk1-Gtl2imprinted cluster on mouse chromosome 12. Nature genetics 2003;35:97-102.

Liu H and Zhang SC. Specification of neuronal and glial subtypes from human pluripotent stem cells. Cell Mol Life Sci. 2011; 68:3995-4008.

Liu S, Zhu J, Jiang T, Zhong Y, Tie Y, Wu Y, Zheng X, Jin Y, Fu H. Identification of lncRNA MEG3 binding protein using ms2-tagged rna affinity purification and mass spectrometry. Appl Biochem Biotechnol 2015;176:1834-1845.

Lu KH, Li W, Liu XH, Sun M, Zhang ML, Wu WQ, Xie WP, Hou YY. Long non-coding RNA MEG3 inhibits NSCLC cells proliferation and induces apoptosis by affecting p53 expression. BMC Cancer. 2013;13:461.

Luo G, Wang M, Wu X, Tao D, Xiao X, Wang L, Min F, Zeng F, Jiang G. Long Non-Coding RNA MEG3 Inhibits Cell Proliferation and Induces Apoptosis in Prostate Cancer. Cell Physiol Biochem. 2015;37:2209-2220.

Lyle R1, Watanabe D, te Vruchte D, Lerchner W, Smrzka OW, Wutz A, Schageman J, Hahner L, Davies C, Barlow DP. The imprinted antisense RNA at the Igf2r locus overlaps but does not imprint Mas1. Nat. Genet. 2000;25:19-21.

Martinez ME, Cox DF, Youth BP, Hernandez A. Genomic imprinting of DIO3, a candidate gene for the syndrome associated with human uniparental disomy of chromosome 14. European Journal of Human Genetics 2016;24:1617-1621.

McMurray EN and Schmidt JV. Identification of imprinting regulators at the Meg3 differentially methylated region. Genomics 2012;100:184-194.

Michalczyk A, Varigos G, Smith L, Ackland ML. Fresh and cultured buccal cells as a source of mRNA and protein for molecular analysis. BioTechniques 2004;37:262-269

Miyoshi N, Wagatsuma H, Wakana S, Shiroishi T, Nomura M, Aisaka K, Kohda T, Surani MA, Kaneko-Ishino T, Ishino F. Identification of an imprinted gene, Meg3/Gtl2 and its human homologue MEG3, first mapped on mouse distal chromosome 12 and human chromosome 14q. Genes Cells 2000;5:211-220.

Mo CF, Wu FC, Tai KY, Chang WC, Chang KW, Kuo HC, Ho HN, Chen HF, Lin SP. Loss of non-coding RNA expression from the DLK1-DIO3 imprinted locus correlates with reduced neural differentiation potential in human embryonic stem cell lines. Stem Cell Res Ther. 2015;6:1.

Mondal T, Subhash S, Vaid R, Enroth S, Uday S, Reinius B, Mitra S, Mohammed A, James AR, Hoberg E, Moustakas A, Gyllensten U, Jones SJ, Gustafsson CM, Sims AH, et al. MEG3 long noncoding RNA regulates the TGF-b pathway genes through formation of RNA–DNA triplex structures. Nat Commun. 2015;6:7743.

Moon YS, Smas CM, Lee K, Villena JA, Kim KH, Yun EJ, Sul HS. Mice Lacking Paternally Expressed Pref-1/Dlk1 Display Growth Retardation and Accelerated Adiposity. Mol Cell Biol. 2002;22:5585-5592.

Müller D, Cherukuri P, Henningfeld K, Poh CH, Wittler L, Grote P, Schlüter O, Schmidt J, Laborda J, Bauer SR, Brownstone RM, Marquardt T. Dlk1 promotes a fast motor neuron biophysical signature required for peak force execution. Science 2014;343:1264-1266.

Murphy SK, Wylie AA, Coveler KJ, Cotter PD, Papenhausen PR, Sutton VR, Shaffer LG, Jirtle LR. Epigenetic Detection of Human Chromosome 14 Uniparental Disomy. Human mutation 2003;22:92-97.

Norrman K, Fischer Y, Bonnamy B, Wolfhagen Sand F, Ravassard P, Semb H. Quantitative comparison of constitutive promoters in human ES cells. PLoS One 2010;5:e12413.

Ogata T and Kagami M. Kagami–Ogata syndrome: a clinically recognizable upd(14)pat and related disorder affecting the chromosome 14q32.2 imprinted region. Journal of Human Genetics 2016;61:87-94.

Ohno, N., Izawa A, Hattori M, Kageyama R, Sudo T. dlk inhibits stem cell factor-induced colony formation of murine hematopoietic progenitors: Hes-1-independent effect. Stem Cells 2001;19**:**71-79.

Peng W, Si S, Zhang Q, Li C, Zhao F, Wang F, Yu J, Ma R. Long non-coding RNA MEG3 functions as a competing endogenous RNA to regulate gastric cancer progression. J Exp Clin Cancer Res. 2015;34:79.

Phillips MD, Kuznetsov SA, Cherman N, Park K, Chen KG, McClendon BN, Hamilton RS, McKay RD, Chenoweth JG, Mallon BS, Robey PG. Directed differentiation of human induced pluripotent stem cells toward bone and cartilage: in vitro versus in vivo assays. Stem Cells Transl Med. 2014;3:867-878.

Qin R, Chen Z, Ding Y, Hao J, Hu J, Guo F. Long non-coding RNA MEG3 inhibits the proliferation of cervical carcinoma cells through the induction of cell cycle arrest and apoptosis. Neoplasma. 2013;60:486-492.

Raghunandan R, Ruiz-Hidalgo M, Jia Y, Ettinger R, Rudikoff E, Riggins P, Farnsworth R, Tesfaye A, Laborda J, Bauer SR. Dlk1 influences differentiation and function of B lymphocytes. Stem Cells Dev. 2008;17:495-507.

Ran FA, Hsu PD, Wright J, Agarwala V, Scott DA, Zhang F. Genome engineering using the CRISPR-Cas9 system. Nat Protoc. 2013;8:2281-308.

Rhee M, Lee SH, Kim JW, Ham DS, Park HS, Yang HK, Shin JY, Cho JH, Kim YB, Youn BS, Sul HS, Yoona KH. Preadipocyte factor 1 induces pancreatic ductal cell differentiation into insulin-producing cells. Sci Rep. 2016;6:23960.

Rinn JL1, Kertesz M, Wang JK, Squazzo SL, Xu X, Brugmann SA, Goodnough LH, Helms JA, Farnham PJ, Segal E, Chang HY. Functional demarcation of active and silent chromatin domains in human HOX loci by noncoding RNAs. Cell 2007;129:1311-1323.

Rosenfeld JA, Fox JE, Descartes M, Brewer F, Stroud T, Gorski JL, Upton SJ, Moeschler JB, Monteleone B, Neill NJ, Lamb AN, Ballif BC, Shaffer LG, Ravnan JB. Clinical features associated with copy number variations of the 14q32 imprinted gene cluster. Am J Med Genet Part A 2015;167A:345-353.

Saleh-Gohari N and Helleday T. Conservative homologous recombination preferentially repairs DNA double-strand breaks in the S phase of the cell cycle in human cells. Nucleic Acids Res. 2004;32:3683-3688.

Schmidt, J.V., Matteson, P.G., Jones, B.K., Guan, X.J., Tilghman, S.M. The Dlk1 and Gtl2 genes are linked and reciprocally imprinted. Genes Dev. 2000;14:1997-2002.

Seitz H, Youngson N, Lin SP, Dalbert S, Paulsen M, Bachellerie JP, Ferguson-Smith AC, Cavaillé J. Imprinted microRNA genes transcribed antisense to a reciprocally imprinted retrotransposon-like gene. Nature Genetics 2003;34:261-262.

Sekita Y, Wagatsuma H, Nakamura K, Ono R, Kagami M, Wakisaka N, Hino T, Suzuki-Migishima R, Kohda T, Ogura A, Ogata T, Yokoyama M, Kaneko-Ishino T, Ishino F. Role of retrotransposon-derived imprinted gene, Rtl1, in the feto-maternal interface of mouse placenta. Nat Genet. 2008;40:243-248.

Shao L and Wu WS. Gene-delivery systems for iPS cell generation. Expert Opin Biol Ther. 2010;10:231-242.

Sharma SM, Fuchsluger T, Ahmad S, Katikireddy KR, Armant M, Dana R, Jurkunas UV. Comparative Analysis of Human-Derived Feeder Layers with 3T3 Fibroblasts for the Ex Vivo Expansion of Human Limbal and Oral Epithelium. Stem Cell Rev. 2012;8:696-705.

Sheng X, Li J, Yang L, Chen Z, Zhao Q, Tan L, Zhou Y, Li J. Promoter hypermethylation influences the suppressive role of maternally expressed 3, a long non-coding RNA, in the development of epithelial ovarian cancer. Oncol Rep. 2014;32:277-285.

Sonoda E, Sasaki MS, Morrison C, Yamaguchi-Iwai Y, Takata M, Takeda S. Sister chromatid exchanges are mediated by homologous recombination in vertebrate cells. Mol Cell Biol. 1999;19:5166-5169.

Spits H and Yssel H. Cloning of Human T and Natural Killer Cells. Methods. 1996 Jun;9:416-421.

Sun L, Li Y, Yang B. Downregulated long non-coding RNA MEG3 in breast cancer regulates proliferation, migration and invasion by depending on p53's transcriptional activity. Biochem Biophys Res Commun. 2016;478:323-329.

Suzuki S, Sargent RG, Illek B, Fischer H, Esmaeili-Shandiz A, Yezzi MJ, Lee A, Yang Y, Kim S, Renz P, Qi Z, Yu J, Muench MO, Beyer AI, Guimarães AO, et al. TALENs facilitate single-step seamless sdf correction of f508del CFTR in airway epithelial submucosal gland cell-derived CF-iPSCs. Mol Ther Nucleic Acids. 2016;5:e273.

Takada S, Tevendale M, Baker J, Georgiades P, Campbell E, Freeman T, Johnson MH, Paulsen M, Ferguson-Smith AC. Delta-like and Gtl2 are reciprocally expressed, differentially methylated linked imprinted genes on mouse chromosome 12. Current Biology 2000;10:1135-1138.

Takahashi K and Yamanaka S. Induction of pluripotent stem cells from mouse embryonic and adult fibroblast cultures by defined factors. Cell 2006;26:663-676.

Takahashi K, Tanabe K, Ohnuki M, Narita M, Ichisaka T, Tomoda K, Yamanaka S. Induction of pluripotent stem cells from adult human fibroblasts by defined factors. Cell 2007;131:861-872.

Temple I. K., Cockwell A., Hassold T., Pettay D., Jacobs P. Maternal uniparental disomy for chromosome 14. J. Med. Genet. 1991;28:511-514.

Temple I. K., Shrubb V., Lever M., Bullman H., Mackay D. J. G. Isolated imprinting mutation of the DLK1/GTL2 locus associated with a clinical presentation of maternal uniparental disomy of chromosome 14. J. Med. Genet.2007;44:637-640.

Terashima M, Tange S, Ishimura A, Suzuki T. MEG3 Long Noncoding RNA Contributes to the Epigenetic Regulation of Epithelial-Mesenchymal Transition in Lung Cancer Cell Lines. J Biol Chem. 2017;292:82-99.

Tian ZZ, Guo XJ, Zhao YM, Fang Y. Decreased expression of long non-coding RNA MEG3 acts as a potential predictor biomarker in progression and poor prognosis of osteosarcoma. Int J Clin Exp Pathol. 2015;8:15138-15142.

Tsai, C.-E., Lin SP, Ito M, Takagi N, Takada S, Ferguson-Smith AC. Genomic imprinting contributes to thyroid hormone metabolism in the mouse embryo. Curr. Biol. 2002;12:1221-1226.

Ulitsky I, Shkumatava A, Jan CH, Sive H, Bartel DP. Conserved function of lincRNAs in vertebrate embryonic development despite rapid sequence evolution. Cell 2011;147:1537-1550.

Unternaehrer JJ and Daley GQ. Induced pluripotent stem cells for modelling human diseases. Philos Trans R Soc Lond B Biol Sci. 2011;366:2274-2285.

Wang D, Garcia-Bassets I, Benner C, Li W, Su X, Zhou Y, Qiu J, Liu W, Kaikkonen MU, Ohgi KA, Glass CK, Rosenfeld MG, Fu XD. Reprogramming transcription by distinct classes of enhancers functionally defined by eRNA. Nature 2011;474:390–394.

Wang JC, Passage MB, Yen PH, Shapiro LJ, Mohandas TK. Uniparental heterodisomy for chromosome 14 in a phenotypically abnormal familial balanced 13/14 robertsonian translocation carrier. Am J Hum Genet. 1991;48:1069-1074.

Wang P, Ren Z, Sun P. Overexpression of the long non-coding RNA MEG3 impairs in vitro glioma cell proliferation. J Cell Biochem. 2012;113:1868-1874.

Wylie AA, Murphy SK, Orton TC, Jirtle RL. Novel imprinted DLK1/GTL2 domain on human chromosome 14 contains motifs that mimic those implicated in IGF2/H19 regulation. Genome Res 2010;10:1711-1718.

Yang J, Cai J, Zhang Y, Wang X, Li W, Xu J, Li F, Guo X, Deng K, Zhong M, Chen Y, Lai L, Pei D, Esteban MA. Induced pluripotent stem cells can be used to model the genomic imprinting disorder Prader-Willi syndrome. J Biol Chem. 2010;285:40303-40311.

Ye L, Chang JC, Lin C, Sun X, Yu J, Kan YW. Induced pluripotent stem cells offer new approach to therapy in thalassemia and sickle cell anemia and option in prenatal diagnosis in genetic diseases.Proc Natl Acad Sci U S A. 2009;106:9826-9830.

Ye L, Muench MO, Fusaki N, Beyer AI, Wang J, Qi Z, Yu J, Kan YW. Blood cell-derived induced pluripotent stem cells free of reprogramming factors generated by Sendai viral vectors. Stem Cells Transl Med. 2013;2:558-566.

Ye L, Wang J, Beyer AI, Teque F, Cradick TJ, Qi Z, Chang JC, Bao G, Muench MO, Yu J, Levy JA, Kan YW. Seamless modification of wild-type induced pluripotent stem cells to the natural CCR5Δ32 mutation confers resistance to HIV infection. Proc Natl Acad Sci U S A. 2014;111:9591-9596.

Yevtodiyenko, A., Carr, M.S., Patel N., Schmidt, J. Analysis of candidate imprinted genes linked to Dlk1-Gtl2 using a congenic mouse line. Mamm. Genome 2002;13:633–638.

Ying L, Huang Y, Chen H, Wang Y, Xia L, Chen Y, Liu Y, Qiu F. Downregulated MEG3 activates autophagy and increases cell proliferation in bladder cancer. Mol Biosyst. 2013;9:407-411.

Zhang CY, Yu MS, Li X, Zhang Z, Han CR, Yan B. Overexpression of long non-coding RNA MEG3 suppresses breast cancer cell proliferation, invasion, and angiogenesis through AKT pathway. Tumour Biol. 2017;39:1010428317701311.

Zhang J, Yao T, Wang Y, Yu J, Liu Y, Lin Z. Long noncoding RNA MEG3 is downregulated in cervical cancer and affects cell proliferation and apoptosis by regulating miR-21. Cancer Biol Ther. 2016;17:104-113.

Zhang L, Yang Z, Trottier J, Barbier O, Wang L. Long noncoding RNA MEG3 induces cholestatic liver injury by interaction with ptbp1 to facilitate shp mrna decay. Hepatology. 2017;65:604-615.

Zhang X, Gejman R, Mahta A, Zhong Y, Rice KA, Zhou Y, Cheunsuchon P, Louis DN, Klibanski A. Maternally expressed gene 3, an imprinted noncoding RNA gene, is associated with meningioma pathogenesis and progression. Cancer Res. 2010;70:2350-2358.

Zhang X, Rice K, Wang Y, Chen W, Zhong Y, Nakayama Y, Zhou Y, Klibanski A. Maternally Expressed Gene 3 (MEG3) Noncoding Ribonucleic Acid: Isoform Structure, Expression, and Functions. Endocrinology. 2010;151:939-947.

Zhou X, Yuan P, Liu Q, Liu Z. LncRNA MEG3 regulates imatinib resistance in chronic myeloid leukemia via suppressing microrna-21. Biomol Ther 20171;25:490-496.

Zhou Y, Zhang X, Klibanski A. *MEG3* noncoding RNA: a tumor suppressor. J Mol Endocrinol. 2012;48: R45-R53.

Zhou Y, Zhong Y, Wang Y, Zhang X, Batista DL, Gejman R, Ansell PJ, Zhao J, Weng C, Klibanski A. Activation of p53 by MEG3 non-coding RNA. J Biol Chem. 2007;282:24731-24742.

Zhuang W, Ge X, Yang S, Huang M, Zhuang W, Chen P, Zhang X, Fu J, Qu J, Li B. Upregulation of lncRNA MEG3 promotes osteogenic differentiation of mesenchymal stem cells from multiple myeloma patients by targeting bmp4 transcription. Stem Cells 2015;33:1985-1997.